

Chapter 3. Source to Exposure

3.1. Introduction

This chapter reviews concepts and findings in atmospheric sciences and exposure assessment that provide a foundation for the detailed presentation of evidence of CO-related health effects in subsequent chapters and for a causality finding regarding climate forcing effects of CO. Section 3.2 provides an overview of the primary and secondary sources of CO as well as the atmospheric chemistry involved in the production and removal of CO by oxidation processes. Section 3.3 provides a description of climate forcing caused directly and indirectly by CO. Descriptions of CO measurement methods, monitor siting requirements, and monitor locations are presented in Section 3.4. Ambient CO concentrations and their spatial and temporal variability are characterized in Section 3.5. The background concentrations of CO useful for risk and policy assessments informing decisions about the NAAQS, referred to as policy-relevant background (PRB) concentrations, are also presented in Section 3.5. Factors related to human exposure to ambient CO, and their implications for epidemiologic studies, are discussed in Section 3.6. Finally, a summary and conclusions of the chapter are presented in Section 3.7.

3.2. CO Sources, Emissions, and Chemistry

3.2.1. Direct CO Emissions

CO is formed primarily by incomplete combustion of carbon-containing fuels and photochemical reactions in the atmosphere. In general, any increase in fuel O₂ content, burn temperature, or mixing time in the combustion zone will tend to decrease production of CO relative to CO₂. CO emissions from large fossil-fueled power plants are typically very low since the boilers at these plants are tuned for highly efficient combustion with the lowest possible fuel consumption. Additionally, by allowing time for the furnace flue gases to mix with air and be oxidized by OH to CO₂ in the hot gas stream before the OH concentrations drop as the flue gases cool, the CO-to-CO₂ ratio in these emissions is shifted toward CO₂.

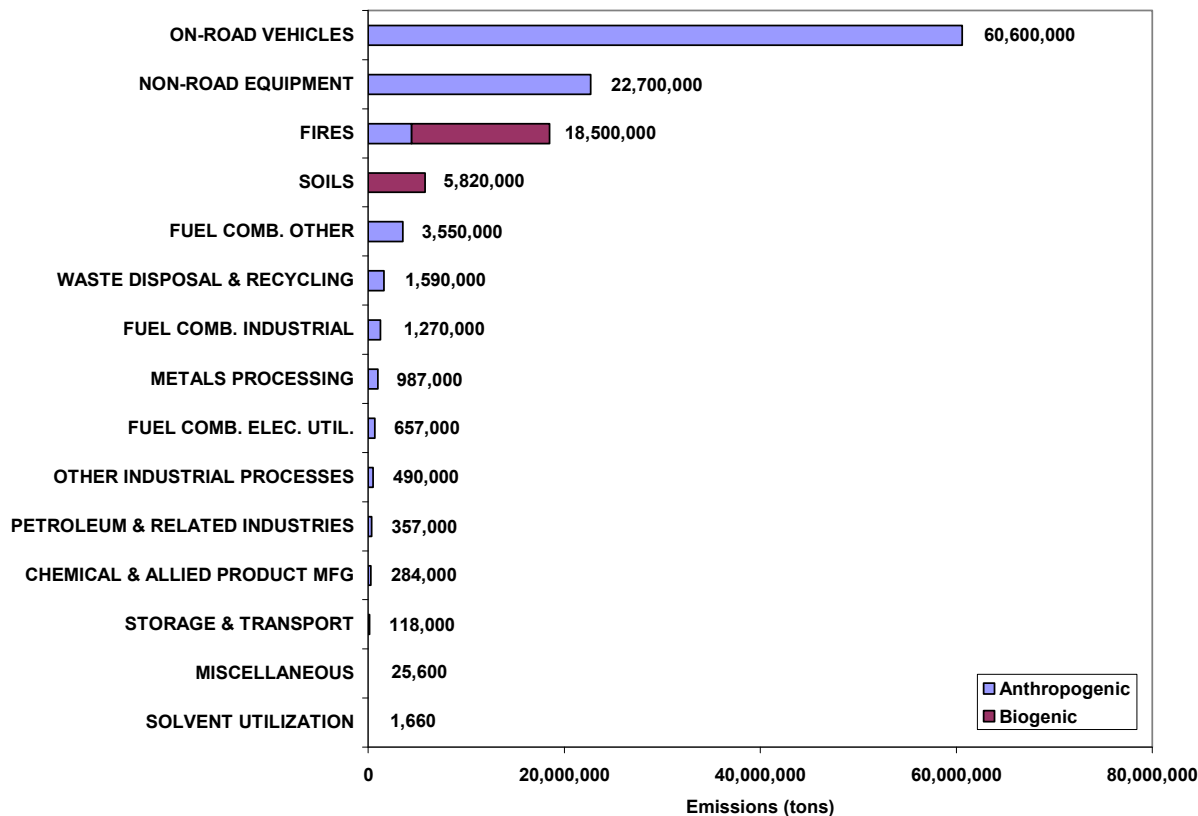
Figure 3-1 lists CO emissions totals in tons segregated by individual source sectors in the U.S. for 2002, which is the most recent publicly available CO emissions data meeting EPA's data quality assurance objectives. In the U.S., direct CO emissions data are tracked in the National Emissions Inventory (U.S. EPA, 2006, [157070](#)), a composite of data from various sources including industries and state, tribal, and local air agencies, and from the Biogenic Emissions Inventory System (BEIS). NEI data are collected for all states, the District of Columbia, the U.S. territories of Puerto Rico and Virgin Islands, and some of the territories of federally recognized American Indian nations. Different data sources use different data collection methods, most of which are based on empirical estimates and engineering calculations rather than measurements. Most fuel combustion and industrial sources, for example, estimate their CO emissions using EPA-approved emission factors, as do on-road and non-road mobile source emitters where models (MOBILE6, MOVES, NONROAD) are available to calculate inventories (U.S. EPA, 2006, [157070](#)). The NEI includes fires of anthropogenic and natural origin. Anthropogenic fires include structural fires, agricultural fires, prescribed burning, and slash burning; forest wildfires are considered to be of natural origin. Estimates of direct CO emission from

Note: Hyperlinks to the reference citations throughout this document will take you to the NCEA HERO database (Health and Environmental Research Online) at <http://epa.gov/hero>. HERO is a database of scientific literature used by U.S. EPA in the process of developing science assessments such as the Integrated Science Assessments (ISAs) and the Integrated Risk Information System (IRIS).

soil are calculated by the EPA using the BEIS model. Although these estimates are generated using well-established approaches, uncertainties are inherent in the emission factors and models used to represent sources for which emissions have not been directly measured. These uncertainties vary by source category, season, and region. Discussion of uncertainties is provided in subsequent paragraphs related to mobile sources, the largest source category.

Nationally, on-road mobile sources in the NEI constituted more than half of total CO emissions in 2002, or ~60.6 MT of ~116.8 MT total, which includes anthropogenic and biogenic emissions reported in the NEI and the BEIS (<http://www.epa.gov/ttnchie1/emch/biogenic>). High concentrations of CO can often occur in areas of heavy traffic. In metropolitan areas in the U.S., for example, as much as 75% of all CO emissions came from on-road vehicle exhaust in the 2002 NEI (U.S. EPA, 2006, [157070](#)). When the emissions from incomplete combustion of fuels powering non-road mobile sources were included, all mobile sources accounted for ~80% of total CO emissions in the U.S. in 2002 (Figure 3-1).

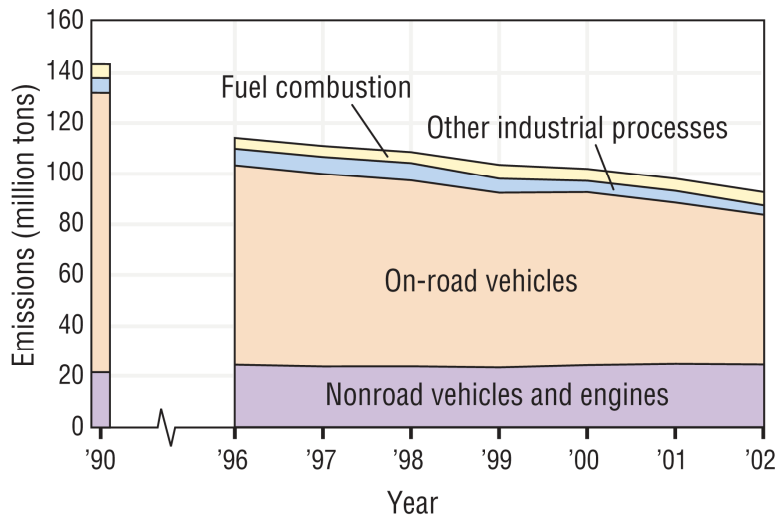
CO emissions from internal combustion engines vary substantially with ambient temperature and operating conditions. Substantial light-duty gasoline vehicle CO emissions occur during the cold start before the catalyst is warmed up. Most emission tests such as the Federal Test Procedure (FTP) which includes a cold start portion and is used to certify that vehicles meet EPA emission standards, are conducted at about 75°F. Lower ambient temperatures result in increased CO emissions because spark ignition engines are required to run richer air:fuel ratios for longer periods of time, and also because the time before the catalyst is warmed up increases compared to the time for catalyst warm-up occurring at 75°F (U.S. EPA, 2006, [199897](#)). Thus, in addition to the vehicle CO emissions standards EPA implemented starting with the 1968 model year, EPA has also implemented a cold temperature CO emission standard for light-duty gasoline vehicles and trucks at 20°F that phased in for 40% of the new fleet in the 1994 model year, 80% for the 1995 model year, and 100% with the 1996 and succeeding model years. The emission standard of 10 g/mile results in a reduction of about 20-30% in CO emissions at 20° F (57 FR 3188-31923 July 17, 1992). Increased vehicle CO emissions can also occur under conditions such as high rates of acceleration, rapid speed fluctuations, heavy-vehicle load demands (such as occur while pulling a trailer or going up a steep hill), and use of air-conditioning. Such driving conditions were not originally fully reflected in the FTP. EPA has issued a Supplemental Federal Test Procedure (SFTP) to control excess CO emissions under these conditions. These regulations were phased in for the 1998-2000 model years (61 FR 54852-54906 October 22, 1996). Moreover, the gasoline-powered spark ignition engines that predominate in light-duty on-road vehicles have higher uncontrolled CO emission rates than other combustion sources because they typically operate closer to the stoichiometric air-to-fuel ratio, have relatively short residence times at peak combustion temperatures, and have very rapid cooling of cylinder exhaust gases. By contrast, the diesel-powered engines that predominate in heavy-duty on-road vehicles and in off-road and non-road fixed combustion sources have much lower engine-out CO emissions than do the spark-ignition engines because the diesels typically operate at very high air-to-fuel ratios, which promote mixing oxygen and fuel, thus improving carbon burn.



Source: U.S. EPA (2006, [157070](#))

Figure 3-1. CO emissions (tons) in the U.S. by source sector in 2002 from the NEI and the BEIS. The “fires” category has been extracted from Tier 3 miscellaneous categories of the NEI, and biogenic fires are those attributed to forest wildfires. The “soils” category comprises the BEIS data. The “roadway vehicles” and “non-road vehicles” categories have been renamed here for clarity.

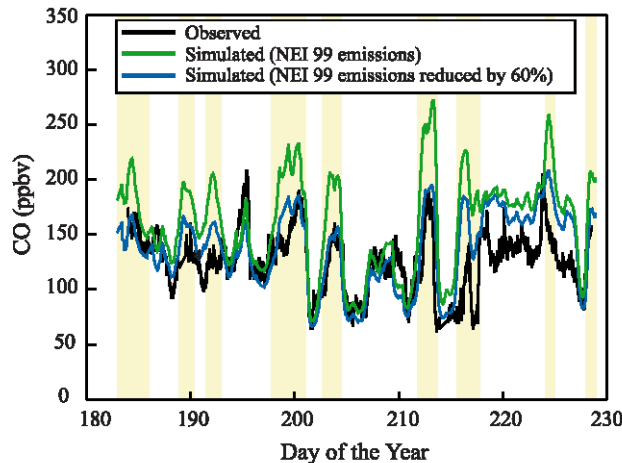
Figure 3-2 shows present and historical CO emissions from the traditionally inventoried anthropogenic source categories: (1) fuel combustion, which includes emissions from coal-, gas-, and oil-fired power plants and industrial, commercial, and institutional sources, as well as residential heaters (e.g., wood-burning stoves) and boilers; (2) industrial processes, which include chemical production, petroleum refining, metals production, and industrial processes other than fuel combustion; (3) on-road vehicles, which include cars, trucks, buses, and motorcycles; and (4) non-road vehicles and engines, such as farm and construction equipment, boats, ships, snowmobiles, aircraft, locomotive, and the two-stroke engines found in lawnmowers, chainsaws, and other small gasoline-powered equipment. Using these NEI data, trends in the national CO emissions can be computed and compared over time. So, for example, the national-scale estimated anthropogenic CO emissions decreased 35% between 1990 and 2002. The trend in Figure 3-2 demonstrates that controls in the on-road vehicle sector have produced nearly all the national-level CO reductions since 1990. (Data are presented here for 1990 and from 1996-2002 because only 1990 data have been updated to be comparable to the more recent inventories made since 1996.)



Source: U.S. EPA (2008, [157076](#))

Figure 3-2. Trends in anthropogenic CO emissions (MT) in the U.S. by source category for 1990 and 1996-2002.

With the exception of this downward trend resulting from emissions controls, anthropogenic CO emissions demonstrate less interannual variability than biogenic emissions (Bergamaschi et al., 2000, [192377](#)). Several recent reports using both ambient concentrations and fuel-based emissions estimates have explored this annual-to-decadal emissions decrease in anthropogenic CO in finer detail; they include Harley et al. (2001, [193922](#); 2005, [088154](#)), Parrish et al. (2002, [052472](#)), Parrish (2006, [090352](#)), Pollack et al. (2004, [184461](#)), and Mobley et al. (2005, [194008](#)). The consistent conclusion from those investigations has been that annual average U.S. on-road vehicle CO emissions have decreased at a rate of ~5% per year since the early 1990s. This can be seen from Figure 3-2 as well. Additional analyses by Harley et al. (2005, [088154](#)) and Parrish (2006, [090352](#)) were also consistent with the suggestion in Pollack et al. (2004, [184461](#)) that the EPA MOBILE6 vehicle emissions model (<http://www.epa.gov/otaq/m6.htm>) now overestimates vehicle CO emissions by a factor of ~2. Field measurements by Bishop and Stedman (2008, [194670](#)) were in accord with Parrish's (2006, [090352](#)) findings that the measured trends of CO and NO_x concentrations from mobile sources in the U.S. indicated that modeled CO emission estimates were substantially too high. Hudman et al. (2008, [191253](#)) found that the NEI overestimated anthropogenic CO emissions by 60% for the eastern U.S. during the period July 1-August 15, 2004 using aircraft observations of CO from the International Consortium for Atmospheric Research on Transport and Transformation (ICARTT) campaign (Fehsenfeld et al., 2006, [190531](#)) and results from a tropospheric chemistry model (GEOS-Chem)(Figure 3-3).



Source: Reprinted with Permission of the American Geophysical Union from Hudman et al. (2008, [191253](#))

Figure 3-3. Surface air CO concentrations at Chebogue Point during the ICARTT campaign. Observations (black) are compared to model results using the 1999 NEI anthropogenic emissions (green) and with these CO emissions reduced by 60% (blue). Yellow bands are periods of U.S. outflow diagnosed by Millet et al. (2006, [195106](#)). Overestimation near day 200 is due to model misplacement of a large Alaskan/Canadian biomass burning plume.

Improvements in emissions technologies not correctly represented in MOBILE emissions models have been suggested as one cause for this discrepancy. For example, Pokharel et al. (2002, [052473](#); 2003, [053740](#)) demonstrated substantial decrements in the CO fraction of tailpipe exhaust in several U.S. cities, and Burgard et al. (2006, [193222](#)) documented improvements in emissions from heavy-duty on-road diesel engines. The Motor Vehicle Emission Simulator (MOVES) model has been designed to address some of the largest errors in the MOBILE model. It was released in final form in December 2009 (<http://www.epa.gov/otaq/models/moves/index.htm>).

Estimates of non-anthropogenic CO emissions are made using the BEIS model with data from the Biogenic Emissions Landcover Database (BELD) and annual meteorological data. National biogenic emissions, excluding fires, were estimated to contribute 5%, or ~5.8 MT, of total CO emissions from all sources in 2002. Biogenic wildfires in 2002 added another 12%, or ~14.1 MT, to the national CO emissions total and were responsible for 76.1% of all CO emissions estimates from fires. This is shown in Figure 3-1 using the NEI and BEIS data. Geogenic emissions of CO, also included in this inventory, include volcanic gases released from molten rock in the Earth's mantle. Mixing ratios of dissolved CO in this rock vary in a range from 0.01 to 2% as a function of the rock stratum surrounding the volcano and other geologic conditions. This high variability and infrequent though often violent release mean geogenic CO measurements are very difficult to make with precision, though on non-local scales the magnitude of their contribution is small relative to anthropogenic sources. Photodecomposition of organic matter in oceans, rivers, lakes, and other surface waters, and from soil surfaces also releases CO (Goldstein and Galbally, 2007, [193247](#)). However, soils can act as a CO source or a sink depending on soil moisture, UV flux reaching the soil surface, and soil temperature (Conrad and Seiler, 1985, [029520](#)). Soil uptake of CO is driven by anaerobic bacteria (Inman et al., 1971, [010972](#)). Emissions of CO from soils appear to occur by abiotic processes, such as thermodecomposition or photodecomposition of organic matter. In general, warm and moist conditions found in most soils favor CO uptake, whereas hot and dry conditions found in deserts and some savannas favor the release of CO (King, 1999, [002828](#)).

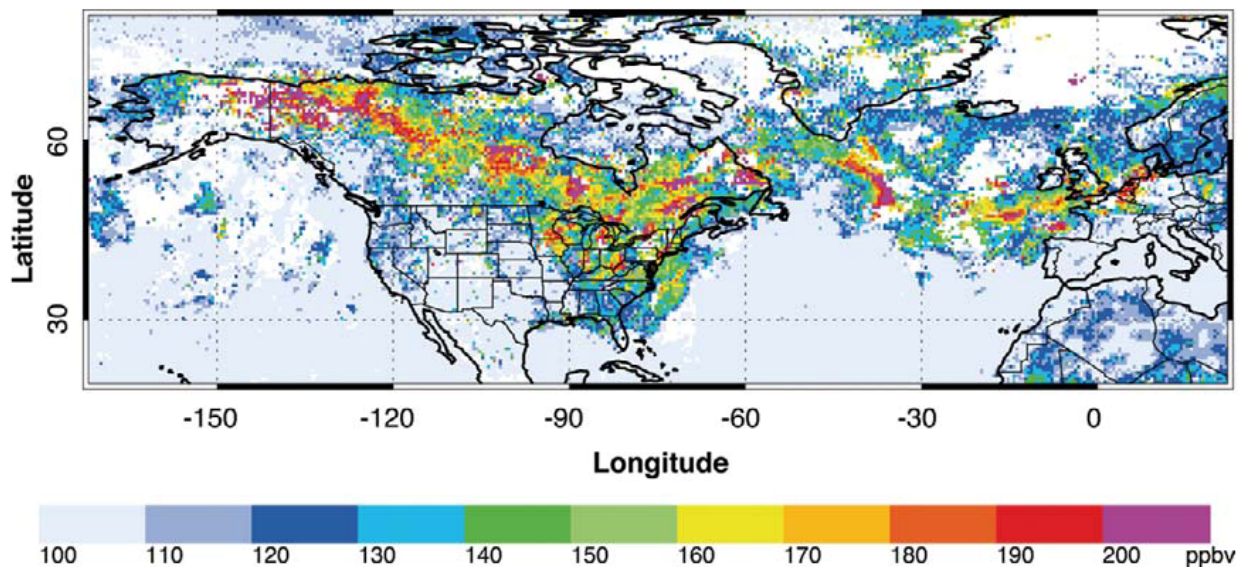
Biomass burning consists of wildfires and the intentional burning of vegetation to clear new land for agriculture and population resettlement; to control the growth of unwanted plants on pasture land; to manage forest resources with prescribed burning; to dispose of agricultural and domestic waste; and as fuel for cooking, heating, and water sterilization. Globally, most wildfires may be ignited directly as the result of human activities, leaving only 10-30% initiated by lightning

(Andreae, 1991, [078147](#)). However, because fire management practices suppress natural wildfires, the buildup of fire fuels increases the susceptibility of forests to more severe but less frequent fires in the future. Thus there is considerable uncertainty in attributing the fraction of wildfire emissions to human activities because the emissions from naturally occurring fires that would have been present in the absence of fire suppression practices are not known.

Biomass burning also exhibits strong seasonality and interannual variability (van der Werf et al., 2006, [157084](#)), with most biomass burned during the local dry season. This is true for both prescribed burns and wildfire. The unusually warm and dry weather in central Alaska and western Yukon in the summer of 2004, for example, contributed to the burning of 11 million acres there. These fires, the largest on record for this region, produced CO emissions easily tracked by the Measurement of Pollution in the Troposphere (MOPITT) instrument on NASA's Terra satellite (Figure 3-4). The high CO concentration measured by MOPITT coincided with the surface location of fires tracked using aerosol plumes identified by the Moderate Resolution Imaging Spectroradiometer (MODIS) also on Terra. Subsequent modeling by Pfister et al. (2005, [093009](#)) showed that the CO contribution from these fires in July 2004 was 33.1 (\pm 5.5) MT that summer, or in the range of the total U.S. anthropogenic CO emissions during the same time. The smoldering phase of combustion yields higher CO emissions than the flaming phase. Using controlled combustion chamber experiments, Lobert et al. (1991, [029473](#)) found that with a wide variety of vegetation types, on average, 84% of the CO from biomass fires was produced during the smoldering phase and 16% during the flaming phase of combustion.

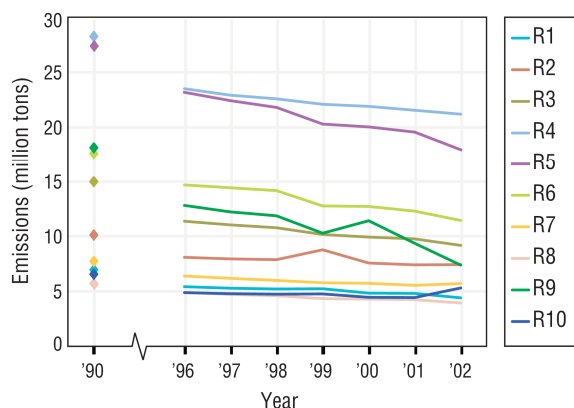
CO emissions data for EPA's 10 administrative Regions in the U.S., depicted in Figure 3-5, show a more nuanced view of the national concentrations and trends described above. Net anthropogenic CO emissions were estimated to have declined in all EPA Regions between 1990 and 2002, with the largest decrease (10.8 MT) occurring in Region 9 and the smallest (1.3 MT) in Region 10.

At state and local levels, CO emissions from on-road mobile sources or from fires can dominate in different locations across the U.S. Figure 3-6 illustrates this variability with CO state-level emissions totals and selected county totals in 2002 for Colorado (Annex A includes analogous data for Alaska, Utah, Massachusetts, Georgia, California, and Alabama). In Colorado, emissions from fires and on-road vehicles were nearly equal: ~0.9 MT from fires and ~1.1 MT from on-road vehicles. Emissions sources varied strongly across counties, however, with urban Denver County dominated by on-road vehicle emissions at 71% and rural Garfield County dominated by fire emissions at 67%.



Source: Reprinted with Permission of the American Meteorological Society from Fishman et al. (2008, [193927](#))

Figure 3-4. CO concentrations centered at ~3,000 m above sea level measured by the MOPITT sensor on the Terra satellite for the period July 15-23, 2004, during intense wildfires in Alaska and the Yukon.

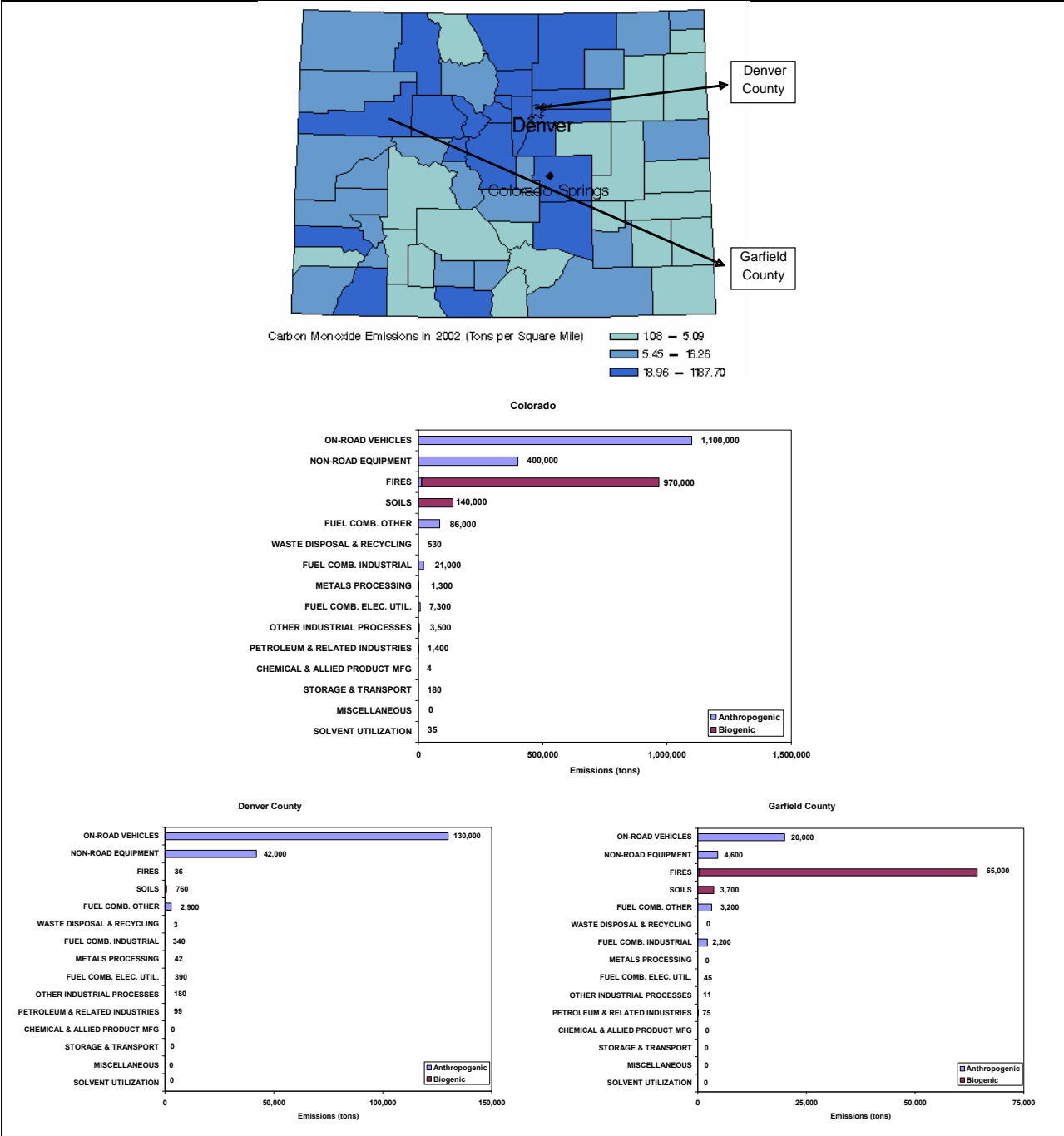


Data are presented for 1990 and 1996-2002, as datasets from these inventory years are all fully up to date. Data are available for inventory years 1991-1995, but these data have not been updated to allow comparison with data from 1990 and 1996-2002.



Source: U.S. EPA (2008, [157076](#))

Figure 3-5. Trends in subnational CO emissions in the 10 U.S. EPA Regions for 1990 and 1996-2002.



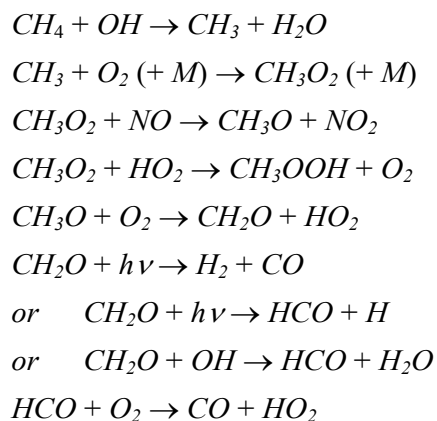
Source: U.S. EPA (2006, 157070)

Figure 3-6. CO emissions density map and distributions for the state of Colorado and for selected counties in Colorado in 2002, from the NEI and the BEIS. The “fires” category has been extracted from Tier 3 miscellaneous categories of the NEI, and biogenic fires are those attributed to wildfires. The “soils” category comprises the BEIS data. The “roadway vehicles” and “non-road vehicles” categories have been renamed here for clarity.

3.2.2. Secondary CO Emissions and Associated Chemistry

Oxidation of anthropogenic and biogenic VOCs constitute important secondary sources of CO. For example, Hudman et al. (2008, [191253](#)) determined that oxidation of isoprene and other biogenic VOCs contributed 9.1 MT of atmospheric CO (with isoprenes contributing 7.1 MT), and oxidation of anthropogenic VOCs contributed another 2.0 MT of CO emissions during the period July 1- August 15, 2004, for the eastern U.S. In contrast, direct anthropogenic CO emissions were estimated to be 5.1 MT for this time period and location. Hence, secondary biogenic formation was found to be a more important source of CO emissions than direct anthropogenic activities for the study period. Hudman et al. (2008, [191253](#)) noted that biogenic CO emissions were highest in the southeastern U.S., where isoprene emissions are also greatest. These estimates were obtained using aircraft measurements from the ICARTT campaign (Fehsenfeld et al., 2006, [190531](#)) and estimates from the GEOS-Chem model (Bey et al., 2001, [051218](#)), configured as described by Hudman et al. (2007, [089474](#)).

Secondary CO production occurs by photooxidation of methane (CH₄) and other VOCs, including nonmethane hydrocarbons (NMHCs) in the atmosphere and organic molecules in surface waters and soils. CH₄ oxidation is summarized in this reaction sequence:



Reaction 3-1

where M is a reaction mediator that is neither created nor destroyed and stabilizes the reaction product.

Photolysis of formaldehyde (CH₂O) proceeds by two pathways. The first produces molecular hydrogen (H₂) and CO with a reaction yield of 55% in conditions of clear skies and low zenith angles; the second yields a hydrogen radical (H) and the formyl radical (HCO). HCO then reacts with O₂ to form hydroperoxy radical (HO₂; OH and HO₂ together are termed HO_x) and CO. Reaction of methyl peroxy radical (CH₃O₂) with HO₂ radicals to form methyl hydroperoxide (CH₃OOH) is also operative, especially in low oxides of nitrogen (NO+NO₂=NO_x) conditions. Heterogeneous removal of the partially water-soluble intermediate products, such as CH₃OOH and CH₂O, will decrease CO yields from CH₄ oxidation.

While oxidation of CH₂O nearly always produces CO and some small quantities of formic acid (CH₂O₂) in the reaction of CH₂O with HO₂ (not shown here), oxidation of acetaldehyde (CH₃CHO) does not always yield two CO molecules. Reaction of CH₃CHO with OH can yield acetyl radicals (CH₃CO) which then will participate with O₂ in a termolecular recombination reaction to form peroxyacetyl radicals, which then can react with nitric oxide (NO) to form CH₃ and CO₂; or the peroxyacetyl radicals can react with NO₂ to form peroxyacetyl nitrate (PAN), CH₃CO₃NO₂. In this way, one carbon atom is oxidized directly to CO₂ without passing through CO. The yield of CO from these pathways depends on the OH concentration and the photolysis rate of CH₃CHO, as well as on the abundance of NO, since peroxyacetyl radicals also will react with other odd hydrogen radicals like HO₂.

Estimating the CO yield from oxidation of hydrocarbons (HCs) larger than CH₄ requires computing the yields of CH₂O, CH₃CHO, CH₃CO, and analogous radicals from oxidation of the parent molecules. Moreover, the extent of heterogeneous removal of soluble intermediate products also affects oxidation of more complex HCs. However, the detailed gas-phase kinetics for many HCs

with more than a few carbons is still unknown. This is especially the case for several important classes of VOCs, including the aromatics, biogenic HCs including isoprene, and their intermediate oxidation products like epoxides, nitrates, and carbonyls. Mass-balance analyses performed on irradiated smog chamber mixtures of aromatic HCs indicate that only about one-half of the carbon is in the form of compounds that can be identified. In addition, reactions like the oxidation of terpenes that produce condensable products are also significant because these reactions produce secondary organic aerosols, thereby reducing the potential yield of CO. The CO yield from oxidation of CH₄, for example, is ~0.9 on a per carbon basis (Kanakidou and Crutzen, 1999, [011760](#)). Yields from other compounds range from <0.1 for anthropogenic alkanes (Altshuller, 1991, [192375](#)) to ~0.9 for ethane; yields from other compounds are given in Table 3-1 taken from Kanakidou and Crutzen (1999, [011760](#)).

Table 3-1. Literature values for CO yields from hydrocarbons in per carbon units, except as noted. Specific hydrocarbons are noted in parentheses.

Reference	CO Yields
Zimmerman et al. (1978, 010758)	0.3 (hydrocarbons)
Brewer et al. (1984, 194402)	0.22-0.27 (isoprene)
Hanst et al. (1980, 011988)	According to chamber experiments, CO and CO ₂ yield:
	~0.85 (ethylene)
	~0.90 (ethane)
	~0.80 (propane)
	~0.58 (n-butane)
	~0.73 (isoprene)
	~0.30 (alpha-pinene)
Crutzen (1987, 002848)	0.9 of CH ₄
Kanakidou et al. (1991, 029701)	0.39 (C ₂ H ₆ and C ₃ H ₈)
Jacob and Wofsy (1990, 029668)	@ low NO _x : 0.2 (isoprene)
	@ high NO _x : 0.6 (isoprene)
Crutzen et al. (1985, 194403)	=0.8 (isoprene + OH)
Kirchhoff and Marinho (1990, 194406)	Isoprene oxidation may form 10 ppbv CO/d over the Amazon (3 km deep boundary layer)
Altshuller (1991, 192375)	Conversion factors of 19 (C ₂ -C ₆) anthropogenic alkenes vary between 0.010 and 0.075
Manning et al. (1997, 194401)	CH ₄ in the SH: 0.7
Kanakidou and Crutzen (1999, 011760)	Annual tropospheric mean conversion factors:
	CH ₄ : 0.9
	Isoprene: 0.4
	Other nonmethane hydrocarbons: 0.7

Source: Adapted with Permission of Elsevier Ltd. from Kanakidou and Crutzen (1999, [011760](#))

The major pathway for removal of CO from the atmosphere is reaction with OH to produce CO₂ and H radicals that rapidly combine with O₂ to form HO₂ radicals, with a rate constant at 1 atm in air of ~2.4×10⁻¹³ cm³/molecule/s (Finlayson-Pitts and Pitts, 2000, [055565](#)). The mean tropospheric photochemical lifetime (τ) of CO in the northern hemisphere is ~57 days (Khalil and Rasmussen, 1990, [012352](#); Thompson and Cicerone, 1986, [019374](#)). Owing to variation in atmospheric water vapor, OH concentration, and insolation, shorter τ are found nearer the tropics and longer ones at higher latitudes. During winter at high latitudes, CO has nearly no photochemical reactivity on urban and regional scales. Because the CO τ is shorter than the ~1 yr characteristic time scale for mixing between the hemispheres and because northern hemisphere CO emissions are higher due to anthropogenic activity (Khalil and Rasmussen, 1990, [012443](#)), a large gradient in concentrations

exists between the hemispheres (Edwards et al., 2004, [199889](#)). In addition, the CO τ at high latitudes is long enough to result in much smaller gradients between 30° latitude and the pole of either hemisphere. The typical residence time of CO in urban areas when assuming a diel-average OH concentration of $3 \times 10^6/\text{cm}^3$ in urban areas is ~ 16 days, so CO will not typically be destroyed in urban areas where it is emitted and will likely be mixed on continental and larger scales. OH concentrations are orders of magnitude lower in indoor environments, and so CO will generally not be affected by indoor air reactions.

3.3. CO Climate Forcing Effects

Recent data do not alter the current well-established understanding of the role of urban and regional CO in continental and global-scale chemistry outlined in the 2000 CO AQCD (U.S. EPA, 2000, [000907](#)) and subsequently confirmed in the recent global assessments of climate change by the Intergovernmental Panel on Climate Change (IPCC) (2001, [156587](#); 2007, [092765](#)). CO is a weak direct contributor to greenhouse warming because its fundamental absorption band near $4.63 \mu\text{m}$ is far from the spectral maximum of Earth's longwave radiation at $\sim 10 \mu\text{m}$. Sinha and Toumi (1996, [193747](#)) estimated the direct RF of CO computed for all-sky conditions at the tropopause, which is the IPCC's preferred form for the calculation (Forster et al., 2007, [092936](#)), to be 0.024 W/m^2 based on an assumed change in CO mean global concentration from 25 to 100 ppb since preindustrial times. The direct RF value similarly projected by Sinha and Toumi (1996, [193747](#)) if the mean global background concentration were to increase from 25 to 290 ppb was 0.057 W/m^2 .

However, because reaction with CO is the major sink for OH on a global scale, increased concentrations of CO can lead to increased concentrations of other trace gases whose loss processes also involve OH chemistry. Some of those trace gases, CH_4 and O_3 for example, absorb infrared radiation from the Earth's surface and contribute to the greenhouse effect directly. Others, including hydrochlorofluorocarbons (HCFCs), methyl chloride, and methyl bromide, can deplete stratospheric O_3 , increasing the surface-incident UV flux.

This indirect effect of CO on stratospheric O_3 concentrations is opposite in sign to the effect of CO on O_3 in the troposphere where CO reacts in a manner similar to other VOCs in the presence of NO_x and UV to create O_3 ; see the detailed description of O_3 formation from VOCs and NO_x in the 2006 O_3 ISA (U.S. EPA, 2006, [088089](#)). Because CO's chemical lifetime is longer than those of the VOCs most important for O_3 formation on urban and regional scales and because CO oxidation has one-to-one stoichiometry (whereby one molecule of CO converts only one molecule of NO to NO_2), CO has a significantly lower O_3 forming potential than other VOCs in the troposphere. Carter (1998, [192380](#)) computed a maximum incremental reactivity for CO of 0.06 g O_3 for 1 g CO , as compared to reactivities of total on-road vehicle exhaust emissions typically in the range of 3 to 4 g O_3 per g VOC . However, because the total mass of CO emissions is substantially greater than those of the other VOCs with higher carbon numbers and faster reactivities, CO can contribute significantly to O_3 formation even though its photochemical processing is slow. Using data from instrumented models, including that of Jeffries (1995, [003055](#)), the NRC (1999, [010614](#)) estimated, for example, that CO can contribute 15-25% of the total O_3 forming potential of gasoline exhaust emissions, although this estimate shows strong regionality. The contribution of CO to urban and regional O_3 concentration is often $<10\%$ owing to its very slow reactivity on these scales and to locally variable radical concentration ratios.

Emissions of CO and the other O_3 precursors, nonmethane VOCs (NMVOCs) and NO_x , affect the oxidizing capacity of the atmosphere largely by perturbing HO_x concentrations. From a climate perspective, this HO_x perturbation chiefly affects the CH_4 τ and production of O_3 in the troposphere. Changes in the concentration of O_3 and hence in its RF occur mainly in the time of a few months. However, Prather (1996, [193195](#)) showed that changes in CH_4 concentration and its RF extend to the "primary mode" timescale of troposphere chemistry of about 14 yr (Derwent et al., 2001, [047912](#); Wild et al., 2001, [193196](#)). The primary mode timescale of CH_4 is in part determined by the positive feedbacks in the CH_4 -OH-CO system in which even low concentration additions of CH_4 produce additional CO through oxidation by OH. That additional CO then further decreases atmospheric OH concentrations when OH oxidizes it to CO_2 . The resulting decreased OH concentration then further increases the CH_4 τ (Daniel and Solomon, 1998, [193235](#); Isaksen and Hov, 1987, [019490](#)). Atmospheric CH_4 concentrations since 1750 have increased by more than a factor of 2, giving an RF

of $\sim 0.6 \text{ W/m}^2$ (Forster et al., 2007, [092936](#)). Roughly 25% of the global mean tropospheric CO is produced by CH₄ oxidation (Wuebbles and Hayhoe, 2002, [044159](#)). Using a 2-D global model on a coarse grid, Wang and Prinn (1999, [011758](#)) showed that increasing CO and CH₄ concentrations leading to decreased OH concentrations can extend the CO τ as well as the CH₄ τ . Wang and Prinn (1999, [011758](#)) varied the CO emissions and other model inputs and parameters in a matrix of simulations that showed, with increased or even constant 20th century CO concentrations, the CO τ was increased by more than 50% in 100 yr. However, Wang and Prinn (1999, [011758](#)) stated that their simulation omitted NMHCs and therefore likely underestimated CO concentrations while under- or overestimating hydroxyl radical concentrations. Likewise, low spatial resolution of the model likely incurred additional error in the solution.

CH₄ is long-lived and, in general, well mixed in the atmosphere. However, the reaction of CH₄ and OH, and hence the CH₄ τ , is governed by the behavior and location of emissions of the short-lived gases, including CO, VOCs, and NO_x. This produces high regional variability and uncertainty in the concentrations and RFs from CO and its related climate forcing gases (Berntsen et al., 2006, [193244](#); Fuglestad et al., 1999, [047431](#)). NO_x, for example, can produce effects on the combined indirect RF opposite in direction to those of CH₄ since under most global background conditions an increase in NO_x increases the global average OH concentration and decreases CH₄ τ and RF (Berntsen et al., 2005, [193241](#); Wild et al., 2001, [193196](#)). Wild et al. (2001, [193196](#)) also showed that emissions changes in CO have effects opposite in sign to those of NO_x because increases in CO act to depress OH concentrations and that the combined effect of CO and NO_x emissions yields a positive RF. The results of this study underscore the need to consider the combined effects of pollutants emitted from similar sources.

Using the 3-D global chemistry model MOZART-2 (Horowitz et al., 2003, [057770](#)), Naik et al. (2005, [193194](#)) simulated changes in global tropospheric O₃ concentrations and RF resulting from differing reductions in emissions of NO_x alone or a combination of NO_x, CO, and NMHCs in nine regions of the Earth. For the reductions in Europe, North America, and Southeast Asia, reducing CO and NMHCs in addition to reducing NO_x lowered the spatial inhomogeneity of the O₃ concentration and RF because CO has a longer lifetime than NO_x.

Wild et al. (2001, [193196](#)) used the University of California-Irvine chemical transport model (CTM) (Wild and Prather, 2000, [052402](#)) driven by the NASA GISS II general circulation model (Rind and Lerner, 1996, [193750](#)) to compute changes in O₃ concentrations and RF from regional emissions of NO_x and CO. Changes in O₃ and CH₄ result from increases in global surface NO_x emissions alone and run for 10-yr periods produced negative net RFs, ranging from -0.2 W/m^2 in East Asia to -0.5 W/m^2 in the Tropics owing to the long-term interdependencies in the CO-CH₄-NO_x system described above. When global CO emissions were increased by an 11 MT pulse for 1 yr together with the same 1-yr pulsed NO_x surface emissions and run again for a 10-yr period, the global net RF rose to 1.7 W/m^2 with an estimated 20% uncertainty based on the spatial variability and short-term reactivity of O₃ (Wild et al., 2001, [193196](#)).

Determining whether several species' τ and RF will increase or decrease in response to pulsed or step-wise emissions of the short-lived O₃ precursor species (NMVOC, CO, and NO_x) is complicated by its global location with respect to the O₃ production response surface. See the description of the O₃ production response surface and its dependence on NO_x and radical concentrations in the 2008 NO_x ISA (U.S. EPA, 2008, [157073](#)) for additional details. Fiore et al. (2002, [051221](#); 2008, [193749](#)) found that O₃ is closely coupled with CH₄ and that their relationship is influenced by regional variation in NO_x concentrations. Using the weighted average results from 12 3-D global chemistry models exercised for the IPCC Third Assessment Report (2001, [156587](#)), Wigley et al. (2002, [047883](#)) confirmed that increases in CO and VOC emissions increased the O₃ RF both directly and indirectly through the CH₄ effects described above. Furthermore, Wigley et al. (2002, [047883](#)) demonstrated that NO_x emissions produced a mix of direct and indirect increases in RF, mostly dominated by the direct effects for all modeled scenarios. Wigley et al. (2002, [047883](#)) concluded that tropospheric O₃ RF influences were larger than CH₄ influences and that the short-lived reactive gases produced 60-80% of that forcing, with the remainder coming from CH₄. Given these chemical interdependencies, calculations of an indirect RF for any of these short-lived O₃ precursor species are most often made for all of the most important ones together.

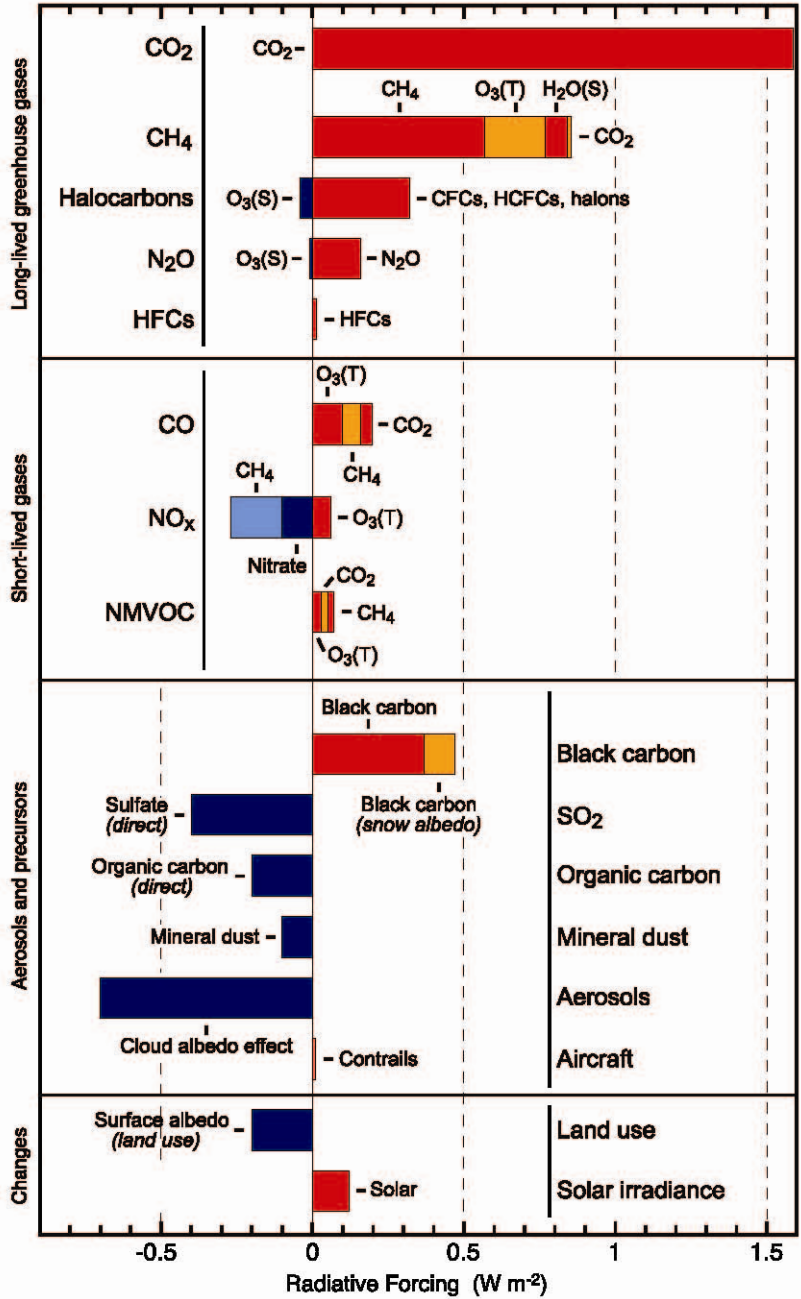
Figure 3-7 illustrates model estimates of the combined RF of increased short-lived O₃ precursor species relative to long-lived GHGs, aerosols, and other changes (Forster et al., 2007, [092936](#)). The combined effect of increased CH₄, CO, NMVOC, and NO_x emissions for the period 1750-2005 has produced tropospheric O₃ concentrations associated with a net RF of $\sim 0.4 \text{ W/m}^2$ with

$\pm 50\%$ uncertainty based on Shindell et al. (2005, [080129](#)). Indirect effects of CO through the GHGs O_3 , CH_4 , and CO_2 were estimated to contribute RF $\sim 0.2 \text{ W/m}^2$, which is more than a factor of 2 larger than the indirect effect of the shorter-lived NMVOCs on the same three GHGs (Forster et al., 2007, [092936](#)). Of the indirect effects on these three GHGs from CO emissions, the O_3 -related component was the largest, accounting for approximately one-half of the forcing (Forster et al., 2007, [092936](#)). In comparison, CO_2 contributed a direct forcing of $1.6 \pm 0.2 \text{ W/m}^2$ over this time period.

Integrated RF estimates over longer time horizons may indicate the future climate effects of present-day emissions. Modeled integrated 20-yr and 100-yr time horizon RFs are presented by Forster et al. (2007, [092936](#)) in Figure 3-8 for year 2000 emissions of short-lived and long-lived GHGs. The integrated RF for CO was estimated to be $\sim 0.2 \text{ W/m}^2\text{-yr}$ with $\sim 50\%$ uncertainty. It can be seen that the integrated RF of CO_2 is much smaller for the 20-yr horizon because the lifetime of CO_2 perturbations is roughly 150 yr. As a result, the RF related to short-lived CO is $\sim 25\%$ of that for CO_2 for the 20-yr horizon ($\sim 0.7 \text{ W/m}^2\text{-yr}$) but only $\sim 7\%$ of that for longer-lived CO_2 over a 100-yr time horizon ($\sim 2.4 \text{ W/m}^2\text{-yr}$). This indirect forcing is just slightly lower than the RF of year 2000 black carbon emissions from fossil fuel and biomass burning on the same horizons according to this assessment.

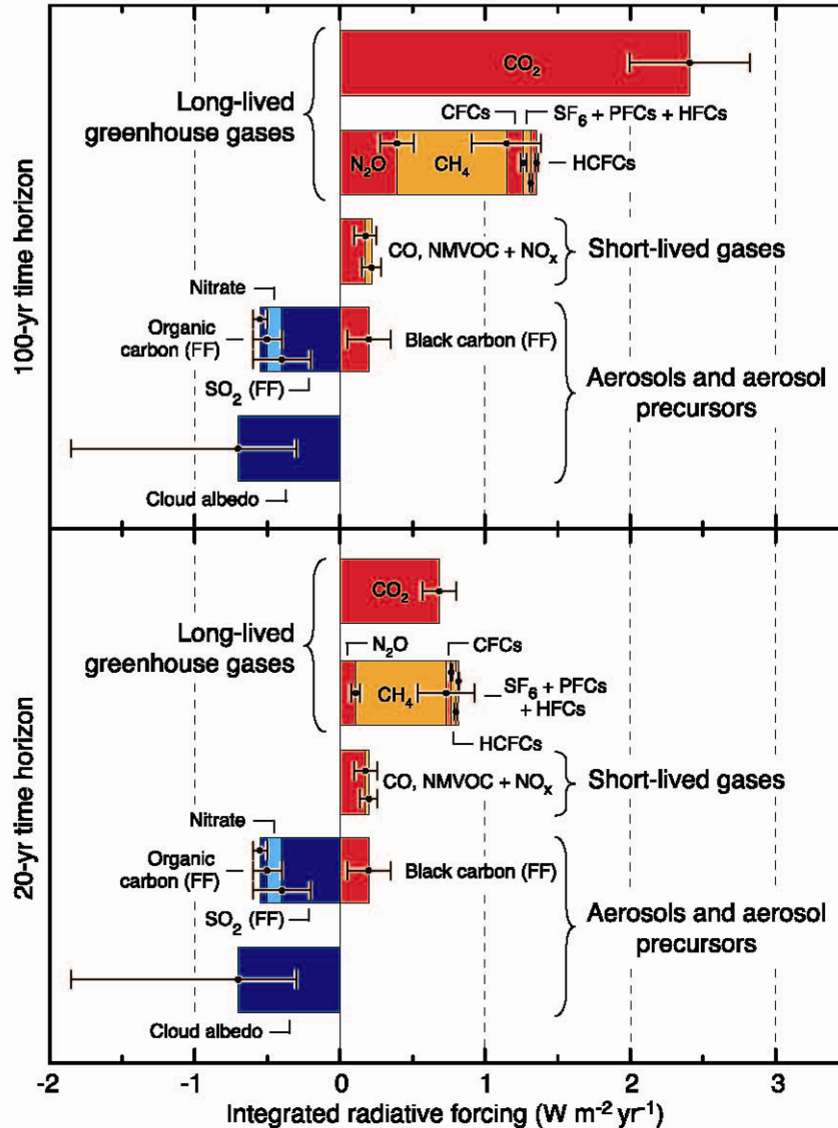
It is also possible to compute individual contributions to the integral RF from CO based on separate emissions sectors. Unger et al. (2009, [193238](#)) used the NASA GISS model for Physical Understanding of Composition-Climate Interactions and Impacts (G-PUCCINI) (Shindell et al., 2006, [193751](#)). Unger et al. (2009, [193238](#)) divided the 1995 global anthropogenic CO emissions total of 933.3 MT/yr into sectors for on-road transport (ORT) and power generation (PG), and then separated contributions from each of these sectors for the U.S. and other large geographic regions of the Earth. ORT CO emissions in the U.S. were 84.1 MT/yr; PG CO emissions were 0.55 MT/yr out of the total U.S. anthropogenic CO emissions of 112.5 MT/yr. Unger et al. (2009, [193238](#)) concluded from analysis of 7-yr runs that the CO indirect CH_4 effects (that is, the CO effects through CH_4 changes as described above) in the 1995 emissions run were -0.004 W/m^2 for the global ORT and -0.022 W/m^2 for the global PG. In the U.S., the indirect CH_4 RF was positive at $+0.009 \text{ W/m}^2$ because the positive effects on $CH_4 \tau$ from the CO emissions dominated over the negative effects from NO_x through OH. This RF fraction from indirect CH_4 is approximately the same as the direct O_3 RF from ORT in the U.S., 0.010 W/m^2 . Because the PG sector emits NO_x but less CO relative to the ORT, the indirect CH_4 RF from the U.S. PG was not dominated by the positive CO effects and remained a net negative at -0.006 W/m^2 (Unger et al., 2009, [193238](#)). The authors acknowledged some uncertainty in this relationship related to the influence of NO_x emissions on CO transformation, but no quantification of uncertainty in these modeled estimates was provided.

These gross emissions sectors can also be subdivided to demonstrate more clearly the localized chemical interdependencies of the CO- CH_4 - NO_x system. Fuglestad et al. (2008, [193242](#)) used the Oslo CTM2 model to simulate effects from all emissions and changes in all transportation subsectors from 1850-2000. Fuglestad et al. (2008, [193242](#)) found that global transport has been responsible for $\sim 15\%$ of the total anthropogenic CO_2 RF and $\sim 15\%$ of the total anthropogenic O_3 RF. Of the total O_3 RF, the largest contributor was the shipping sector at 0.03 W/m^2 , because its high NO_x -to-CO and NO_x -to-VOC ratios produced OH increases and hence CH_4 decreases in regions of naturally low NO_x . For the shipping segment of the transport sector, the high NO_x emissions there reduced the $CH_4 \tau$ but increased O_3 . The global mean effect from these two was small and still smaller than the direct negative effect from SO_4^{2-} aerosols. In the on-road segment of global transportation, emissions of CO and VOCs together with NO_x produce an O_3 RF larger than the negative RF from CH_4 .



Source: Reprinted with Permission of Cambridge University Press from Forster et al. (2007, [092936](#))

Figure 3-7. Components of RF in 2005 resulting from emissions since 1750. (S) and (T) indicate stratospheric and tropospheric changes, respectively.



Source: Reprinted with Permission of Cambridge University Press from Forster (2007, [092936](#))

Figure 3-8. Integrated RF of year 2000 emissions over 20-yr and 100-yr time horizons. The values provided refer to global annual emissions, but effects are expected to vary regionally for short-lived gases.

Caution is warranted in interpreting RF estimates. RF values are global model calculations using the assumption that global climate sensitivities are equal for all forcing mechanisms, whether CO₂, SO₄²⁻ and other aerosols, or the short-lived gases like CO (Berntsen et al., 2005, [193241](#); Berntsen et al., 2006, [193244](#)). That assumption is under challenge now by GCM results using regionalized RF values separately for different forcing mechanisms and with CO₂, O₃, and solar input changes (Joshi et al., 2003, [193752](#)). Joshi et al. (2003, [193752](#)) found that global climate system sensitivities from non-CO₂ RF varied by $\pm 30\%$ compared to CO₂ RF. Other GCM experiments by Lelieveld et al. (2002, [190361](#)), Rotstayn and Penner (2001, [193754](#)), Menon et al. (2002, [155978](#)), and Kristjansson (2002, [045282](#)) have indicated that regionally changing RF can induce changes in large-scale circulation patterns that control the regionalized cycles of flooding and drought through disruptions in regional temperature and hydrologic cycles. However, such regionalized patterns resulting from GCM experiments are so uncertain and so widely variable across models that even the sign of these regionalized changes can vary with model type and any of

the models' unconstrained assumptions (Berntsen et al., 2006, [193244](#)). Even with such uncertainty and variability, though, the consensus of the climate community is that the climate effects of changes to emissions of the long- and especially the short-lived pollutants, including CO, very likely depend on location.

Global warming potential (GWP) is a widely used relative measure of the potential effect of different emissions on climate, usually defined as the time-integrated RF from an instantaneous pulsed release of 1 kg of a trace gas relative to the effects from a pulsed release of 1 kg of CO₂. Because the greenhouse warming effects from CO are nearly completely indirect and because CO concentrations are spatially heterogeneous, neither the IPCC nor EPA computes direct GWPs for CO, just as they do not for tropospheric O₃, NO, NO₂, or VOCs (U.S. EPA, 2008, [184463](#)). IPCC does estimate indirect GWP for CO using the integrated indirect RF (Forster et al., 2007, [092936](#)). However, the indirect GWP values evaluated and summarized by IPCC are global and cannot reflect effects of localized emissions or emissions changes, making the values for the short-lived species NMVOC, CO, and NO_x more uncertain than the values for the long-lived, well-mixed species as a result of the OH chemistry described above. Moreover, urban- and regional-scale oxidation of CO to CO₂ under current atmospheric conditions proceeds very slowly, and IPCC considers production of CO₂ through this pathway to be double counting of CO effects (Forster et al., 2007, [092936](#)). Variation in the CO GWP range of estimates can be attributed to the unusually large heterogeneity in model type and form, pulsed or stepped emissions increase, time-horizon unit, and integral or differential indirect effects in several combinations (with or without NO_x emissions changes, including or excluding CO₂ effects).

Even with such variability in methods and tools, the CO GWPs have been largely in agreement for approximately 10 yr. The IPCC estimated the indirect GWP of CO to be 1.9 (Forster et al., 2007, [092936](#)). Daniel and Solomon (1998, [193235](#)) used a global box model for changes through CH₄ and O₃ effects from pulsed CO emissions and estimated a CO GWP exclusive of the effect through CO₂ to be between 1 and 4.4. Using the STOCHEM CTM, Derwent et al. (2001, [047912](#)) estimated a pulsed emissions CO GWP, again exclusive of effects through CO₂, to be 1.5. Johnson and Derwent (1996, [193192](#)) had previously computed and integrated GWP of 2.1 for the CH₄ and O₃ effect from a step-wise emissions change using a 2-D and a 100-yr time horizon. Derwent et al. (2001, [047912](#)) and Collins et al. (2002, [044156](#)) subsequently differentiated that integral for each effect and reported GWP for step-wise CO emissions changes on a 100-yr time horizon of 1.0, 0.6, and 1.6 through the effects on CH₄, O₃, and CO₂, respectively. Berntsen et al. (2005, [193241](#)) used the model LMDz v3.3 (Hauglustaine et al., 2004, [193191](#)) to compute 100-yr GWP values for pulsed CO emissions through all indirect effects to be 1.9 as resolved for Europe and 2.4 for Asia, demonstrating the strong regionality in the indirect effects from these short-lived precursors. Most recently, Shindell et al. (2009, [201599](#)) compared GWPs separately for CO, CH₄, and NO_x with and without interactions with aerosols. When including direct and indirect radiative effects related to interaction of CO with aerosols, the GWP for CO was estimated to rise from a range of 1-3 to a range of 3-8.

3.4. Ambient Measurements

3.4.1. Ambient Measurement Instruments

For enforcement of the air quality standards set forth under the Clean Air Act, EPA has established provisions in the Code of Federal Regulations (CFR) under which analytical methods can be designated as federal reference methods or federal equivalent methods (FRM or FEM, respectively). Measurements for determinations of NAAQS compliance must be made with FRMs or FEMs. As of August 2009, 20 automated FRMs and no FEMs had been approved for CO (<http://www.epa.gov/ttn/amt/criteria.html>).

All EPA FRMs for CO operate on the principle of nondispersive infrared (NDIR) detection and can include the gas filter correlation (GFC) methodology. NDIR is an automated and continuous method based on the specific absorption of infrared radiation by the CO molecule. Most commercially available analyzers incorporate a gas filter to minimize interferences from other gases and operate near atmospheric pressure. NDIR is based on the physics of CO's characteristic infrared

absorption near 4.63 μm . NDIR methods have several practical advantages over other techniques for CO detection in that they are not sensitive to flow rate changes, require no wet chemicals, are reasonably independent of ambient air temperature changes, are sensitive over wide concentration ranges, and have fast response times. An extensive and comprehensive review of NDIR, GFC, and alternative, non-FRM techniques for CO detection, including tunable diode laser spectroscopy, gas chromatography, mercury liberation, and resonance fluorescence, was made for the 2000 CO AQCD (U.S. EPA, 2000, [000907](#)), and the reader is directed there for additional information. The description here is limited to a brief outline of the FRM NDIR and GFC techniques.

GFC spectroscopy analyzers are used most frequently now in documenting compliance with ambient air standards. A GFC monitor has all of the advantages of an NDIR instrument and the additional advantages of smaller size, no interference from CO_2 , and very small interference from water vapor. During operation, air flows continuously through a sample cell. Radiation from the infrared source is directed by optical transfer elements through two main optical subsystems: (1) the rotating gas filter; and (2) the optical multipass (sample) cell. The beam exits the sample cell through an interference filter, which limits the spectral passband to a few of the strongest CO absorption lines. Detection of the transmitted radiation occurs at the infrared detector. The gas correlation cell is constructed with two compartments, one filled with 0.5 atm CO, and a second with pure nitrogen gas (N_2). Radiation transmitted through the CO is completely attenuated at the wavelengths where CO absorbs strongly. The radiation transmitted through the N_2 is reduced by coating the exit window of the cell with a neutral attenuator so that the amounts of radiation transmitted by the two cells are made approximately equal in the passband that reaches the detector. In operation, radiation passes alternately through the two cells as they are rotated to establish a signal modulation frequency. If CO is present in the sample, the radiation transmitted through the CO is not appreciably changed, whereas that through the N_2 cell is changed. This imbalance is linearly related to CO concentrations in ambient air.

Specifications for CO monitoring are designed to help states demonstrate whether they have met compliance criteria; operational parameters required under 40 CFR 53 are provided in Table 3-2. Given the 1-h level of the NAAQS of 35 ppm and the 8-h level of the NAAQS of 9 ppm, a 1.0 ppm limit of detection (LOD) is sufficient for demonstration of compliance, where the LOD is set at three times an instrument's noise level when analyzing a zero air sample to ensure that reported signals are in response to actual ambient CO concentrations. However, with ambient CO levels now routinely at or below 1 ppm, there is greater uncertainty in the monitoring data because a large percentage is below the LOD. For this reason, a new generation of ambient CO monitors has been designed for measurements below 0.5 ppm, with $\text{LOD} = 0.04$ ppm. Additionally, CO measurements at concentrations below 0.5 ppm are needed to support additional objectives, such as validating the inputs to CTMs, improving estimates of low-concentration CO exposure, and assessing differences between CO levels in urban and rural areas, because background CO concentrations are on the order of 0.1 ppm. Effective LOD is influenced by instrumental noise and drift and by the amount of water vapor in the air. Recent improvements in the instruments' optical components and dehumidification of the air stream help to reduce the amount of noise and drift in the CO measurements. Newer GFC instruments have been designed for automatic zeroing to minimize drift (U.S. EPA, 2000, [000907](#)).

Table 3-2. Performance specifications for analytical detection of CO, based on 40 CFR Part 53.

Parameter	Specification
Range	0-50 ppm
Noise	0.5 ppm
LOD	1.0 ppm
Interference equivalent	
Each interfering substance	±1.0 ppm
Total interfering substances	1.5 ppm
Zero drift	
12 h	±1.0 ppm
24 h	±1.0 ppm
Span drift, 24 h	
20% of upper range limit	±10.0%
80% of upper range limit	±2.5%
Lag time	10 min
Rise time	5 min
Fall time	5 min
Precision	
20% of upper range limit	0.5 ppm
80% of upper range limit	0.5 ppm

Currently, 24 models of CO monitors are in use; the models are listed in Annex A, Table A-1. Among them, 20 are older NDIR instruments listed to have an LOD of 0.5 ppm, and 4 are GFC instruments listed to have an LOD of 0.04 ppm. States do not routinely report the operational LOD, precision, and accuracy of the monitors to EPA's Air Quality System (AQS). When the monitored value is below the LOD, some states report the raw monitored data, while others report the concentration as 50% of the LOD (0.25 ppm for high-LOD instruments and 0.02 ppm for low-LOD instruments) when reported data are below the LOD. Among several of the older instruments still in use (Federal Reference Method codes 008, 012, 018, 033, 041, 050, 051, and 054), performance testing has shown effective LODs of 0.62-1.05 ppm, with 24-h drift ranging from 0.044-0.25 ppm and precision ranging from 0.022-0.067 ppm at 20% of the upper range limit of the instrument (Michie et al., 1983, [194043](#)). Among newer GFC instruments, manufacturer-declared LODs range from 0.02-0.04 ppm, with 24-h zero drift varying between 0.5% within 1 ppm and 0.1 ppm and precision varying from 0.5% to 0.1 ppm.

Comparison of older and newer monitors with LOD = 0.5 ppm and 0.04 ppm, respectively, calls attention to several data quality issues with the older monitors; Figure 3-9 illustrates this point with data from two co-located monitors with LODs of 0.5 ppm and 0.04 ppm, in Charlotte, NC. First, the data appearing below the LOD of 0.5 ppm for the older monitor comprise 58% of the data obtained by that monitor. In contrast, no data from the 0.04 ppm LOD monitor are reported below 0.04 ppm. Below 0.5 ppm, observations obtained with the older monitor are on average more than five times higher than those from the newer monitor. Second, the data from the older monitor are reported in units of 0.1 ppm, as seen in the lower resolution of the data with respect to the x-axis. Last, it is possible from the data that the older monitor exhibits some upward drift, since newer models have automatic zeroing functions. Above 0.5 ppm, the slope of the scatterplot is 0.95, suggesting that readings from the older monitor are on average 5% higher than those from the newer monitor. The median data are 0.4 ppm for the older monitor and 0.24 ppm for the newer monitor. However the mean from the older monitor is 0.5 ppm, in contrast with 0.330 ppm for the newer monitor. The 99th percentile is 1.8 ppm for the older monitor, in contrast with the newer monitor, whose 99th percentile level is 1.485 ppm.

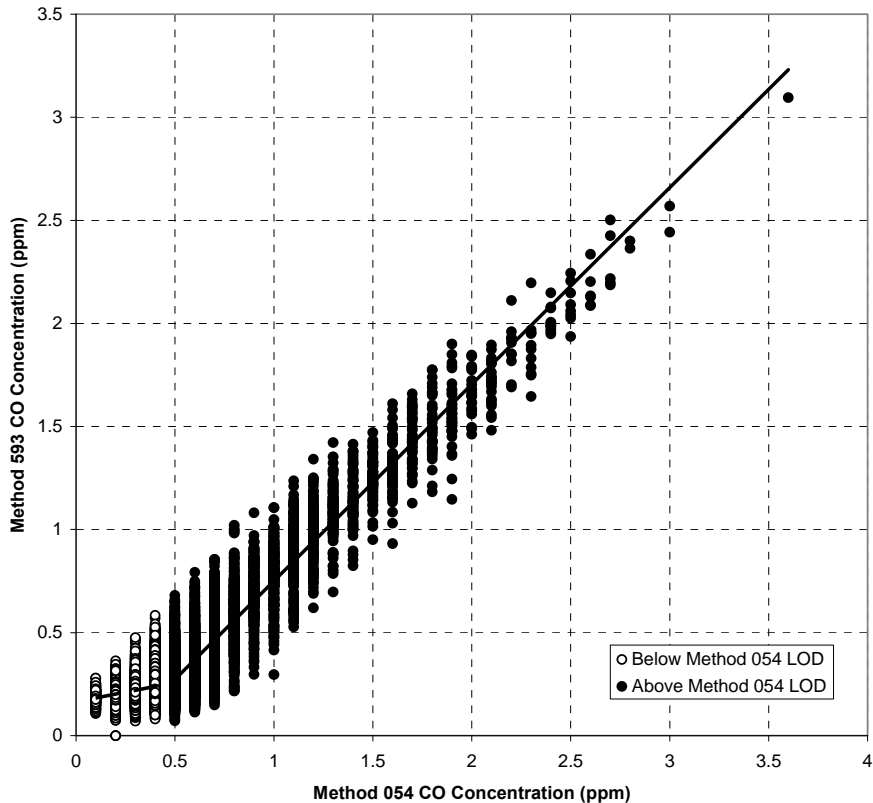


Figure 3-9. Scatterplot comparing data from co-located monitors in Charlotte, NC. Data from Method 054 are from an older model (Thermo Electron Model 48C, Waltham, MA) with LOD = 0.5 ppm, while data from Method 593 are from a newer instrument (Teledyne API Model 300EU, San Diego, CA) with LOD = 0.04 ppm. Above the Method 054 LOD, the methods vary linearly as: $[\text{Method 593}] = 0.95[\text{Method 054}] - 0.20$ ($R^2 = 0.88$, $n = 6990$); below the Method 054 LOD, the regression changes to $[\text{Method 593}] = 0.19[\text{Method 054}] + 0.16$ ($R^2 = 0.07$, $n = 9856$).

3.4.2. Ambient Sampling Network Design

3.4.2.1. Monitor Siting Requirements

Minimum monitoring requirements for CO were revoked in the 2006 revisions to ambient monitoring requirements (71 FR 61236, October 17, 2006). This action was made to allow for reductions in measurements of CO and some other pollutants (SO₂, NO₂, and Pb) where measured levels were well below the applicable NAAQS and air quality problems were not expected. CO monitoring activities have been maintained at some State and Local Air Monitoring Stations (SLAMS), and these measurements of CO using FRM are required to continue until discontinuation is approved by the EPA Regional Administrator. CO monitors are typically sited at the following spatial scales (40 CFR Part 58 Appendix D):

- **Microscale:** Data represent concentrations within a 100 m radius of the monitor. For CO, microscale monitors are sited 2-10 m from a roadway. Measurements are intended to represent the near-road or street canyon environment.

- Middle scale: Data represent concentrations averaged over areas defined by 100-500 m radii. Measurements are intended to represent several city blocks.
- Neighborhood scale: Data represent concentrations averaged over areas defined by 0.5-4.0 km radii. Measurements are intended to represent extended portions of a city.

In 2007, there were 376 CO monitors reporting values to the EPA Air Quality System (AQS) database. Where CO monitoring is ongoing, 40 CFR Part 58 requires at least one CO monitor to capture maximum levels in a given region. This requirement is met with a monitor situated at the CFR-defined microscale distance from the side of a roadway for CO. Microscale monitor locations also have sample inlets mounted at 3 ± 0.5 m above ground level, unlike the monitors sampling for larger scales, whose inlet heights can vary between 2 and 15 m. For the CFR-defined neighborhood scale monitoring, the minimum monitor distance from a major roadway is directly related to the average daily traffic counts on that roadway to ensure that measurements are not substantially influenced by any one roadway. For example, the minimum distance of a neighborhood scale CO monitor from a roadway with an average daily traffic count of 15,000 vehicles per day is 25 m, while the minimum distance is 135 m for a roadway with an average daily traffic count of 50,000 vehicles per day. Occasionally, CO monitors are sited at urban (covering areas of 4-50 km) or regional (covering areas of tens to hundreds of km) scale. More detail on siting requirements can be found in 40 CFR Part 58 Appendices D and E.

In addition to monitoring for determining compliance with the NAAQS, EPA is currently in the process of implementing plans for a new network of multipollutant stations called National Core (NCore) that is intended to meet multiple monitoring objectives. A subset of the SLAMS network, NCore stations are intended to address integrated air quality management needs to support long-term trends analysis, model evaluation, health and ecosystem studies, as well as the more traditional objectives of NAAQS compliance and Air Quality Index reporting. The complete NCore network, required to be fully implemented by January 1, 2011, will consist of approximately 60 urban and 20 rural stations and will include some existing SLAMS sites that have been modified for the additional measurements. Each state will contain at least one NCore station, and 46 of the states plus Washington, DC, will have at least one urban station. CO will be measured using 0.04 ppm LOD monitors at all sites, as will SO₂, NO, and NO_y¹; surface meteorology will also be measured at NCore sites. The advantage to the NCore strategy is that time-resolved, simultaneous measurements of multiple pollutants will be obtained at each site. The disadvantage is that the NCore network will be sparse, and so spatial variability will be difficult to ascertain from the data obtained.

3.4.2.2. Spatial and Temporal Coverage

Figure 3-10 depicts the distribution of the 376 regulatory CO monitors operating in the U.S. in 2007. Data from 291 of the 376 CO monitors operating year-round at 290 sites in the years 2005-2007 met the data completeness criteria for inclusion in the multiyear ambient data analyses for this assessment. Completeness criteria require that data be collected for 75% of the hours in a day, 75% of the days in a quarter, and 3 complete quarters for all 3 yr; criteria for Region 10 were relaxed to 2 complete quarters because it contains Alaska. The greatest density of monitors is in the CSAs for Los Angeles, and San Francisco, CA; and along the Mid-Atlantic seaboard. Monitors are also located in regions where biomass burning is more prevalent, such as Anchorage, AK, but not all of these monitors report values from all seasons of all years. The number of monitors per sampling scale is provided in Table 3-3, and locations of monitors with nearby roadway types and traffic counts are provided in Annex A, Tables A-2 through A-7, for each monitoring scale. Twenty-four percent of the monitors meeting completeness criteria are categorized as “Null”, meaning that no scale has been identified for those monitors. Furthermore, given the overlap between scales regarding the type of road at which the monitor is sited, it is possible that scale has been misclassified for some of the monitors.

¹ NCore sites must measure, at a minimum, PM_{2.5} particle mass using continuous and integrated/filter-based samplers, speciated PM_{2.5}, PM_{10-2.5} particle mass, speciated PM_{10-2.5}, O₃, SO₂, CO, NO/NO_y, wind speed, wind direction, relative humidity, and ambient temperature.

Table 3-3. Counts of CO monitors by sampling scale meeting 75% completeness criteria for use in the U.S. during 2005-2007.

Monitoring Scale	Count
Microscale	57
Middle Scale	31
Neighborhood Scale	119
Urban Scale	11
Regional Scale	2
Null	71

Figure 3-10 also shows the locations of the newer 0.04 ppm LOD CO monitors throughout the U.S in 2007, indicated by blue and purple triangles. The newer monitors included in the analysis are located in: Baton Rouge, LA; Boston, MA; Charlotte, NC; Dallas, TX; Decatur, GA; Houston, TX; Portland, OR; Presque Isle, ME; San Jose, CA; and rural locations within Georgia and South Carolina. Other 0.04 ppm LOD monitors not meeting completeness criteria for the 2005-2007 analysis were located in: Beltsville, MD; Cedar Rapids, IA; Davenport, IA; Des Moines, IA; Nederland, TX; Northbrook, IL; Plant City, FL; Seattle, WA; Thomaston, CT; Tulsa, OK; Westport, CT; and rural locations in Maryland and Wisconsin. A listing of 0.04 ppm and 0.5 ppm LOD monitors meeting completeness criteria by state for 2005-2007 is provided in Annex A, Table A-8.

Eleven metropolitan regions were chosen for closer investigation of monitor siting based on their relevance to the health studies assessed in subsequent chapters of this ISA and to demonstrate specific points about geospatial distributions of CO emissions and concentrations. These regions were: Anchorage, AK; Atlanta, GA; Boston, MA; Denver, CO; Houston, TX; Los Angeles, CA; New York City, NY; Phoenix, AZ; Pittsburgh, PA; Seattle, WA; and St. Louis, MO. Core-Based Statistical Areas (CBSAs) and Combined Statistical Areas (CSAs), as defined by the U.S. Census Bureau (<http://www.census.gov/>), were used to determine which counties, and hence, which monitors, to include for each metropolitan region.¹ As an example, Figure 3-11 through Figure 3-14 display CO monitor density with respect to population density (for total population and elderly adults aged 65 and over) for the Denver and Los Angeles CSAs (Annex A, Figures A-7 through A-22 show analogous plots for the other nine metropolitan regions). Figure 3-18 and Figure 3-21 and additional figures in Annex A show the locations of CO monitors for the 11 CSAs/CBSAs in relation to major roadways, including interstate highways, U.S. highways, state highways, and other major roadways required for traffic network connectivity. In the examples shown for Denver and Los Angeles, the monitors were typically located near high population density neighborhoods within the CSA. The Los Angeles CSA monitors appear to be distributed fairly evenly across the city of Los Angeles, while the Denver CSA had three monitors in the city center and two in the suburbs of the Denver CSA. Regional background sites were not included on the maps unless they lay within the CSA/CBSA.

¹ A CBSA represents a county-based region surrounding an urban center of at least 10,000 people determined using 2000 census data and replaces the older Metropolitan Statistical Area (MSA) definition from 1990. The CSA represents an aggregate of adjacent CBSAs tied by specific commuting behaviors. The broader CSA definition was used when selecting monitors for the cities listed above with the exception of Anchorage and Phoenix, which are not contained within a CSA. Therefore, the smaller CBSA definition was used for these metropolitan areas.

CO Monitor Locations in United States in 2007

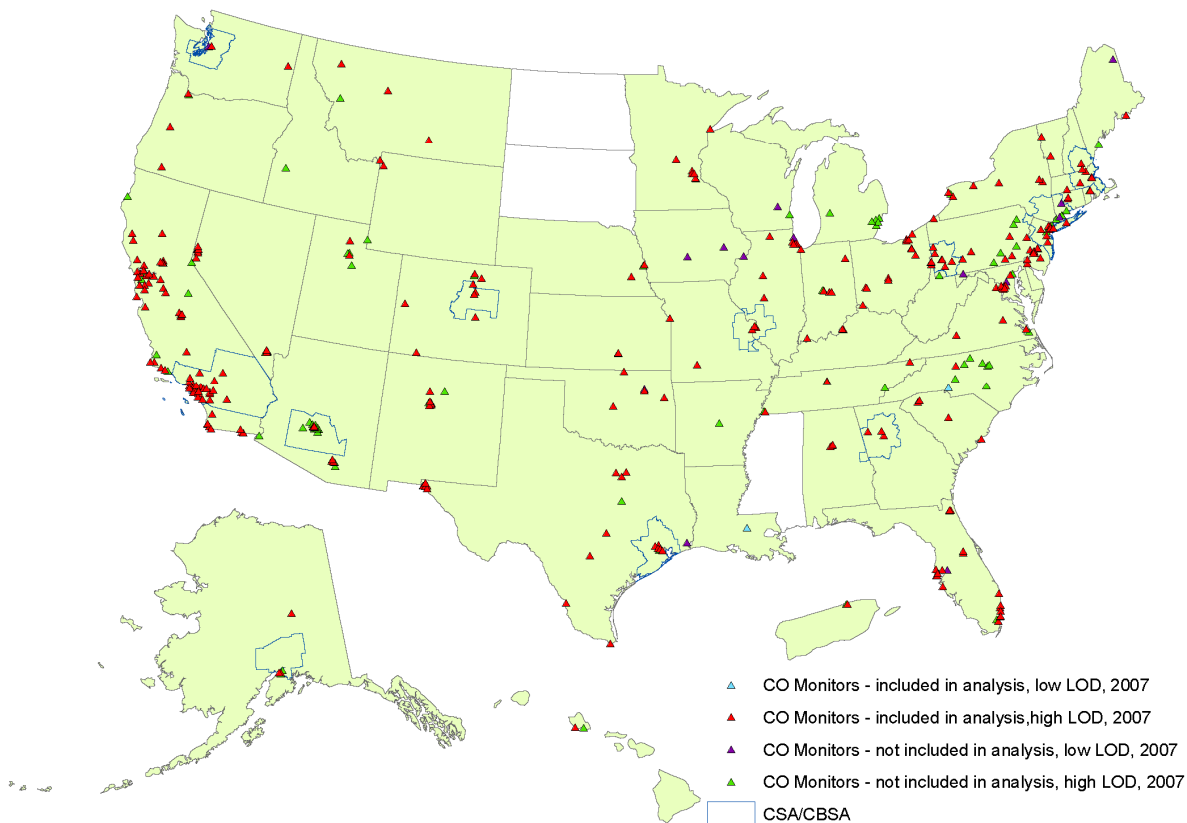


Figure 3-10. Map of CO monitor locations in the U.S. in 2007. Locations are indicated with triangles: blue and red triangles show locations of the sites used in data analysis for this assessment; purple and green triangles are at locations with monitors which did not meet the data completeness requirements for analysis; blue lines mark the boundaries of the 11 CSAs/CBSAs used in the data analysis for this assessment.

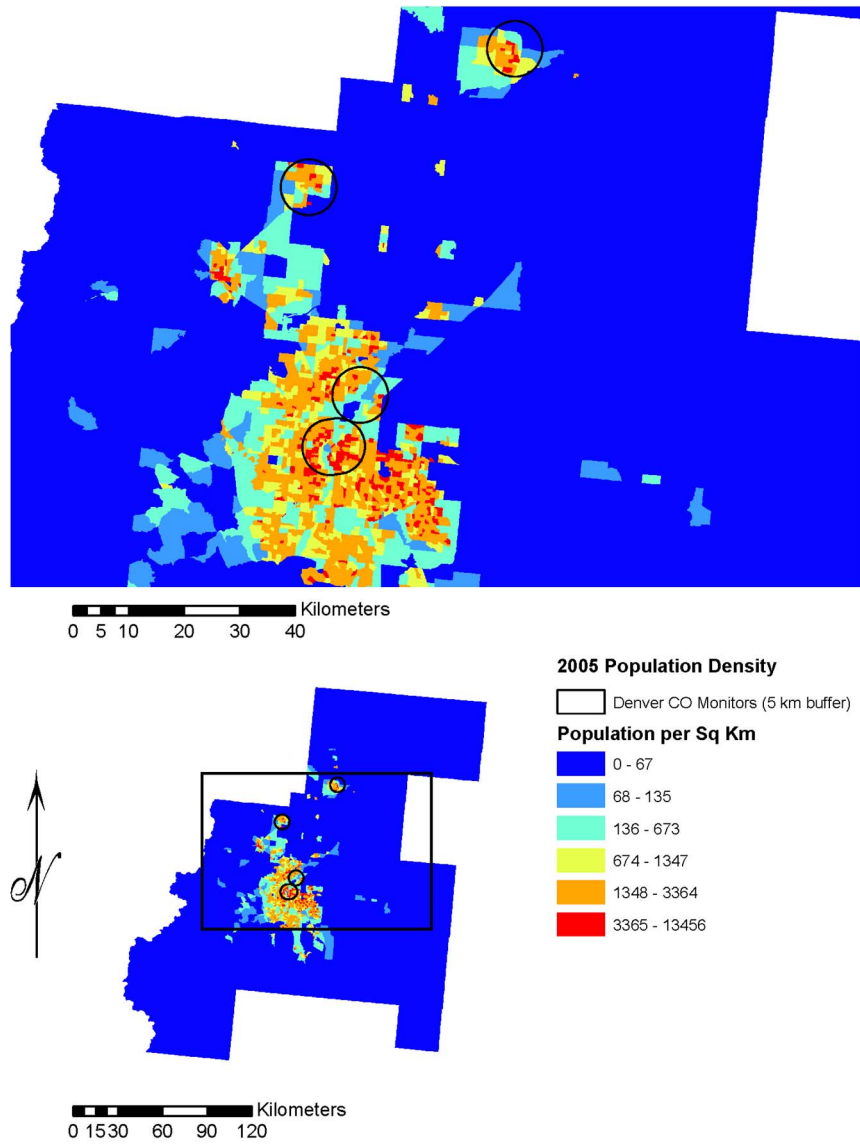


Figure 3-11. Map of CO monitor locations with respect to population density in the Denver, CO CSA, total population. The circles indicate 5 km buffers around the monitors.

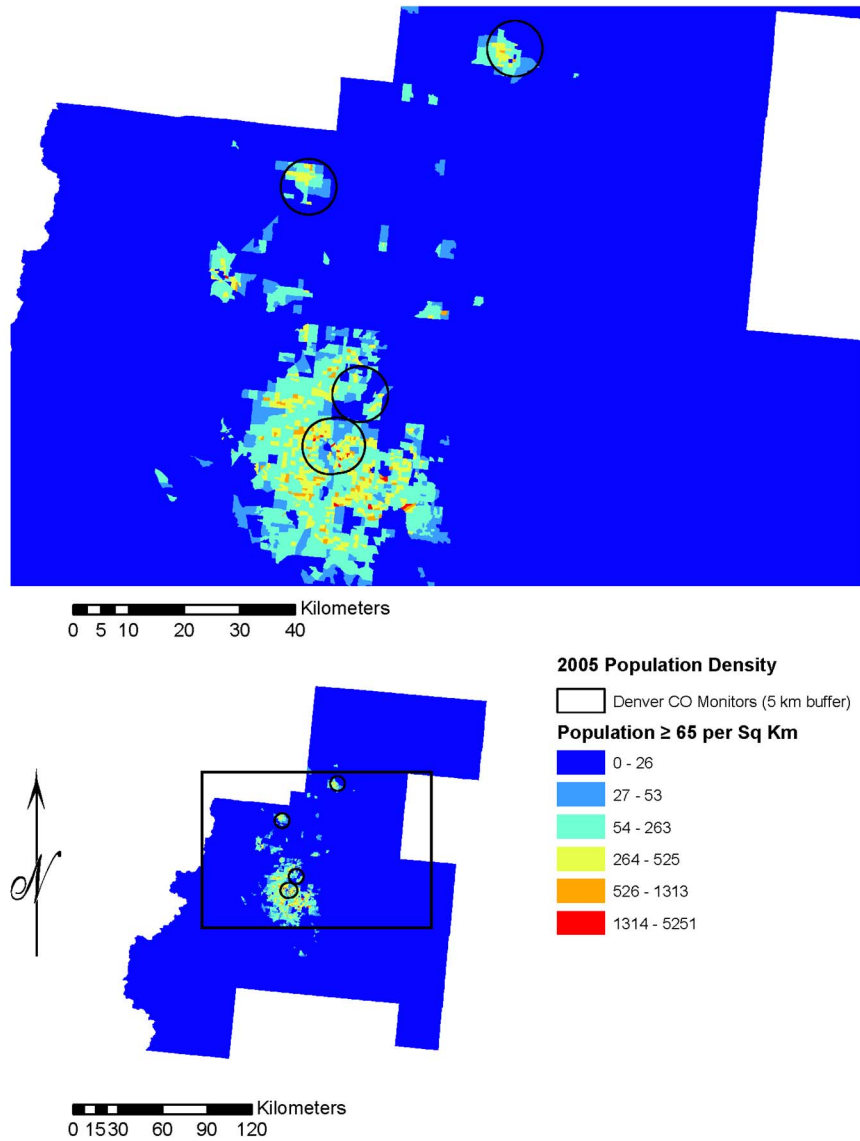


Figure 3-12. Map of CO monitor locations with respect to population density in the Denver, CO CSA, age 65 and older. The circles indicate 5 km buffers around the monitors.

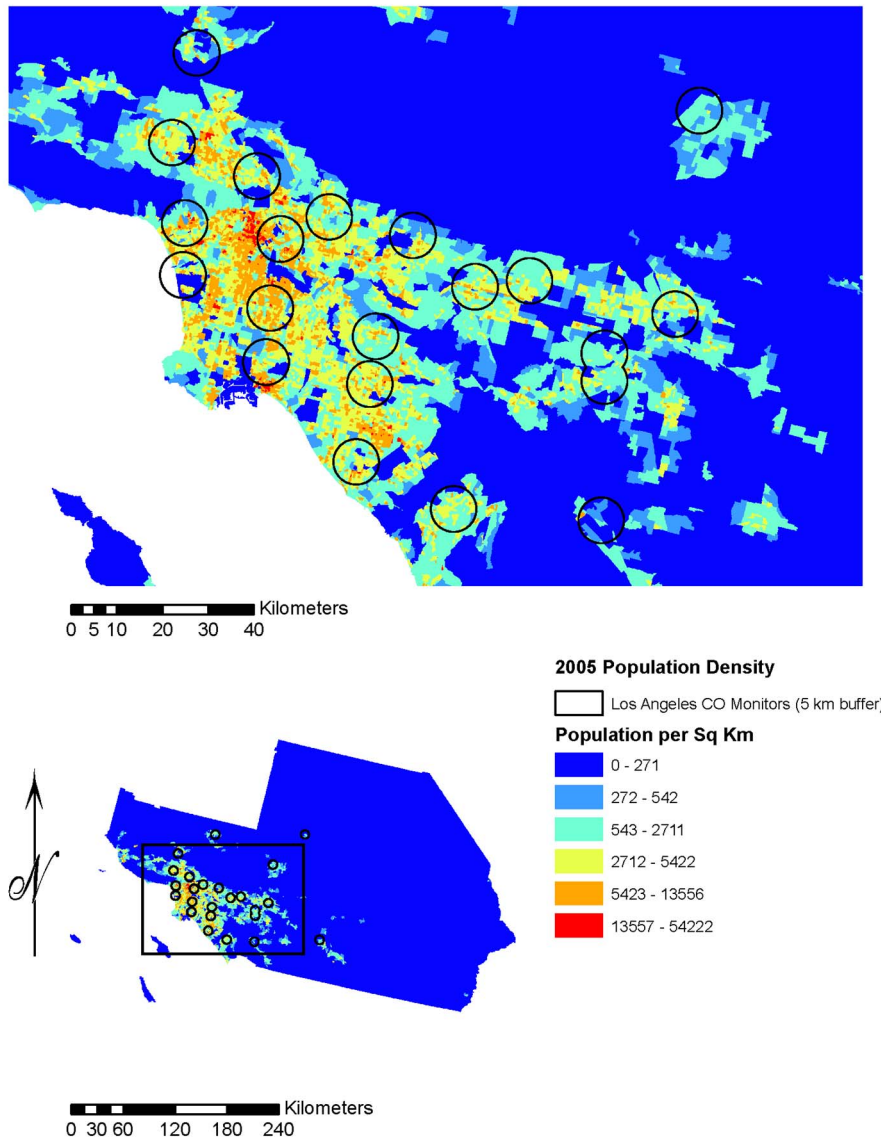


Figure 3-13. Map of CO monitor locations with respect to population density in the Los Angeles, CA CSA, total population. The circles indicate 5 km buffers around the monitors.

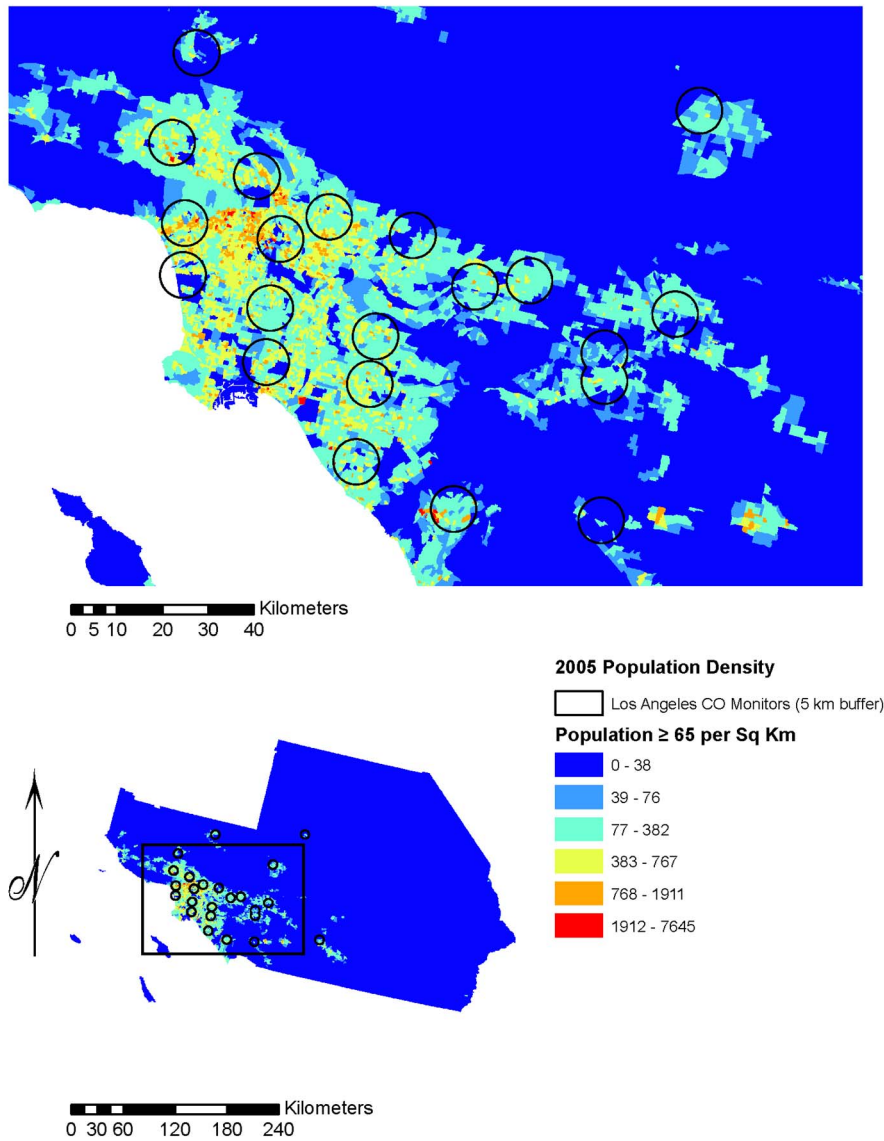


Figure 3-14. Map of CO monitor locations with respect to population density in the Los Angeles, CA CSA, age 65 and older. The circles indicate 5 km buffers around the monitors.

Ambient monitors for CO and other criteria pollutants are located to monitor compliance rather than population exposures. However, CO monitors submitting data to the AQS are often used for exposure assessment. For this reason, data are presented here to assess population density in the vicinity of CO monitors. Table 3-4 and Table 3-5 show the population density around CO monitors for the total population and for elderly adults aged 65 and over for each CSA/CBSA. The percentage of population within specific radii of the monitors for each city was, for the most part, similar between the total and elderly populations. In the cases of Anchorage, Denver, Phoenix, and St. Louis however, the percentage of the elderly population within given radii of the monitors was considerably different compared with the total population. Between-city disparities in population density were larger. Los Angeles, with 85%, and Denver, with 68%, had the largest proportion of the total population within 15 km of a monitor. Seattle, with 18%, had the lowest population coverage in large part because ambient CO concentrations there require only a single CO monitor. For the elderly population, Los Angeles, at 83%, Anchorage, at 73%, and Denver, at 70%, had the greatest population coverage within 15 km of a monitor; Seattle, at 18%, again had the lowest coverage. Proximity to monitoring stations is considered further in Sections 3.5 and 3.6 regarding spatial variability within cities. In combination, these data illustrate that population coverage varies by monitor and across cities.

Table 3-4. Proximity to CO monitors for the total population by city.

Region	Total CSA/ CBSA N	≤ 1 km		≤ 5 km		≤ 10 km		≤ 15 km	
		N	%	N	%	N	%	N	%
Anchorage, AK	352,225	5,391	1.53	131,608	37.36	212,834	60.43	239,842	68.09
Atlanta, GA	5,316,742	5,480	0.10	149,772	2.82	672,701	12.65	1,444,986	27.18
Boston, MA	7,502,707	95,732	1.28	1,180,054	15.73	2,432,846	32.43	3,418,353	45.56
Denver, CO	2,952,039	26,096	0.88	497,598	16.86	1,091,444	36.97	1,720,360	58.28
Houston, TX	5,503,320	29,068	0.53	599,796	10.90	1,669,117	30.33	2,506,830	45.55
Los Angeles, CA	17,655,319	202,340	1.15	4,064,309	23.02	11,928,427	67.56	15,074,972	85.38
New York, NY	22,050,940	201,350	0.91	3,711,369	16.83	8,385,801	38.03	12,454,837	56.48
Phoenix, AZ	3,818,147	47,478	1.24	503,433	13.19	1,033,102	27.06	1,581,887	41.43
Pittsburgh, PA	2,515,383	29,136	1.16	369,965	14.71	895,252	35.59	1,359,596	54.05
Seattle, WA	3,962,434	4,814	0.12	94,649	2.39	279,976	7.07	699,490	17.65
St. Louis, MO	2,869,955	16,638	0.58	255,499	8.90	886,412	30.89	1,303,636	45.42

Table 3-5. Proximity to CO monitors for adults aged 65 and older by city.

Region	Total CSA/ CBSA	≤ 1 km		≤ 5 km		≤ 10 km		≤ 15 km	
	N	N	%	N	%	N	%	N	%
Anchorage, AK	17,742	361	2.03	8,986	50.65	12,038	67.85	12,990	73.22
Atlanta, GA	362,201	423	0.12	12,758	3.52	54,148	14.95	111,232	30.71
Boston, MA	945,790	8,272	0.87	131,198	13.87	297,392	31.44	430,502	45.52
Denver, CO	232,974	2,541	1.09	42,760	18.35	102,783	44.12	163,682	70.26
Houston, TX	377,586	1,703	0.45	42,312	11.21	130,567	34.58	182,049	48.21
Los Angeles, CA	1,626,663	17,974	1.10	380,079	23.37	1,069,188	65.73	1,355,461	83.33
New York, NY	2,710,675	29,534	1.09	427,601	15.77	940,121	34.68	1,429,215	52.73
Phoenix, AZ	388,150	2,877	0.74	35,839	9.23	77,244	19.90	125,300	32.28
Pittsburgh, PA	449,544	5,383	1.20	66,967	14.90	166,440	37.02	255,220	56.77
Seattle, WA	390,372	556	0.14	12,142	3.11	31,036	7.95	69,858	17.90
St. Louis, MO	358,747	3,203	0.89	42,890	11.96	127,274	35.48	184,491	51.43

3.5. Environmental Concentrations

3.5.1. Spatial Variability

3.5.1.1. National Scale

The current NAAQS designates that the level of the NAAQS is not to be exceeded more than once per year at a given monitoring site. Figure 3-15 and Figure 3-16 show the second-highest 1-h and second-highest 8-h county-average CO concentrations, respectively, over the U.S. along with estimates of the fraction of the U.S. total population exposed to those concentrations. Although 93% of the U.S. counties are not represented in AQS reporting, based on their population densities and proximity to sources, those counties are not expected to have higher concentrations than the ones analyzed here in the absence of extreme events such as wildfires. Continuous hourly averages are reported from U.S. monitoring stations. One-hour (1-h) and 8-h CO data were available for 243 counties and autonomous cities or municipalities (e.g., Anchorage, AK, Washington, DC) where CO monitors met the 75% data completeness criteria used in this analysis for the years 2005-2007. In 2007, no monitored location reported a second-highest 1-h CO concentration above 35 ppm (Figure 3-15). Moreover, only two monitored locations, one in Weber County, UT and the other in Jefferson County, AL (including Birmingham, AL), reported second-highest 1-h CO concentrations between 15.1 and 35.0 ppm. Figure 3-16 shows that only 5 counties reported second-highest 8-h CO concentrations above 5.0 ppm: Jefferson County, AL; Imperial County, CA; Weber County, UT; Philadelphia County, PA; and Anchorage Municipality, AK.

Carbon Monoxide – Second Highest 1-hour Average, 2007

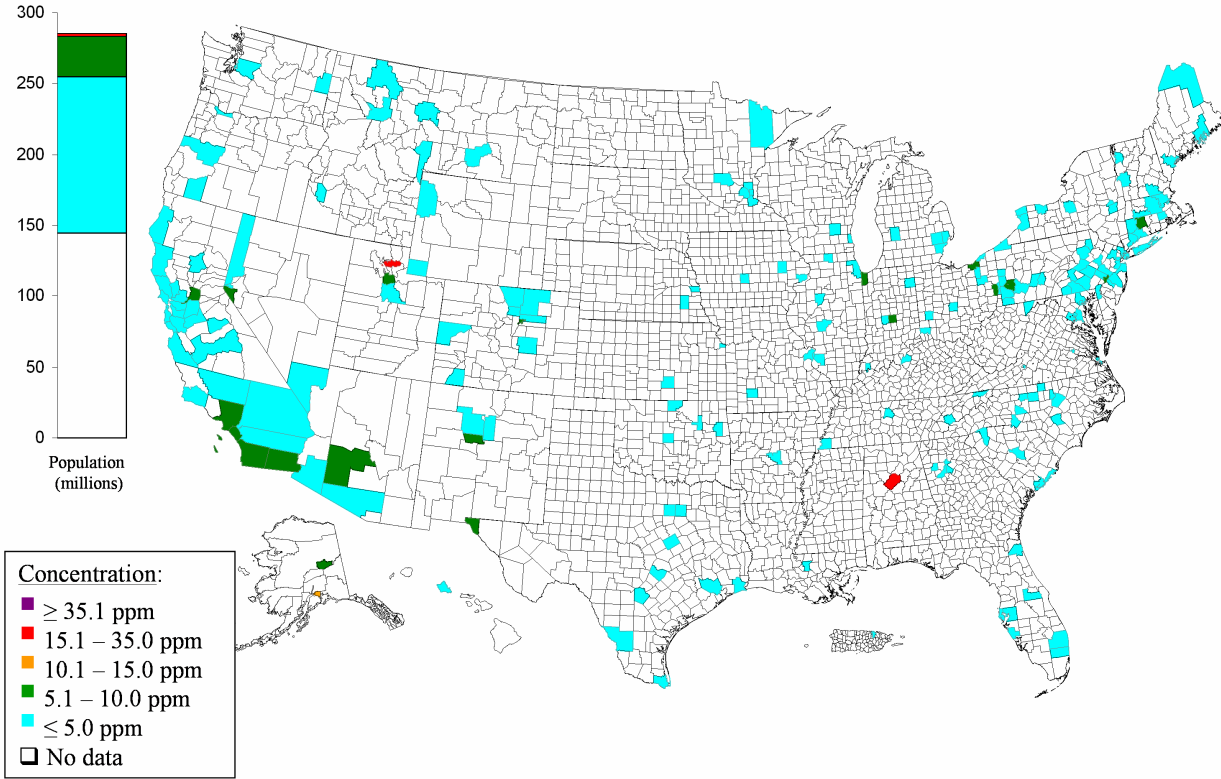


Figure 3-15. County-level map of second-highest 1-h avg CO concentrations in the U.S. in 2007. The bar on the left shows the total U.S. population living in counties with CO concentrations in the range indicated. Note that approximately 150 million people live in counties with no CO monitors.

Carbon Monoxide – Second Highest 8-hour Average, 2007

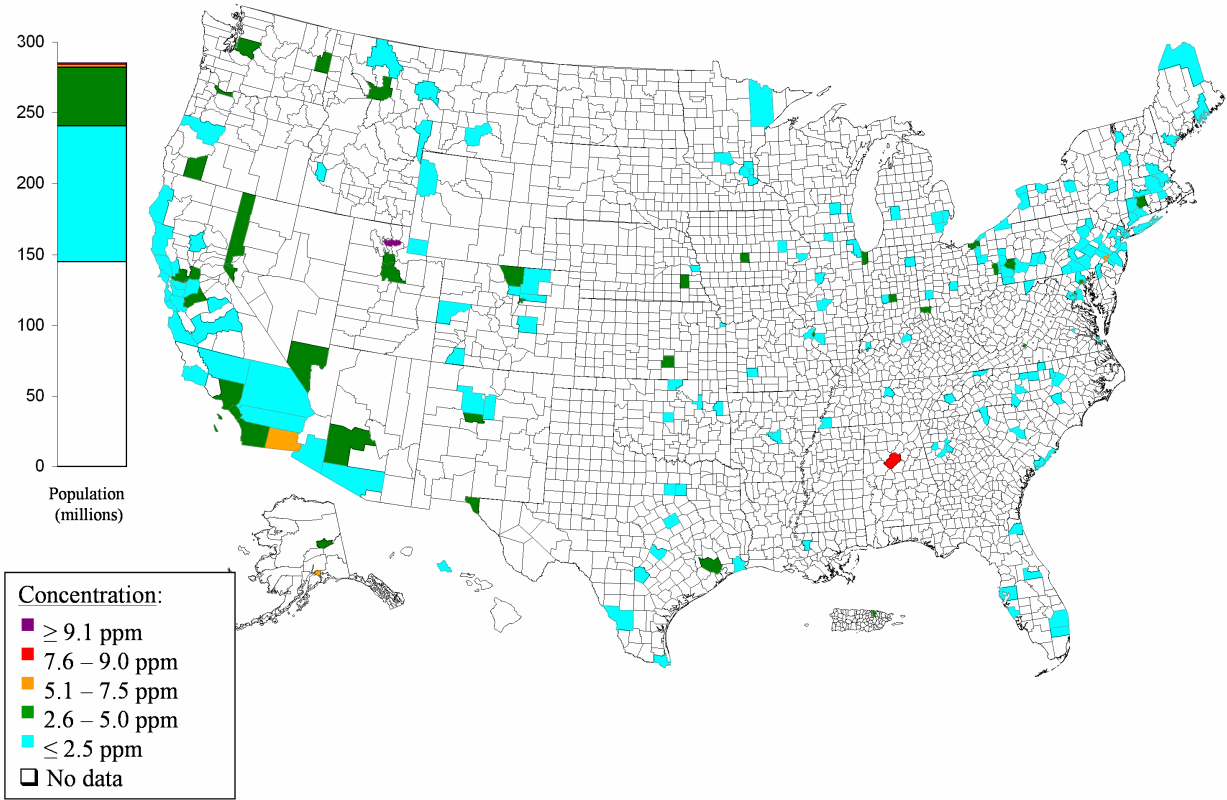


Figure 3-16. County-level map of second-highest 8-h avg CO concentrations in the U.S. in 2007. The bar on the left shows the total U.S. population living in counties with CO concentrations in the range indicated. Note that approximately 150 million people live in counties with no CO monitors.

Table 3-6. Distribution of 1-h avg CO concentration (ppm) derived from AQS data.

	N	Mean	Min	Percentiles									Max
				1	5	10	25	50	75	90	95	99	
NATIONWIDE STATISTICS (N = NUMBER OF OBSERVATIONS)													
2005-2007	7,180,700	0.5	0.0	0.0	0.0	0.1	0.2	0.4	0.6	0.9	1.2	2.1	39.0
2005	2,391,962	0.5	0.0	0.0	0.0	0.1	0.2	0.4	0.6	1.0	1.3	2.3	22.3
2006	2,402,153	0.5	0.0	0.0	0.0	0.1	0.2	0.4	0.6	0.9	1.2	2.1	35.3
2007	2,386,585	0.4	0.0	0.0	0.0	0.1	0.2	0.3	0.5	0.8	1.1	1.9	39.0
Winter (December - February)	1,752,340	0.6	0.0	0.0	0.0	0.1	0.3	0.4	0.7	1.2	1.6	2.7	20.0
Spring (March - May)	1,826,167	0.4	0.0	0.0	0.0	0.1	0.2	0.3	0.5	0.8	1.0	1.7	35.3
Summer (June - August)	1,811,082	0.4	0.0	0.0	0.0	0.0	0.2	0.3	0.5	0.7	0.9	1.5	39.0
Fall (September - November)	1,791,111	0.5	0.0	0.0	0.0	0.1	0.2	0.4	0.6	1.0	1.3	2.2	24.1
NATIONWIDE STATISTICS, POOLED BY SITE (N = NUMBER OF SITES)													
2005-2007	285	0.5	0.0	0.0	0.1	0.2	0.3	0.4	0.6	0.7	0.8	1.0	1.5
2005	285	0.5	0.0	0.0	0.1	0.2	0.4	0.5	0.6	0.8	0.9	1.3	1.6
2006	285	0.5	0.0	0.0	0.1	0.2	0.3	0.4	0.6	0.7	0.8	1.2	1.4
2007	285	0.4	0.0	0.0	0.1	0.2	0.3	0.4	0.5	0.7	0.7	1.1	1.5
Winter (December - February)	285	0.6	0.0	0.0	0.2	0.2	0.4	0.5	0.7	0.9	1.1	1.5	1.6
Spring (March - May)	285	0.4	0.0	0.0	0.1	0.2	0.3	0.4	0.5	0.7	0.7	1.0	1.6
Summer (June - August)	285	0.4	0.0	0.0	0.1	0.2	0.3	0.4	0.5	0.6	0.7	1.1	1.5
Fall (September - November)	285	0.5	0.0	0.0	0.1	0.2	0.4	0.4	0.6	0.8	0.9	1.1	1.5
STATISTICS FOR INDIVIDUAL CSAS/CBSAS (2005-2007) (N = NUMBER OF OBSERVATIONS)													
Anchorage ^a	25,672	1.1	0.0	0.1	0.2	0.3	0.5	0.7	1.3	2.3	3.1	5.0	13.1
Atlanta	76,683	0.5	0.0	0.0	0.2	0.2	0.3	0.4	0.6	0.8	1.1	1.6	10.8
Boston	171,975	0.4	0.0	0.0	0.0	0.1	0.2	0.4	0.5	0.7	0.9	1.4	10.0
Denver	129,038	0.5	0.0	0.0	0.1	0.2	0.3	0.4	0.6	1.0	1.3	2.2	9.3
Houston	123,925	0.3	0.0	0.0	0.0	0.0	0.2	0.3	0.4	0.6	0.8	1.4	4.6
Los Angeles	592,960	0.5	0.0	0.0	0.0	0.1	0.2	0.3	0.6	1.0	1.4	2.3	8.4
New York	226,673	0.5	0.0	0.0	0.1	0.1	0.3	0.5	0.6	0.9	1.1	1.6	5.8
Phoenix	127,477	0.8	0.0	0.0	0.1	0.2	0.3	0.5	1.0	1.9	2.5	3.6	7.8
Pittsburgh	179,758	0.3	0.0	0.0	0.0	0.0	0.1	0.2	0.4	0.6	0.8	1.2	6.7
Seattle	25,818	0.8	0.0	0.1	0.2	0.3	0.4	0.6	0.9	1.3	1.6	2.5	5.9
St. Louis	77,142	0.4	0.0	0.0	0.1	0.2	0.3	0.4	0.5	0.7	0.9	1.4	5.7
Not in the 11 cities	5,449,251	0.5	0.0	0.0	0.0	0.1	0.2	0.4	0.6	0.9	1.2	2.1	39.0

^aCO monitoring is only available for quarters 1 and 4; since monitoring data are not available year-round, Anchorage is not included in the nationwide statistics shown in this table.

Table 3-6 contains the distribution of hourly CO measurements reported to AQS for 2005-2007. All monitoring locations meeting the 75% data completeness criteria have been included in this table. Several monitors in EPA Region 10, including four in Alaska, did not meet the data completeness criteria since CO reporting was only required during the first and fourth quarters of each year at these sites. Anchorage was included in the table, however, for an approximate comparison with the other CSAs and CBSAs reporting year-round measurements to AQS. Anchorage and other partial-year monitors were not, however, included in the national statistics shown in the table. AQS site number 371190041, located in Charlotte, NC, was the only site with co-located monitors both meeting the data completeness criteria and, therefore, the nationwide data in the table was derived from 286 monitors located at 285 sites. In Section 3.5.1.3, the nationwide 1-h avg statistics shown in Table 3-6 (along with the nationwide 24-h avg, 1-h daily max and 8-h daily max statistics) are further divided by monitoring scale (microscale, middle scale, etc.) to address issues relating to the near-road environment.

The nationwide mean, median, and interquartile range for 1-h measurements reported for 2005-2007 were 0.5, 0.4 and 0.4 ppm, respectively, and these statistics did not change by more than 0.1 ppm over the 3-yr period. More than 50% of the data nationwide were below the LOD for the majority of monitors in use. The largest recorded second-highest 1-h concentration, 26.3 ppm, for this period was reported in 2006 in Birmingham, AL (AQS site ID: 010736004). The highest 1-h concentration, 39 ppm, between 2005 and 2007, was reported in Ogden, UT (AQS site ID: 490570006) on August 28, 2007. An annual outdoor barbeque festival held in Ogden on that day resulted in a period of elevated CO concentrations. The seasonally stratified concentrations in Table 3-6 are generally highest in the winter (December-February) and fall (September-November) and decrease on average during the spring (March-May) and summer (June-August).

Nationwide statistics pooled by site are listed in the center rows of Table 3-6 and illustrate the distribution of the site average CO concentrations recorded at the 285 monitoring sites for 2005-2007 (Figure 3-10). The site reporting the highest 3-yr pooled 1-h avg CO concentration, 1.5 ppm, was located in San Juan, Puerto Rico (AQS site ID: 721270003). The 11 individual CSAs/CBSAs discussed earlier are included in the table, none of which reported concentrations above the value of the 1-h NAAQS. Four of the 11 cities (Boston, Houston, Pittsburgh and St. Louis) had 95th percentile 1-h CO concentrations below 1 ppm; the 95th percentile concentrations for the remaining cities were below 3.1 ppm. Lack of year-round monitoring in Anchorage prevented a direct comparison with the other metropolitan regions. However, Anchorage exhibited a 1-h CO distribution shifted higher in concentration when compared to the U.S. average during fall or winter. The 99th percentile 1-h avg concentration in Anchorage was 5.0 ppm; the other selected cities with year-round monitoring had 99th percentile concentrations ranging from 0.9 ppm to 2.5 ppm.

Table 3-7. Distribution of 24-h avg CO concentration (ppm) derived from AQS data.

	N	Mean	Min	Percentiles									Max
				1	5	10	25	50	75	90	95	99	
NATIONWIDE STATISTICS (N = NUMBER OF OBSERVATIONS)													
2005-2007	303,843	0.5	0.0	0.0	0.0	0.1	0.3	0.4	0.6	0.9	1.1	1.7	7.0
2005	101,184	0.5	0.0	0.0	0.0	0.1	0.3	0.4	0.6	0.9	1.1	1.8	5.8
2006	101,652	0.5	0.0	0.0	0.0	0.1	0.3	0.4	0.6	0.9	1.1	1.6	7.0
2007	101,007	0.4	0.0	0.0	0.0	0.1	0.2	0.4	0.5	0.8	1.0	1.6	6.9
Winter (December-February)	74,144	0.6	0.0	0.0	0.1	0.2	0.3	0.5	0.7	1.1	1.3	2.0	7.0
Spring (March - May)	77,317	0.4	0.0	0.0	0.0	0.1	0.2	0.4	0.5	0.7	0.9	1.4	6.4
Summer (June - August)	76,562	0.4	0.0	0.0	0.0	0.1	0.2	0.3	0.5	0.7	0.8	1.3	6.9
Fall (September - November)	75,820	0.5	0.0	0.0	0.0	0.1	0.3	0.4	0.6	0.9	1.1	1.7	5.8
NATIONWIDE STATISTICS, POOLED BY SITE (N = NUMBER OF SITES)													
2005-2007	285	0.5	0.0	0.0	0.1	0.2	0.3	0.4	0.6	0.7	0.8	1.0	1.5
2005	285	0.5	0.0	0.0	0.1	0.2	0.4	0.5	0.6	0.8	0.9	1.3	1.6
2006	285	0.5	0.0	0.0	0.1	0.2	0.3	0.4	0.6	0.7	0.8	1.2	1.4
2007	285	0.4	0.0	0.0	0.1	0.2	0.3	0.4	0.5	0.7	0.7	1.1	1.5
Winter (December - February)	285	0.6	0.0	0.0	0.2	0.2	0.4	0.5	0.7	0.9	1.1	1.5	1.6
Spring (March - May)	285	0.4	0.0	0.0	0.1	0.2	0.3	0.4	0.5	0.7	0.7	1.0	1.6
Summer (June - August)	285	0.4	0.0	0.0	0.1	0.2	0.3	0.4	0.5	0.6	0.7	1.1	1.5
Fall (September - November)	285	0.5	0.0	0.0	0.1	0.2	0.4	0.4	0.6	0.8	0.9	1.1	1.5
STATISTICS FOR INDIVIDUAL CSAS/CBSAS (2005-2007) (N = NUMBER OF OBSERVATIONS)													
Anchorage ^a	1,074	1.1	0.0	0.2	0.2	0.4	0.6	0.9	1.4	1.9	2.4	3.3	4.6
Atlanta	3,229	0.5	0.0	0.1	0.2	0.2	0.3	0.4	0.6	0.8	0.9	1.2	1.6
Boston	7,446	0.4	0.0	0.0	0.1	0.1	0.3	0.4	0.5	0.7	0.8	1.1	2.2
Denver	5,363	0.5	0.0	0.1	0.2	0.2	0.3	0.5	0.6	0.9	1.1	1.5	2.3
Houston	5,188	0.3	0.0	0.0	0.0	0.1	0.2	0.3	0.4	0.5	0.6	0.9	1.9
Los Angeles	25,803	0.5	0.0	0.0	0.1	0.1	0.2	0.4	0.6	1.0	1.2	1.7	3.8
New York	9,513	0.8	0.0	0.0	0.1	0.2	0.4	0.5	0.6	0.8	1.0	1.3	2.5
Phoenix	5,348	0.8	0.0	0.1	0.2	0.3	0.4	0.6	1.1	1.6	1.9	2.5	3.4
Pittsburgh	7,497	0.3	0.0	0.0	0.0	0.0	0.1	0.2	0.4	0.6	0.7	1.0	1.9
Seattle	1,079	0.8	0.1	0.2	0.3	0.4	0.5	0.7	0.9	1.2	1.4	1.8	2.4
St. Louis	3,216	0.4	0.0	0.0	0.1	0.2	0.3	0.4	0.5	0.7	0.8	1.0	1.9
Not in the 11 cities	230,161	0.5	0.0	0.0	0.0	0.1	0.2	0.4	0.6	0.8	1.1	1.6	7.0

^aCO monitoring is only available for quarters 1 and 4; since monitoring data are not available year-round, Anchorage is not included in the nationwide statistics shown in this table.

Table 3-7 contains the distribution of 24-h avg CO concentrations derived from the 1-h concentrations reported to AQS and summarized in Table 3-6. The nationwide mean, median, and interquartile range for 24-h avg values during 2005-2007 were 0.5, 0.4 and 0.3 ppm, respectively. These were similar to those for the 1-h values and showed more than half the data falling below the LOD for the majority of monitors in the field. The maximum 24-h avg concentration in these years, 7 ppm, was reported in Birmingham, AL (AQS site ID: 010736004). The 99th percentile 24-h avg

concentrations ranged from 0.9 ppm to 2.5 ppm in the selected cities with year-round monitoring; Anchorage had a 99th percentile concentration of 3.3 ppm.

Table 3-8. Distribution of 1-h daily max CO concentration (ppm) derived from AQS data.

	N	Mean	Min	Percentiles									Max
				1	5	10	25	50	75	90	95	99	
NATIONWIDE STATISTICS (N = NUMBER OF OBSERVATIONS)													
2005-2007	303,843	0.9	0.0	0.0	0.1	0.3	0.4	0.7	1.2	1.8	2.4	3.8	39.0
2005	101,184	1.0	0.0	0.0	0.2	0.3	0.5	0.8	1.3	2.0	2.6	4.1	22.3
2006	101,652	0.9	0.0	0.0	0.1	0.3	0.4	0.7	1.2	1.9	2.4	3.9	35.3
2007	101,007	0.8	0.0	0.0	0.1	0.2	0.4	0.7	1.1	1.7	2.1	3.4	39.0
Winter (December - February)	74,144	1.2	0.0	0.0	0.2	0.3	0.5	0.9	1.6	2.5	3.1	4.7	20.0
Spring (March - May)	77,317	0.8	0.0	0.0	0.1	0.3	0.4	0.7	1.0	1.6	2.0	3.0	35.3
Summer (June - August)	76,562	0.7	0.0	0.0	0.1	0.2	0.4	0.6	0.9	1.3	1.6	2.5	39.0
Fall (September - November)	75,820	1.0	0.0	0.0	0.2	0.3	0.5	0.8	1.3	2.0	2.5	3.8	24.1
NATIONWIDE STATISTICS, POOLED BY SITE (N = NUMBER OF SITES)													
2005-2007	285	0.9	0.1	0.1	0.3	0.5	0.6	0.8	1.1	1.5	1.7	2.3	3.9
2005	285	1.0	0.1	0.1	0.4	0.5	0.7	0.9	1.2	1.6	2.0	2.5	3.7
2006	285	0.9	0.1	0.1	0.3	0.5	0.6	0.9	1.1	1.6	1.8	2.3	4.8
2007	285	0.8	0.1	0.1	0.3	0.4	0.6	0.8	1.0	1.4	1.6	2.0	3.1
Winter (December - February)	285	1.2	0.0	0.1	0.4	0.6	0.8	1.0	1.5	2.1	2.5	3.4	4.1
Spring (March - May)	285	0.8	0.1	0.1	0.3	0.4	0.6	0.8	1.0	1.3	1.5	2.1	4.0
Summer (June - August)	285	0.7	0.0	0.1	0.2	0.3	0.5	0.6	0.8	1.1	1.3	2.2	3.3
Fall (September - November)	285	1.0	0.1	0.1	0.3	0.5	0.7	0.9	1.2	1.7	2.0	2.4	4.1
STATISTICS FOR INDIVIDUAL CSAS/CBSAS (2005-2007) (N = NUMBER OF OBSERVATIONS)													
Anchorage ^a	1,074	2.6	0.0	0.3	0.6	0.8	1.3	2.2	3.5	5.0	6.1	7.6	13.1
Atlanta	3,229	0.8	0.0	0.2	0.3	0.3	0.4	0.7	1.1	1.4	1.7	2.2	10.8
Boston	7,446	0.7	0.0	0.1	0.2	0.3	0.4	0.6	0.9	1.2	1.6	2.6	10.0
Denver	5,363	1.2	0.1	0.2	0.4	0.5	0.7	1.0	1.5	2.2	2.7	3.9	9.3
Houston	5,188	0.7	0.0	0.0	0.1	0.2	0.4	0.6	0.8	1.3	1.7	2.6	4.6
Los Angeles	25,803	1.0	0.0	0.1	0.2	0.3	0.5	0.8	1.3	2.0	2.6	4.0	8.4
New York	9,513	0.9	0.0	0.1	0.2	0.4	0.6	0.8	1.1	1.5	1.8	2.5	5.8
Phoenix	5,348	1.9	0.0	0.3	0.5	0.6	0.9	1.6	2.5	3.5	4.1	5.3	7.8
Pittsburgh	7,497	0.6	0.0	0.0	0.1	0.2	0.5	0.8	1.1	1.4	2.0	2.0	6.7
Seattle	1,079	1.5	0.2	0.4	0.5	0.7	0.9	1.3	1.8	2.4	2.9	4.3	5.9
St. Louis	3,216	0.8	0.0	0.1	0.3	0.4	0.5	0.6	0.9	1.3	1.7	2.7	5.7
Not in the 11 cities	230,161	0.9	0.0	0.0	0.1	0.2	0.4	0.7	1.2	1.8	2.4	3.8	39.0

^aCO monitoring is only available for quarters 1 and 4; since monitoring data are not available year-round, Anchorage is not included in the nationwide statistics shown in this table.

Table 3-8 contains the distribution of 1-h daily max CO concentrations derived from 1-h values reported to AQS for all monitors meeting the inclusion criteria described earlier. The nationwide mean, median, and interquartile range for 1-h daily max concentrations reported for 2005-2007 were 0.9, 0.7 and 0.8 ppm, respectively. Roughly one-third of the 1-h daily max data fall below the LOD for the majority of CO monitors reporting to AQS. The 99th percentile 1-h daily max

concentrations ranged from 2.0 ppm to 5.3 ppm in the selected cities with year-round monitoring; Anchorage had a 99th percentile concentration of 7.6 ppm.

Table 3-9. Distribution of 8-h daily max CO concentration (ppm) derived from AQS data.

	N	Mean	Min	Percentiles									
				1	5	10	25	50	75	90	95	99	Max
NATIONWIDE STATISTICS (N = NUMBER OF OBSERVATIONS)													
2005-2007	303,843	0.7	0.0	0.3	0.3	0.3	0.3	0.5	0.8	1.3	1.7	2.6	10.9
2005	101,184	0.7	0.0	0.3	0.3	0.3	0.3	0.6	0.9	1.4	1.8	2.8	9.7
2006	101,652	0.7	0.0	0.3	0.3	0.3	0.3	0.5	0.8	1.3	1.7	2.6	9.8
2007	101,007	0.6	0.0	0.3	0.3	0.3	0.3	0.5	0.8	1.2	1.5	2.3	10.9
Winter (December - February)	74,144	0.9	0.0	0.3	0.3	0.3	0.4	0.7	1.1	1.7	2.1	3.2	9.8
Spring (March - May)	77,317	0.6	0.0	0.3	0.3	0.3	0.3	0.5	0.7	1.1	1.3	2.0	9.6
Summer (June - August)	76,562	0.5	0.0	0.3	0.3	0.3	0.3	0.4	0.6	0.9	1.1	1.7	10.9
Fall (September - November)	75,820	0.7	0.0	0.3	0.3	0.3	0.3	0.6	0.9	1.4	1.8	2.7	9.0
NATIONWIDE STATISTICS, POOLED BY SITE (N = NUMBER OF SITES)													
2005-2007	285	0.7	0.2	0.3	0.3	0.4	0.5	0.6	0.8	1.0	1.2	1.7	2.1
2005	285	0.7	0.3	0.3	0.3	0.4	0.5	0.6	0.9	1.1	1.4	1.9	2.2
2006	285	0.7	0.2	0.3	0.3	0.4	0.5	0.6	0.8	1.1	1.2	1.8	2.4
2007	285	0.6	0.2	0.3	0.3	0.4	0.5	0.6	0.7	1.0	1.1	1.6	2.0
Winter (December - February)	285	0.9	0.2	0.3	0.4	0.4	0.6	0.8	1.1	1.4	1.7	2.4	2.6
Spring (March - May)	285	0.6	0.2	0.3	0.3	0.4	0.4	0.5	0.7	0.9	1.1	1.6	2.2
Summer (June - August)	285	0.5	0.2	0.3	0.3	0.3	0.4	0.5	0.6	0.8	0.9	1.5	2.0
Fall (September - November)	285	0.7	0.2	0.3	0.3	0.4	0.5	0.6	0.9	1.2	1.3	1.8	2.2
STATISTICS FOR INDIVIDUAL CSAS/CBSAS (2005-2007) (N = NUMBER OF OBSERVATIONS)													
Anchorage ^a	1,074	1.7	0.3	0.3	0.4	0.6	0.9	1.5	2.3	3.3	3.9	5.0	6.5
Atlanta	3,229	0.6	0.0	0.2	0.2	0.3	0.4	0.5	0.8	1.1	1.3	1.7	2.5
Boston	7,446	0.6	0.3	0.3	0.3	0.3	0.3	0.5	0.7	0.9	1.1	1.8	5.8
Denver	5,363	0.8	0.3	0.3	0.3	0.3	0.5	0.7	1.0	1.4	1.8	2.4	3.4
Houston	5,188	0.5	0.3	0.3	0.3	0.3	0.3	0.4	0.6	0.9	1.1	1.7	3.3
Los Angeles	25,803	0.7	0.3	0.3	0.3	0.3	0.3	0.6	0.9	1.5	1.8	2.7	6.2
New York	9,513	0.7	0.3	0.3	0.3	0.3	0.4	0.6	0.9	1.2	1.4	1.8	3.0
Phoenix	5,348	1.3	0.3	0.3	0.3	0.4	0.6	1.0	1.8	2.5	3.0	3.8	5.8
Pittsburgh	7,497	0.5	0.3	0.3	0.3	0.3	0.3	0.3	0.6	0.9	1.0	1.5	3.7
Seattle	1,079	1.1	0.3	0.3	0.4	0.5	0.7	1.0	1.4	1.8	2.2	3.2	4.0
St. Louis	3,216	0.6	0.3	0.3	0.3	0.3	0.3	0.5	0.7	0.9	1.2	1.9	4.2
Not in the 11 cities	230,161	0.7	0.0	0.3	0.3	0.3	0.3	0.5	0.8	1.3	1.6	2.5	10.9

^aCO monitoring is only available for quarters 1 and 4; since monitoring data is not available year-round, Anchorage is not included in the nationwide statistics shown in this table.

Table 3-9 contains the distribution of 8-h daily max concentrations derived from the 1-h CO concentrations reported to AQS. This was done by first calculating the average concentration for each successive 8-h period, thereby producing 24 8-h avg per day. The maximum of these values for a given monitor within a given day (midnight-to-midnight) was used as the 8-h daily max statistic for that monitor and day. The nationwide mean, median, and interquartile range for 8-h daily max

concentrations reported for 2005-2007 were 0.7, 0.5, and 0.5 ppm, respectively. Half of the 8-h daily max concentrations fell below the LOD for the majority of CO monitors in the field. The highest 8-h daily max concentration, 10.9 ppm, was recorded at a monitor located 5 mi north of Newkirk, OK (AQS site ID: 400719010). The 99th percentile 8-h daily max concentrations ranged from 1.5 ppm to 3.8 ppm in the selected cities with year-round monitoring; Anchorage had a 99th percentile 8-h daily max concentration of 5.0 ppm.

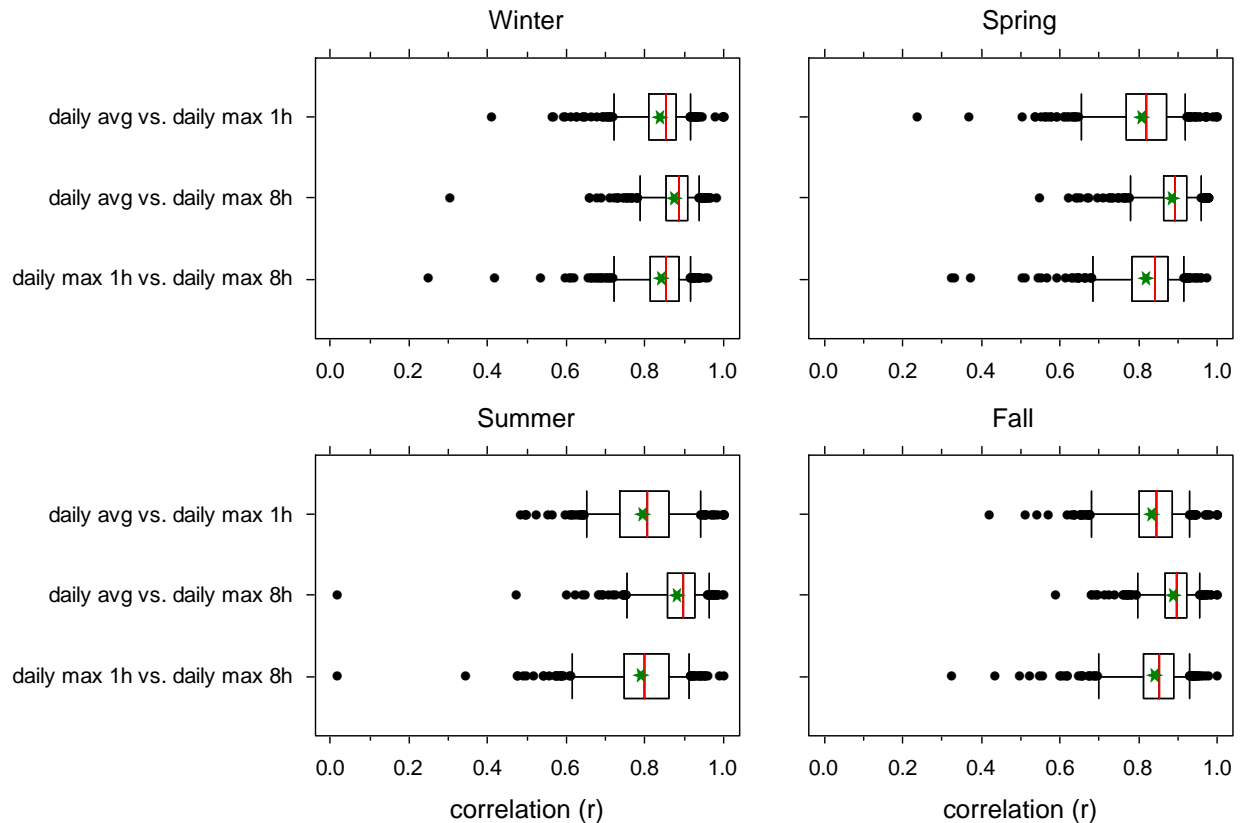


Figure 3-17. Seasonal plots showing the variability in correlations between 24-h avg CO concentration with 1-h daily max and 8-h daily max CO concentrations and between 1-h daily max and 8-h daily max CO concentrations. Red bars denote the median, green stars denote the arithmetic mean, the box incorporates the IQR and the whiskers extend to the 5th and 95th percentiles. Correlations outside the 5th and 95th percentiles are shown as individual points.

Table 3-7 through Table 3-9 show distributions of CO data based on the 24-h avg, 1-h daily max and 8-h daily max concentration. The current standards are based on 1-h and 8-h calculations. While the nationwide concentrations vary in absolute magnitude based on these three statistics, the shape of the distributions are quite similar up to the 99th percentile. The relative increase from the 99th percentile to the max for the 1-h daily max is larger than for the 24-h or 8-h daily max. This is to be expected since this statistic is more sensitive to short-term (less than 8 h) increases in CO concentration. Box plots showing the range in Pearson correlation coefficients (r) between the different statistics are shown in Figure 3-17. Included are the correlation of the 24-h avg with the 1-h daily max and 8-h daily max, as well as the correlation between the 1-h daily max and 8-h daily max, all calculated using the same 2005-2007 data set stratified by season. Correlations are generally quite high across all seasons and all comparisons, with median $r > 0.8$. Correlations are higher on average in the wintertime compared to the summertime for the two comparisons involving the 1-h daily max

statistic. The correlations between the 24-h avg and the 8-h daily max are the highest in all seasons, which is in agreement with the distributional similarities shown in the preceding tables.

3.5.1.2. Urban Scale

This section describes urban variability in CO concentrations reported to AQS at the individual CSA/CBSA level. Denver, CO, and Los Angeles, CA, were selected for this assessment to illustrate the variability in CO concentrations measured across contrasting metropolitan regions. Information on the other nine cities evaluated for this assessment is included in Appendix A. Maps of the Denver CSA and the Los Angeles CSA shown in Figure 3-18 and Figure 3-21, respectively, illustrate the location of all CO monitors meeting the inclusion criteria described earlier. Letters on the maps identify the individual monitor locations and correspond with the letters provided in the accompanying concentration box plots (Figure 3-19 and Figure 3-22) and pair-wise monitor comparison tables (Table 3-10 and Table 3-11). The box plots for each monitor include the hourly CO concentration median and interquartile range with whiskers extending from the 5th to the 95th percentile. Data from 2005-2007 were used to generate the box plots, which are stratified by season as follows: 1 = winter (December-February), 2 = spring (March-May), 3 = summer (June-August), and 4 = fall (September-November). The comparison tables include the Pearson correlation coefficient (r), the 90th percentile of the absolute difference in concentrations (P90) in ppm, the coefficient of divergence (COD) and the straight-line distance between monitor pairs (d) in km. The COD provides an indication of the variability across the monitoring sites within each CSA/CBSA and is defined as follows:

$$COD_{jk} = \sqrt{\frac{1}{p} \sum_{i=1}^p \left(\frac{X_{ij} - X_{ik}}{X_{ij} + X_{ik}} \right)^2}$$

Equation 3-1

where X_{ij} and X_{ik} represent the observed hourly concentrations for time period i at sites j and k , and p is the number of paired hourly observations. A COD of 0 indicates there are no differences between concentrations at paired sites (spatial homogeneity), while a COD approaching 1 indicates extreme spatial heterogeneity. Pearson correlation is also plotted as a function of distance for Denver and Los Angeles in Figure 3-20 and Figure 3-23, respectively. Similar maps, box plots, and comparison tables for the nine remaining CSAs/CBSAs are included in Annex A.

The information contained in these figures and tables should be used with some caution since many of the reported concentrations for the years 2005-2007 are near or below the monitors' stated LOD. Because ambient concentrations are now in large part very near or below the 0.5 ppm LOD for the majority of FRMs and the coarsely reported measurement resolution is 0.1 ppm, the comparison statistics shown in these tables might be biased to exhibit specious heterogeneity in the box plots.

Denver Combined Statistical Area

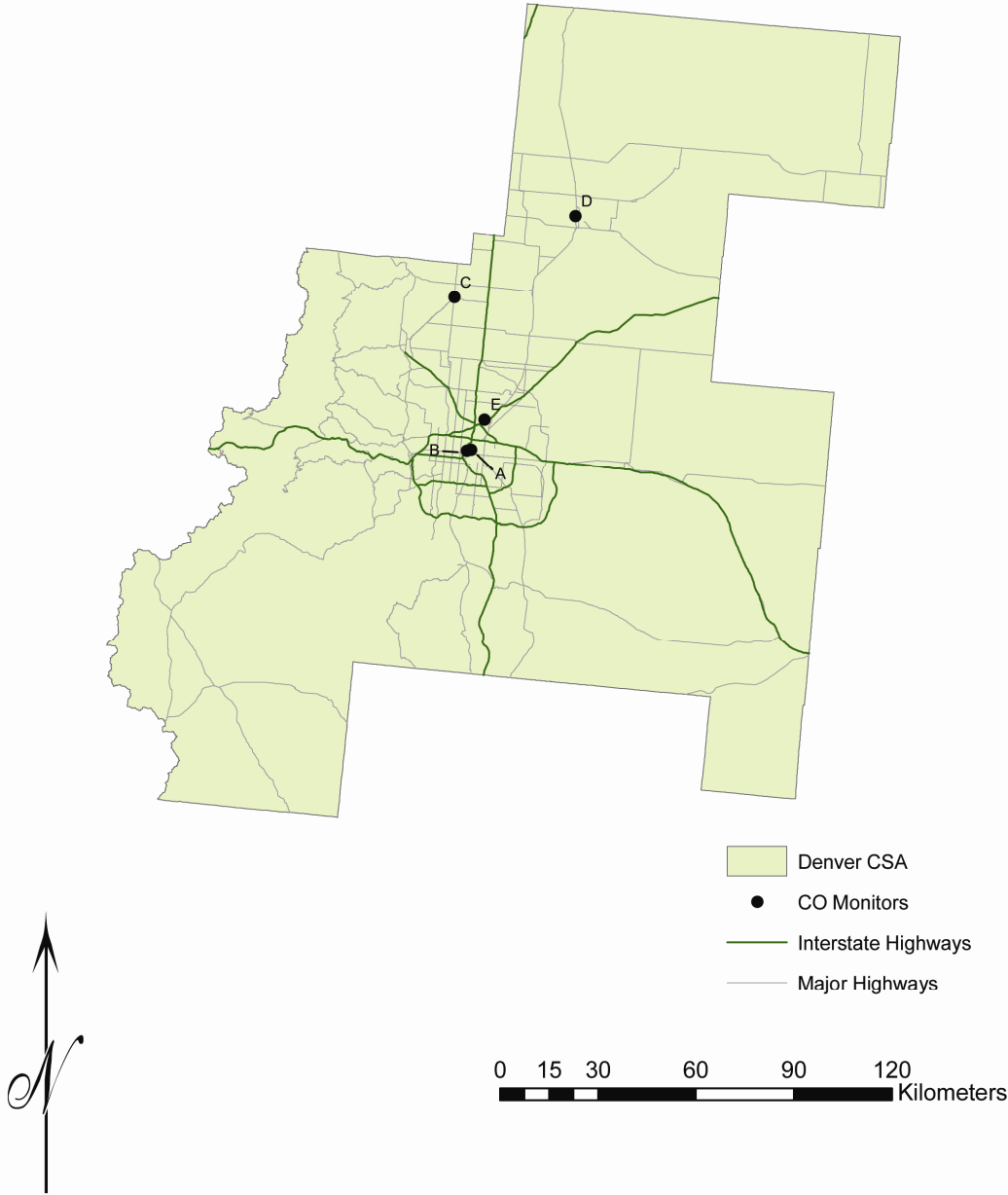


Figure 3-18. Map of CO monitor locations and major highways for Denver, CO.

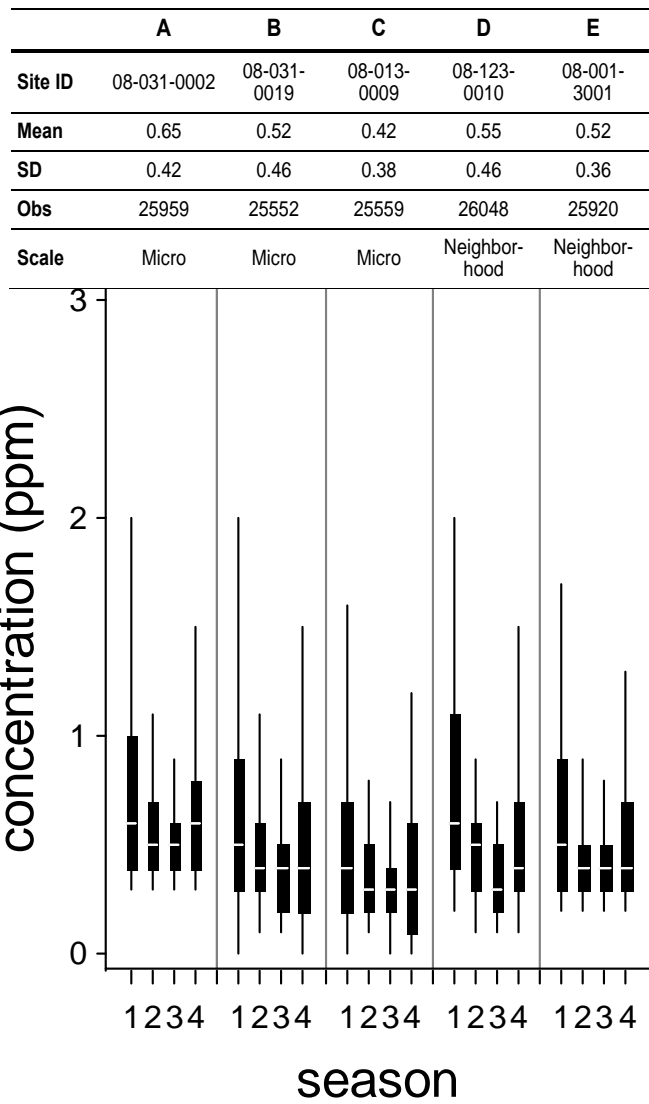


Figure 3-19. Box plots illustrating the distribution of 2005-2007 hourly CO concentrations in Denver, CO. The data are stratified by season along the x-axis where 1 = winter, 2 = spring, 3 = summer, and 4 = fall. The box plots show the median and interquartile range with whiskers extending from the 5th to the 95th percentile. Identifiers and statistics for each site are shown at the top of the figure.

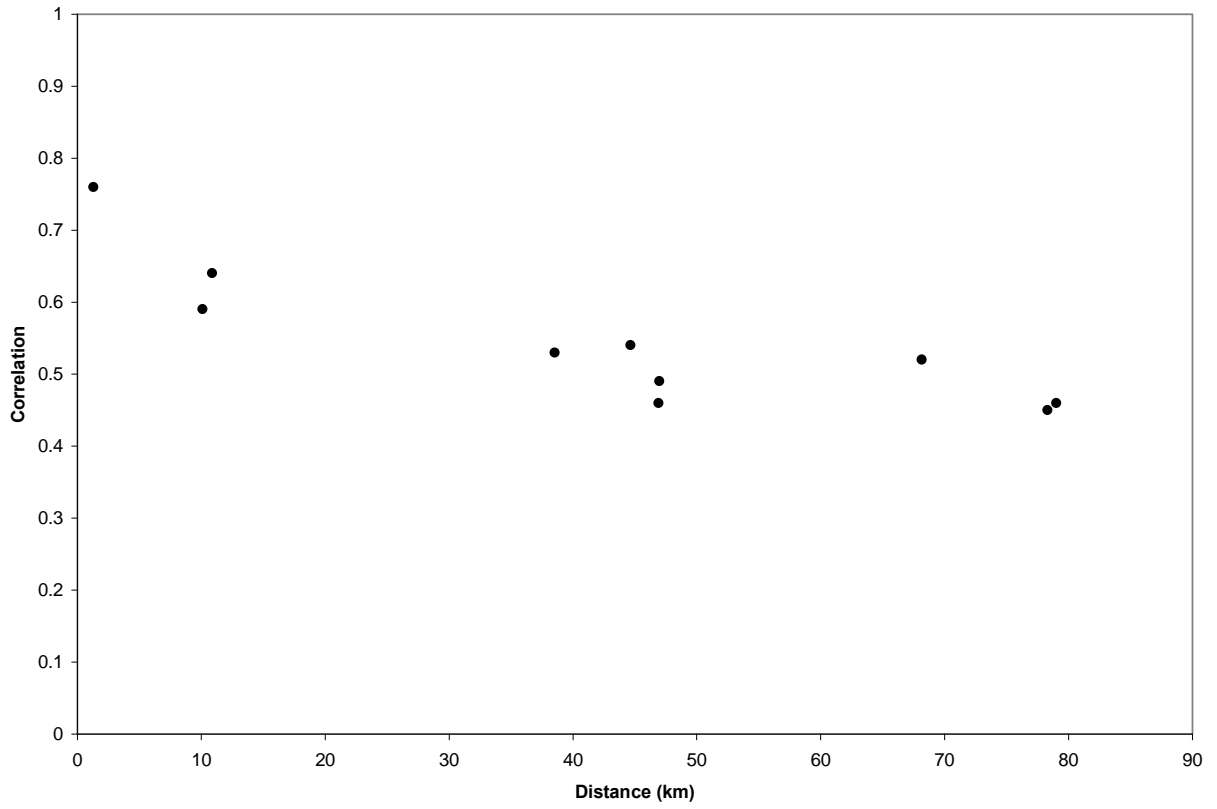


Figure 3-20. Intersampler correlation versus distance for monitors located within the Denver CSA.

Los Angeles Combined Statistical Area



Figure 3-21. Map of CO monitor locations and major highways for Los Angeles, CA.

	A	B	C	D	E	F	G	H
Site ID	06-065-1003	06-059-1003	06-037-9033	06-037-1301	06-071-9004	06-065-9001	06-037-5005	06-059-0007
Mean	0.67	0.31	0.23	0.98	0.53	0.29	0.24	0.42
SD	0.42	0.47	0.29	0.89	0.38	0.20	0.37	0.46
Obs	24885	24760	24135	24825	24844	24792	24965	24264
Scale	Micro	Middle	Middle	Middle	Middle	Neighborhood	Neighborhood	Urban

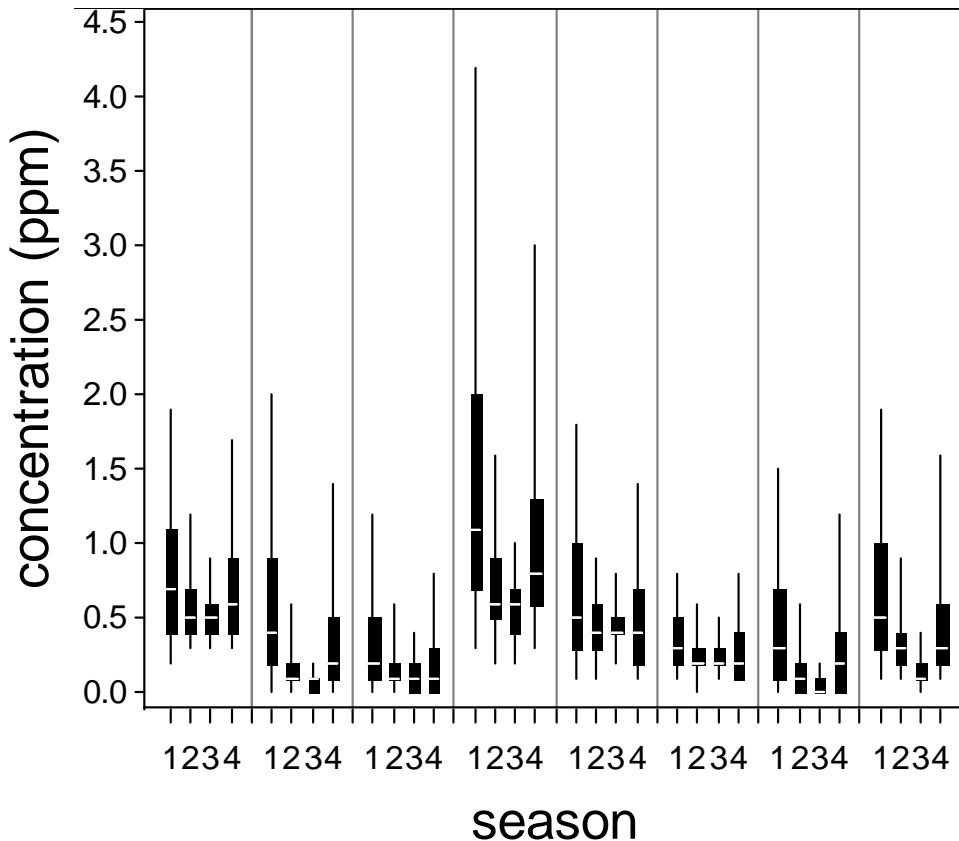
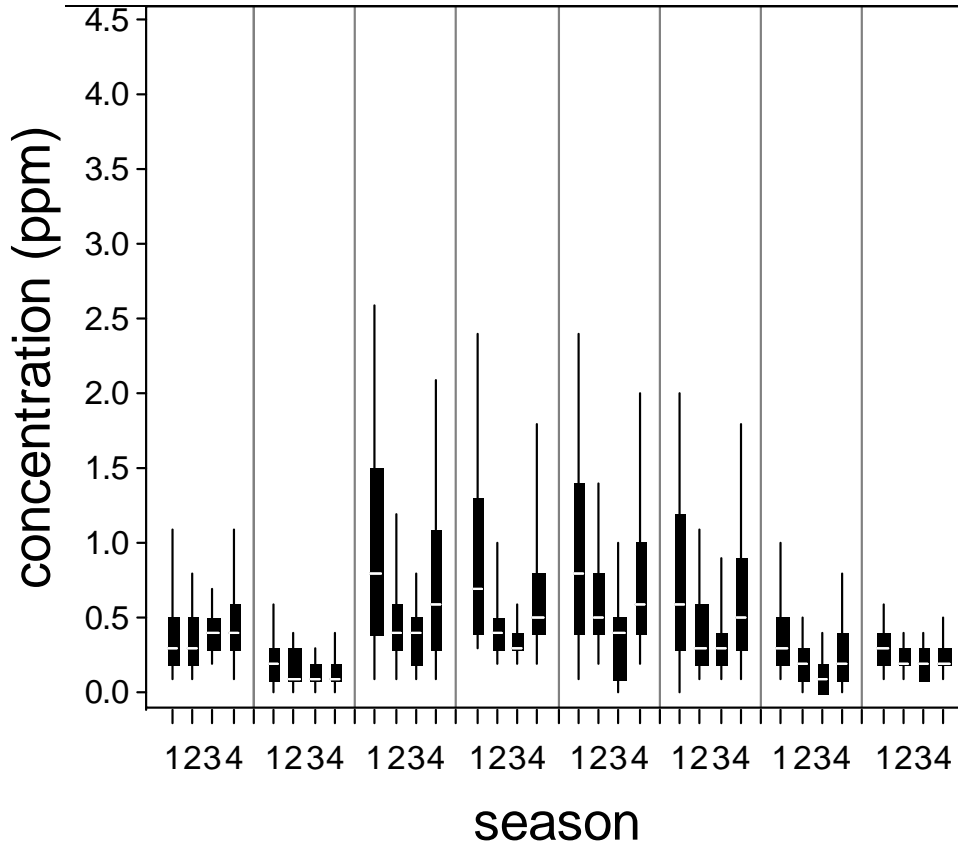


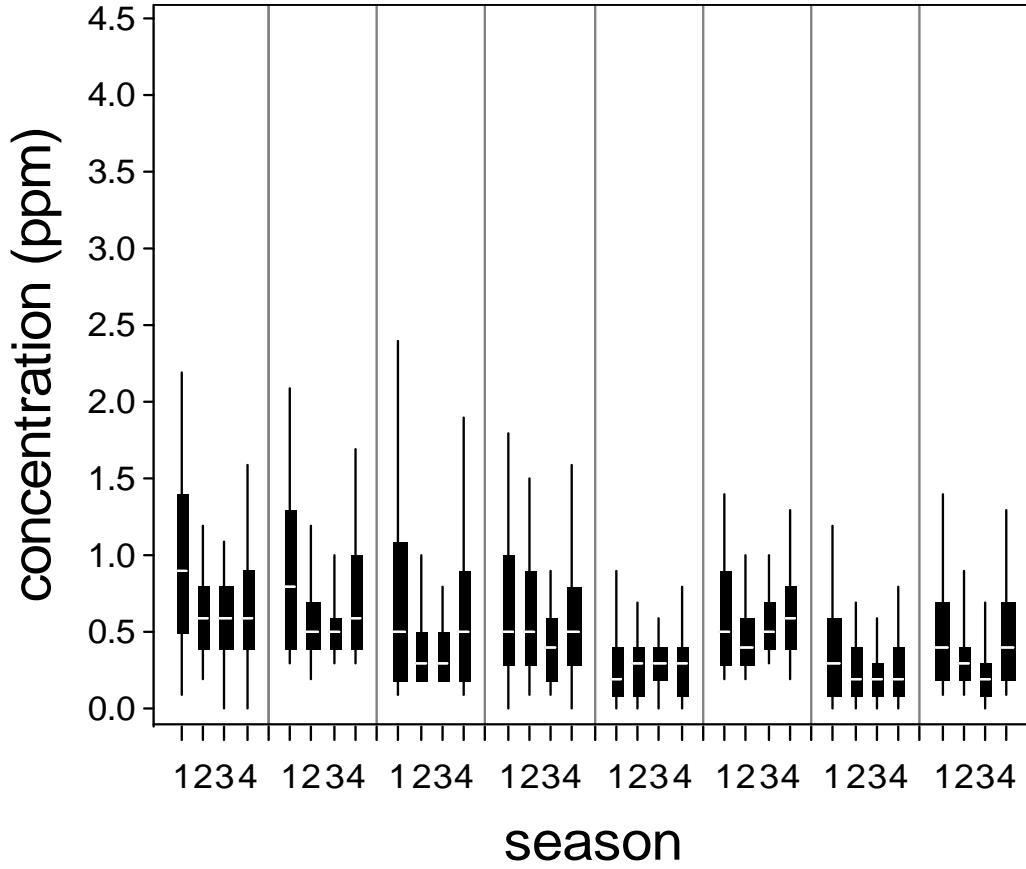
Figure 3-22. Box plots illustrating the distribution of 2005-2007 hourly CO concentrations in Los Angeles, CA. The data are stratified by season along the x-axis where 1 = winter, 2 = spring, 3 = summer, and 4 = fall. The box plots show the median and interquartile range with whiskers extending from the 5th to the 95th percentile. Identifiers and statistics for each site are shown at the top of the figure (monitors without scale designations in AQS are labeled Null). Part 1 of 3 of Figure 3-22. See the next two pages for parts 2 and 3 of Figure 3-22.

	I	J	K	L	M	N	O	P
Site ID	06-037-0002	06-071-0001	06-037-1002	06-059-5001	06-037-4002	06-037-1103	06-059-2022	06-065-5001
Mean	0.42	0.17	0.66	0.62	0.69	0.56	0.26	0.25
SD	0.27	0.17	0.59	0.55	0.56	0.50	0.25	0.14
Obs	2,5001	24105	24892	24705	24259	24645	24831	24938
Scale	Null							



Part 2 of 3 for Figure 3-22

	Q	R	S	T	U	V	W	X
Site ID	06-037-2005	06-037-1701	06-037-1201	06-065-8001	06-037-6012	06-071-1004	06-071-0306	06-037-0113
Mean	0.72	0.69	0.57	0.60	0.30	0.59	0.30	0.41
SD	0.48	0.45	0.54	0.46	0.25	0.32	0.28	0.36
Obs	24804	24912	24281	24778	24860	24767	24796	24916
Scale	Null							



Part 3 of 3 for Figure 3-22

Table 3-11. Table of intersampler comparison statistics, as defined in the text, including Pearson r, P90 (ppm), COD and d (km) for each pair of hourly CO monitors reporting to AQS for 2005-2007 in Los Angeles, CA. The table is grouped and identified by monitoring scale (monitors without scale designations in AQS are labeled Null).

	Micro	Middle				Neighbor-hood		Urban	Null																
	A	B	C	D	E	F	G	H	I	J	K	L	M	N	O	P	Q	R	S	T	U	V	W	X	
Micro	A	1.00	0.56	0.56	0.54	0.73	0.72	0.45	0.62	0.54	0.35	0.70	0.66	0.46	0.62	0.61	0.48	0.53	0.78	0.73	0.67	0.54	0.70	0.55	0.57
		0.0	0.8	0.9	1.1	0.5	0.7	0.9	0.7	0.7	1.0	0.6	0.6	0.8	0.6	0.8	0.9	0.7	0.4	0.6	0.6	0.8	0.5	0.8	0.7
		0.00	0.66	0.67	0.30	0.30	0.46	0.73	0.46	0.33	0.68	0.29	0.24	0.39	0.37	0.58	0.47	0.35	0.19	0.29	0.37	0.53	0.20	0.54	0.42
Middle	B	57.1	104.6	74.8	21.3	30.5	95.0	51.3	52.6	110.6	88.2	51.0	74.1	77.4	43.3	80.1	70.1	35.0	108.0	6.1	114.5	27.4	62.8	98.1	
		1.00	0.55	0.67	0.50	0.46	0.60	0.75	0.14	0.28	0.70	0.72	0.64	0.58	0.62	0.34	0.50	0.60	0.57	0.40	0.25	0.36	0.55	0.47	
		0.0	0.6	1.3	0.7	0.5	0.5	0.5	0.7	0.7	0.9	0.7	0.9	0.8	0.5	0.6	0.9	0.9	0.8	0.9	0.7	0.8	0.6	0.7	
Neighborhood	C	0.00	0.66	0.70	0.64	0.59	0.69	0.55	0.64	0.69	0.63	0.62	0.64	0.63	0.56	0.59	0.68	0.66	0.62	0.67	0.67	0.65	0.62	0.59	
		0	112.0	38.6	76.9	55.1	55.8	17.3	51.2	158.5	66.3	27.9	29.5	51.6	23.7	129.6	54.0	46.3	80.7	59.3	96.2	54.9	107.5	64.4	
		1.00	0.55	0.50	0.50	0.39	0.56	0.27	0.45	0.59	0.63	0.43	0.53	0.51	0.41	0.45	0.61	0.53	0.41	0.40	0.49	0.67	0.42		
Urban	D	0.00	0.72	0.64	0.57	0.74	0.60	0.62	0.62	0.62	0.85	0.64	0.69	0.63	0.61	0.56	0.70	0.66	0.62	0.67	0.62	0.65	0.57	0.60	
		0	82.5	100.4	132.5	84.4	94.7	62.2	104.0	57.4	84.2	94.0	67.5	122.7	171.9	59.6	75.4	64.0	99.2	48.4	77.9	75.4	74.9		
		1.00	0.44	0.39	0.63	0.71	0.21	0.33	0.70	0.78	0.70	0.74	0.57	0.28	0.53	0.65	0.49	0.35	0.23	0.39	0.51	0.50			
Null	E	0.0	1.3	1.6	1.5	1.1	1.5	1.7	0.9	0.9	1.0	1.0	1.5	1.7	1.0	1.0	1.2	1.2	1.6	1.3	1.5	1.3			
		0.00	0.42	0.56	0.76	0.51	0.44	0.73	0.35	0.30	0.39	0.41	0.65	0.56	0.39	0.29	0.41	0.45	0.60	0.35	0.61	0.50			
		0	88.6	86.0	20.4	27.4	35.0	152.6	29.1	23.8	11.8	15.3	59.5	154.5	23.8	45.0	42.1	73.7	58.2	57.0	103.4	26.4			
Micro	F	0.0	0.6	0.8	0.6	0.6	0.6	0.8	0.7	0.7	0.9	0.6	0.6	0.7	0.7	0.6	0.6	0.7	0.6	0.6	0.5	0.6	0.6		
		0.00	0.42	0.72	0.64	0.46	0.35	0.65	0.35	0.33	0.46	0.39	0.56	0.43	0.41	0.31	0.32	0.41	0.51	0.29	0.52	0.41			
		0	48.0	108.0	68.5	59.9	90.2	96.3	65.7	90.1	87.9	64.6	73.3	78.6	44.2	116.3	17.7	119.3	32.7	44.9	109.1				
Neighborhood	G	1.00	0.43	0.53	0.56	0.30	0.58	0.55	0.36	0.53	0.51	0.49	0.47	0.69	0.66	0.66	0.56	0.68	0.49	0.55					
		0.0	0.5	0.6	0.4	0.4	1.0	0.8	1.1	0.8	0.3	0.3	0.9	0.8	0.8	0.3	0.6	0.4	0.5						
		0.00	0.70	0.42	0.38	0.58	0.46	0.43	0.54	0.46	0.50	0.32	0.53	0.46	0.40	0.49	0.47	0.43	0.47	0.39					
Urban	H	0	106.1	58.7	74.8	137.8	106.5	63.7	81.1	93.4	32.4	75.7	89.2	58.1	125.1	36.6	135.3	54.8	92.3	112.0					
		1.00	0.58	0.19	0.18	0.64	0.59	0.59	0.42	0.26	0.40	0.51	0.52	0.43	0.24	0.27	0.41	0.27	0.41	0.59					
		0.0	0.6	0.7	0.6	1.0	0.8	1.0	0.8	0.5	0.5	1.0	1.0	0.9	0.9	0.6	0.9	0.6	0.9	0.6					
Null	I	0.00	0.71	0.72	0.75	0.72	0.72	0.75	0.73	0.73	0.70	0.75	0.73	0.70	0.75	0.73	0.72	0.74	0.73	0.73	0.72	0.69			
		0	47.4	51.0	166.0	27.0	44.2	26.4	22.7	78.3	174.8	34.4	63.9	29.1	93.7	48.7	75.8	118.6	11.4						
		1.00	0.29	0.31	0.72	0.81	0.63	0.70	0.67	0.37	0.54	0.69	0.61	0.49	0.29	0.47	0.54	0.59							
Micro	J	0.0	0.6	0.8	0.7	0.5	0.8	0.6	0.5	0.7	0.8	0.7	0.7	0.7	0.6	0.7	0.7	0.6	0.6	0.5	0.6	0.5			
		0.00	0.43	0.62	0.41	0.38	0.48	0.40	0.46	0.41	0.52	0.44	0.41	0.49	0.53	0.45	0.50	0.39	0.54	0.50	0.38				
		0	33.9	144.7	51.8	10.5	23.2	37.3	32.9	129.2	37.7	31.4	68.3	51.7	81.8	41.6	93.7	53.7							
Neighborhood	K	1.00	0.17	0.43	0.34	0.17	0.46	0.42	0.33	0.41	0.57	0.44	0.47	0.43	0.61	0.24	0.45								
		0.0	0.6	1.0	0.8	1.1	0.8	0.5	0.5	0.8	0.7	0.8	0.5	0.5	0.6	0.5	0.6	0.5							
		0.00	0.62	0.35	0.33	0.47	0.38	0.52	0.36	0.43	0.33	0.33	0.43	0.47	0.30	0.50	0.38								
Urban	L	0	117.7	36.5	23.6	42.4	29.0	60.6	131.4	18.7	17.7	56.5	49.2	61.9	27.4	68.4	50.0								
		1.00	0.35	0.34	0.24	0.34	0.33	0.29	0.31	0.40	0.31	0.19	0.25	0.36	0.43	0.25									
		0.0	1.2	1.0	1.3	1.0	0.4	0.3	1.1	1.1	1.0	1.1	0.5	0.8	0.4	0.7									
Null	M	0.00	0.67	0.66	0.70	0.66	0.63	0.55	0.71	0.68	0.64	0.69	0.62	0.66	0.59	0.62									
		0	142.7	137.1	159.7	143.4	152.3	123.6	131.7	113.3	158.2	105.4	148.8	103.7	51.0	161.1									
		1.00	0.75	0.62	0.84	0.69	0.40	0.67	0.78	0.74	0.52	0.39	0.59	0.58	0.69										
Micro	N	0.00	0.26	0.41	0.29	0.56	0.46	0.39	0.26	0.28	0.42	0.52	0.29	0.53	0.38										
		0	43.6	40.8	14.7	84.6	167.7	18.1	53.5	20.0	85.3	30.1	63.8	97.8	18.9										
		1.00	0.62	0.74	0.67	0.40	0.58	0.77	0.61	0.50	0.34	0.54	0.58	0.59											
Neighborhood	O	0.00	0.7	0.5	0.8	1.0	0.7	0.5	0.7	0.5	0.7	0.8	0.9	0.6	0.8	0.6									
		0.00	0.37	0.31	0.54	0.42	0.37	0.20	0.29	0.38	0.52	0.25	0.51	0.37											
		0	24.6	29.8	41.5	130.6	28.1	24.3	61.5	50.2	73.4	35.8	86.4	48.5											
Urban	P	1.00	0.60	0.48	0.24	0.41	0.52	0.44	0.31	0.15	0.28	0.43	0.43												
		0.0	0.8	1.1	1.2	0.9	0.8	0.9	1.0	1.2	0.9	1.1	0.9												
		0.00	0.45	0.58	0.53	0.46	0.38	0.44	0.48	0.60	0.41	0.59	0.48												
Null	Q	0	27.1	52.1	152.4	34.7	48.6	52.3	74.0	69.4	60.3	109.6	35.2												
		1.00	0.63	0.32	0.67	0.77	0.64	0.49	0.34	0.57	0.51	0.71													
		0.0	0.8	1.0	0.7	0.5	0.7	0.8	0.9	0.6	0.8	0.6													
Micro	R	0.00	0.55	0.46	0.44	0.33	0.34	0.45	0.52	0.36	0.53	0.38	0.53	0.38											
		0	70.2	157.4	11.7	43.8	31.8	75.1	44.7	55.2	95.9	21.2													
		1.00	0.44	0.55	0.70	0.55	0.43	0.28	0.57	0.45	0.57														
Neighborhood	S	0.0	0.3	0.9	0.9	0.8	0.9	0.5	0.7	0.4	0.6														
		0.00	0.47	0.62	0.58	0.54	0.59	0.59	0.56	0.56	0.50														
		0	107.9	69.5	48.9	101.2	47.5	114.6	52.6	102.5	85.9														

Legend
r
P90
COD
d

	Micro	Middle	Neighbor-hood	Urban	Null									
Null	P					1.00	0.39	0.47	0.42	0.40	0.40	0.47	0.38	0.35
						0.0	1.0	1.0	0.9	0.9	0.4	0.7	0.4	0.6
						0.00	0.54	0.47	0.40	0.50	0.45	0.43	0.44	0.38
						0	149.6	114.2	187.6	82.4	192.2	104.2	102.8	178.1
	Q						1.00	0.65	0.54	0.39	0.32	0.53	0.46	0.49
							0.0	0.6	0.8	0.8	1.0	0.7	0.9	0.8
							0.00	0.34	0.42	0.46	0.58	0.35	0.59	0.49
							0	35.4	38.0	67.2	46.2	46.0	84.3	31.6
	R							1.00	0.70	0.60	0.47	0.78	0.58	0.63
								0.0	0.6	0.7	0.9	0.5	0.9	0.7
								0.00	0.30	0.38	0.53	0.18	0.54	0.41
								0	73.4	31.8	79.6	12.0	62.4	65.0
	S								1.00	0.62	0.53	0.58	0.55	0.64
									0.0	0.7	0.8	0.6	0.8	0.7
									0.00	0.40	0.49	0.30	0.50	0.34
									0	105.2	20.4	83.8	115.6	17.8
	T									1.00	0.46	0.54	0.38	0.55
										0.0	0.9	0.6	0.9	0.7
										0.00	0.56	0.37	0.58	0.46
										0	110.8	22.8	57.0	96.1
U									1.00	0.53	0.39	0.36		
									0.0	0.6	0.5	0.6		
									0.00	0.51	0.54	0.50		
									0	88.3	110.7	37.4		
V										1.00	0.47	0.50		
										0.0	0.7	0.6		
										0.00	0.52	0.40		
										0	52.7	76.4		
W											1.00	0.41		
											0.0	0.6		
											0.00	0.50		
											0	115.3		
X												1.00		
												0.0		
												0.00		
													0	

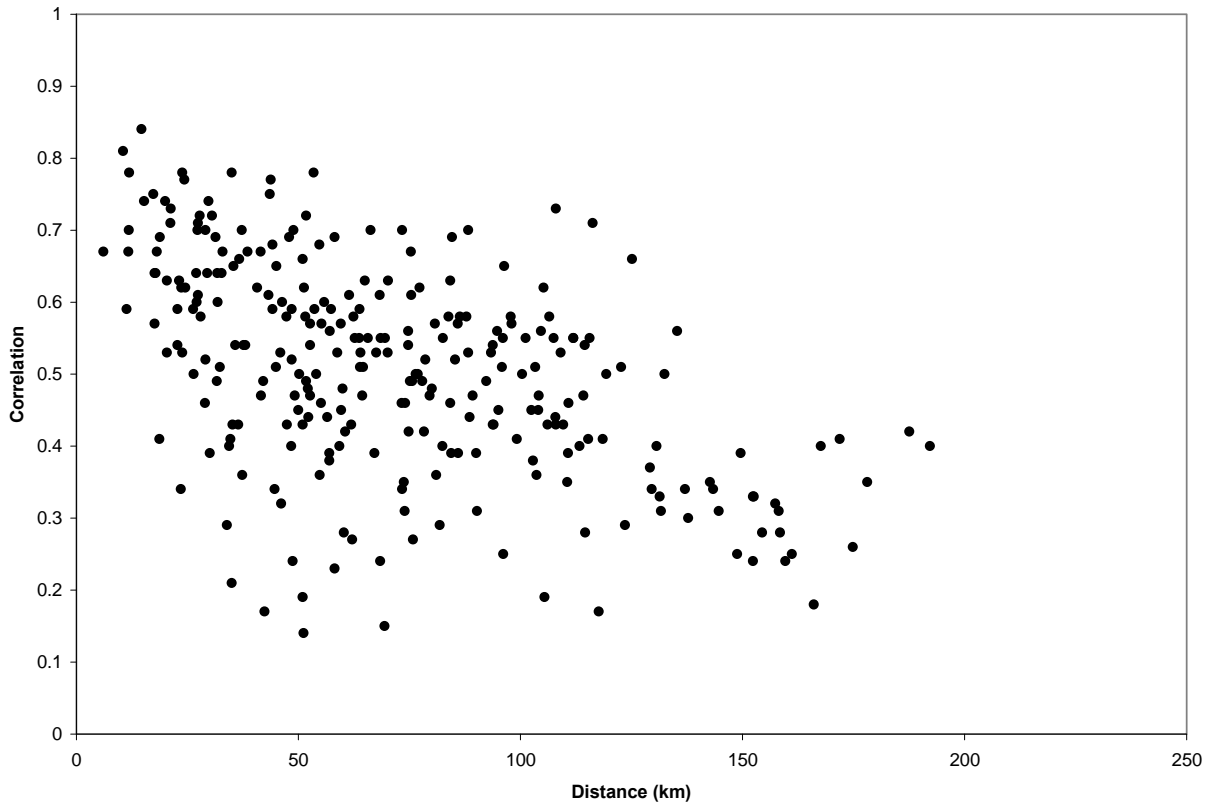


Figure 3-23. Intersampler correlation versus distance for monitors located within the Los Angeles CSA.

The Denver CSA in Figure 3-18 incorporates an area of 33,723 km² with a maximum straight-line distance between CO monitors of 79 km. Of the five CO monitors meeting the inclusion criteria, three were sited for microscale monitoring and two were sited for neighborhood scale monitoring. Sites A and B are located in downtown Denver while Site E is located in an industrial region north of town and surrounded on three sides by three heavily-traveled interstate highways. Sites C and D are located in two smaller towns (Longmont and Greeley, respectively) north of Denver. The means and seasonal patterns shown in Figure 3-19 are similar for all five monitors within this CSA. The highest annual mean concentration (0.7 ppm) was observed at Site A, a downtown microscale monitor, while the lowest annual mean concentration (0.4 ppm) was observed at Site C, a microscale monitor in Longmont. The step-wise nature of the box plots is attributed to the 0.1 ppm resolution of the CO monitors used in the Denver CSA. Because these monitors have LOD of 0.5 ppm, it is also likely that the means and statistical distributions are biased as well.

The Los Angeles CSA in Figure 3-21 incorporates an area of 88,054 km² and a maximum straight-line distance between monitors of 192 km, making it more than twice the size of the Denver CSA. Of the 11 CSAs/CBSAs investigated, Los Angeles had the largest number of CO monitors (N = 24) meeting the inclusion criteria. One monitor was sited for microscale, four for middle scale, two for neighborhood scale, and one for urban scale. The remaining 16 monitors did not contain a siting classification in AQS. The monitors were evenly distributed around the Los Angeles and Riverside areas, with outlying monitors in Santa Clarita (Site U), Lancaster (Site C), Victorville (Site W), Barstow (Site J) and Palm Springs (Site P). A large amount of variability is present in the means and seasonal patterns displayed in Figure 3-22. Generally speaking, lower annual mean concentrations (<0.3 ppm) were measured in the outlying towns including those listed above as well as Lake Elsinore (Site F) and Mission Viejo (Site O). In addition, a neighborhood scale upwind background site (Site G) located on the grounds of the Los Angeles International Airport and 1.5 km from the

Pacific Ocean reported a relatively low mean annual concentration of 0.2 ppm. The highest annual mean concentration (1.0 ppm) was observed at Site D, a middle scale maximum concentration site located 25 m from a busy surface street and adjacent to the Imperial Shopping Mall. This site is also 180 m from a major highway intersection and 350 m from Interstate 105. The step-wise nature of the box plots is attributed to the 0.1 ppm resolution of the CO monitors used in the Los Angeles CSA. Because these monitors have LOD of 0.5 ppm, it is also likely that the means and statistical distributions are biased as well.

The pair-wise comparisons for measurements at the monitors in each of the 11 CSAs/CBSAs included in this analysis reveal a wide range of response between monitors in each city and among the cities judged against each other (Table 3-10, Table 3-11 and Annex Tables A-9 through A-16). While this wide range is produced by the interactions of many physical and chemical elements, the location of each monitor and the uniqueness of its immediate surroundings can often explain much of the agreement or lack thereof.

For the monitor comparisons within the Denver CSA (Table 3-10 and Figure 3-20), the correlations tend to be inversely related to the monitor separation distance, with the highest correlation ($r = 0.76$) for the two downtown Denver monitors (Sites A and B) separated by 1.3 km and the lowest correlations ($r \leq 0.46$) between the downtown Denver monitors and the Greeley monitor (Site D) located roughly 80 km north. While Sites A and B have a high correlation, the comparative magnitudes of the concentrations measured at these two sites, as determined by the P90 and COD, is comparable to comparisons with much less proximal monitors. This is likely caused by the location of these two monitors on opposite sides of downtown Denver, as illustrated by the aerial view of monitors A and B in Figure 3-24. While there is no prevailing wind direction in Denver, the wind comes from the south-southwest with a slightly higher frequency than other directions, making Site A downwind of the urban core more frequently than Site B. Assuming traffic within the urban core is a major source of CO, this would explain the higher mean concentrations measured at Site A relative to Site B despite their close proximity.

Greater variability in the pair-wise comparison statistics is observed in the Los Angeles CSA compared to the Denver CSA, partially due to the greater number of monitors spread over a larger area. Factors other than the distance between monitors, however, can contribute substantially to concentration disparities observed between monitors. To illustrate this point, Site S (located in Reseda, a suburb in the Simi Valley northwest of Los Angeles) correlates well ($r = 0.73$) with Site A (located 108 km to the southeast in Riverside). In fact, Site S correlates well ($r > 0.62$) with Sites A, E, F and T, all east of Los Angeles and all over 100 km away. Site S is located in a densely populated urban area with a mixture of commercial and residential land whereas the other four sites are located in less densely populated regions with commercial, residential and undeveloped land. Sites S and T contain no monitoring scale information in AQS, but Sites A, E and F are classified as microscale, middle scale and neighborhood scale, respectively. In contrast to the above example, Sites I and Q are located only 19 km apart in Azusa and Pasadena, respectively, and they correlate less well ($r = 0.41$). While these two locations are relatively close in proximity with similar topography, the siting of the two monitors is quite different. Site I in Azusa is located 700 m from I-210 in a mixed use community containing warehouses, small industry, housing and a gravel operation (Figure 3-25) while Site Q in Pasadena is located between a large residential neighborhood and the California Institute of Technology campus (Figure 3-26). Neither of these sites has monitoring scale designations reported in AQS. The contrasting CO emission sources surrounding these two monitors result in disparate concentrations with poor correlations despite their close proximity. Topography and micrometeorology can also play an important role in the correlation between monitors. For example, Sites C and P are isolated from the other sites in the Los Angeles CSA by the San Gabriel Mountains and the San Bernardino Mountains, respectively, resulting in lower than average concentrations (Figure 3-22) and relatively low pair-wise correlations (Table 3-11) for these two sites. This analysis demonstrates that agreement between monitors on an urban scale is a complex function of monitor siting, location relative to sources, geography, and micrometeorology.



Figure 3-24. Aerial view of the location of CO monitors A and B (marked by the red pins) in Denver, CO, depicting their proximity to the urban core. Scale: 1 cm = 145 m.

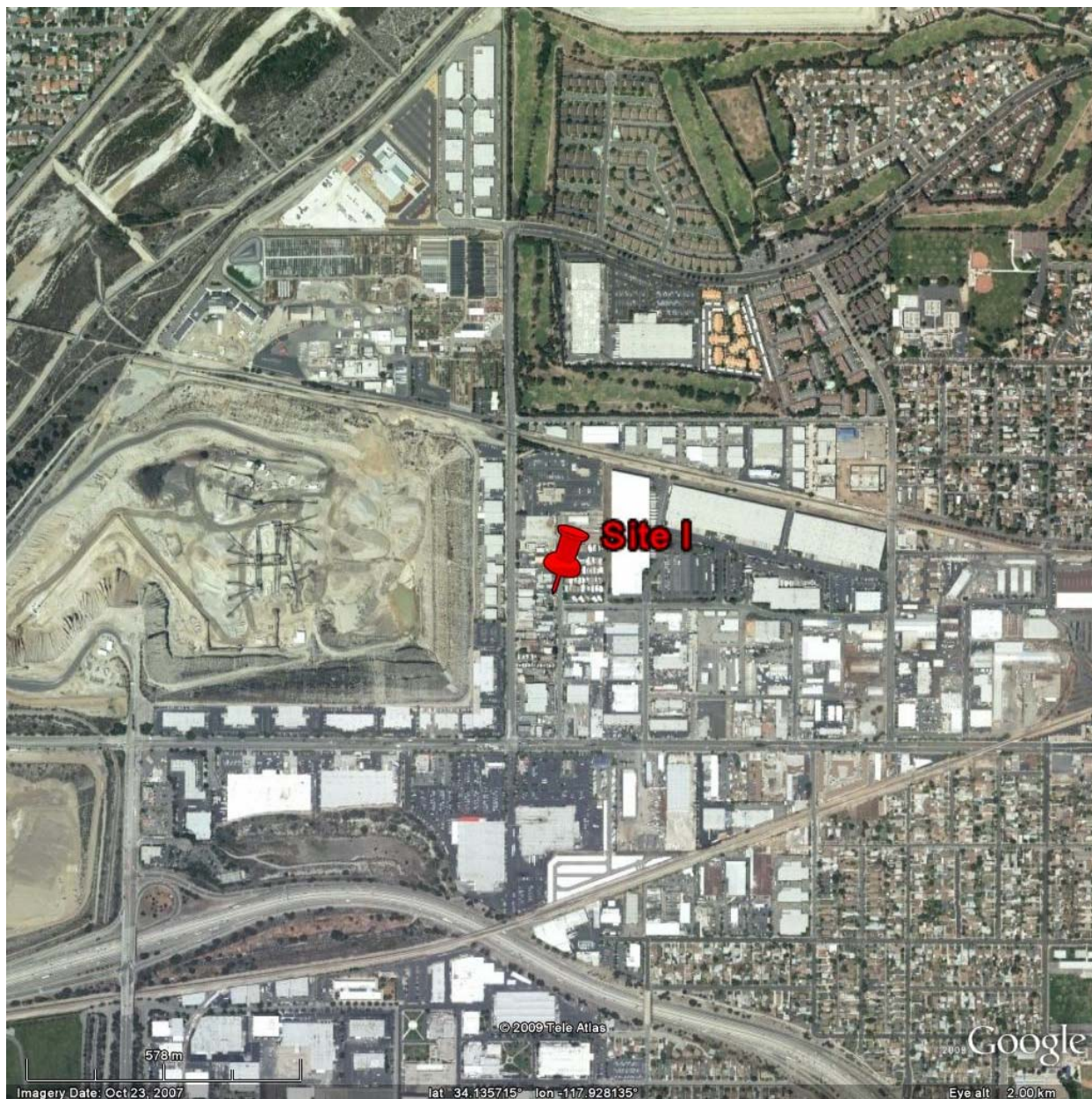


Figure 3-25. Aerial view of the location of CO monitor I (marked by the red pin) in Azusa, CA (Los Angeles CSA), depicting its proximity to mixed use land. Scale: 1 cm = 145 m.

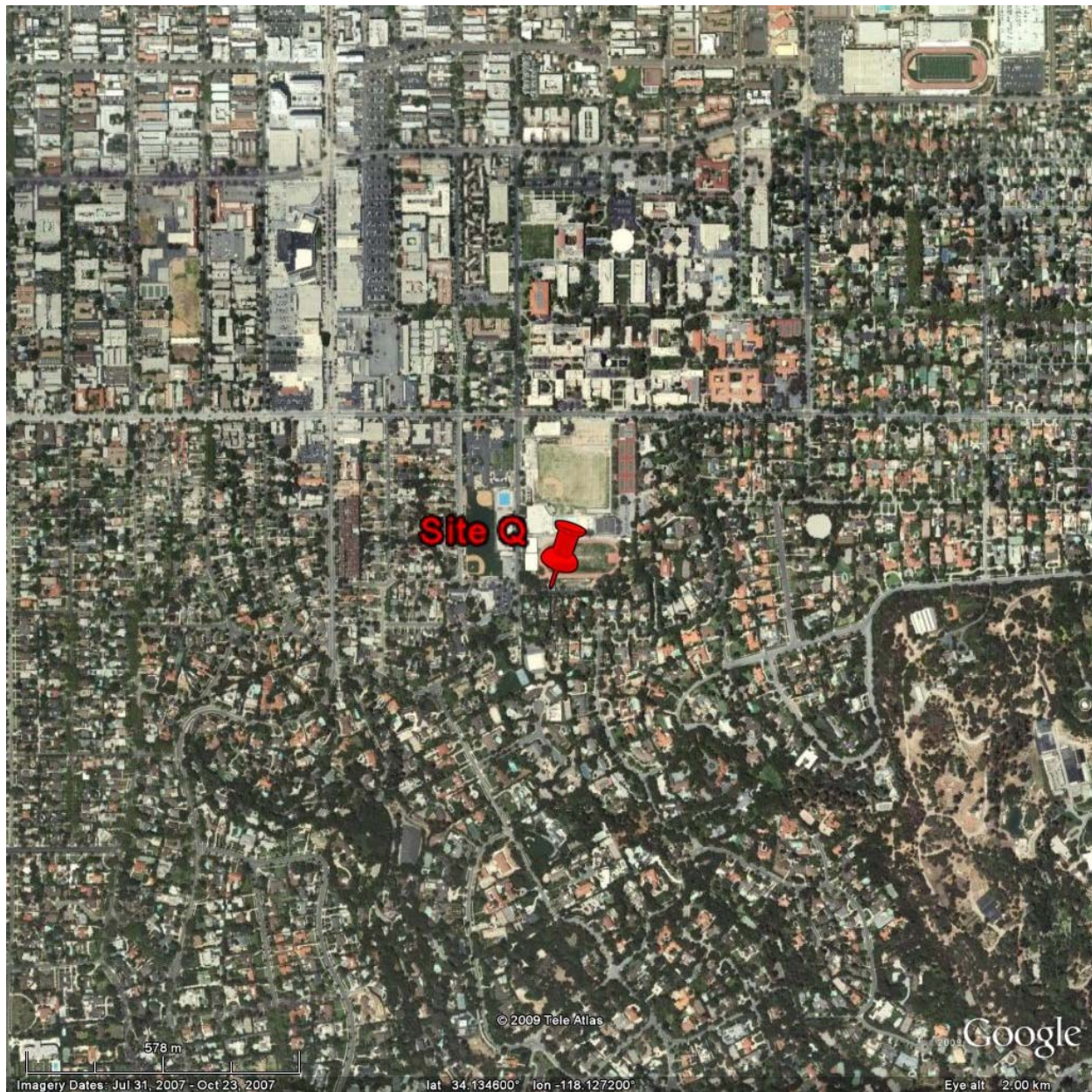


Figure 3-26. Aerial view of the location of CO monitor Q (marked by the red pin) in Pasadena, CA (Los Angeles CSA), depicting its proximity to a residential neighborhood. Scale: 1 cm = 145 m.

3.5.1.3. Micro- to Neighborhood Scale and the Near-Road Environment

Table 3-12 shows the 2005-2007 nationwide distributional data for all hourly, 1-h daily max, 1-h daily avg, and 8-h daily max CO concentrations broken down by spatial sampling scale. The different sampling scales included in the table (microscale, middle scale, neighborhood scale and urban scale) were defined in Section 3.4.2.1. While monitors classified under all four scales are used for highest concentration monitoring and regulatory compliance, individual monitors are classified by spatial scale to be used for addressing more particular monitoring objectives. Microscale, middle scale, and neighborhood scale monitors are used to quantify source impacts while neighborhood scale and urban scale monitors are used for population-oriented monitoring (40 CFR Part 58 Appendix D). For CO, traffic is the major source in an urban setting and therefore microscale data are sited “to represent distributions within street canyons, over sidewalks, and near major roadways” with at least one monitor sited to capture maximum concentrations, while middle scale monitors are sited to represent “air quality along a commercially developed street or shopping plaza, freeway corridors, parking lots and feeder streets” (40 CFR Part 58 Appendix D). The data used to create Table 3-12 were subject to the same 75% completeness criteria described in Section 3.5.1.1. More than 50% of the reported hourly data fell below the reported LOD (reported as 0.5 ppm for the majority of monitors reporting to AQS).

Table 3-12. National distribution of all hourly observations, 1-h daily max, 1-h daily average, and 8-h daily max concentration (ppm) derived from AQS data, based on monitor scale designations, 2005-2007.

Time Scale	n	Mean	Min	PERCENTILES									Max
				1	5	10	25	50	75	90	95	99	
ALL HOURLY													
Microscale	1,428,745	0.6	0.0	0.0	0.1	0.2	0.3	0.5	0.8	1.1	1.4	2.2	19.6
Middle Scale	771,941	0.5	0.0	0.0	0.0	0.1	0.2	0.4	0.6	1.0	1.3	2.3	18.9
Neighborhood Scale	2,878,993	0.4	0.0	0.0	0.0	0.0	0.2	0.3	0.5	0.8	1.1	2.1	35.3
Urban Scale	279,311	0.3	0.0	0.0	0.0	0.0	0.1	0.3	0.5	0.7	0.9	1.6	10.8
1-H DAILY MAX													
Microscale	59,905	1.2	0.0	0.2	0.3	0.4	0.7	1.0	1.5	2.1	2.5	3.9	19.6
Middle Scale	32,659	1.0	0.0	0.1	0.2	0.3	0.5	0.8	1.2	2.0	2.5	4.0	18.9
Neighborhood Scale	121,328	0.9	0.0	0.0	0.1	0.2	0.4	0.6	1.1	1.8	2.4	4.0	35.3
Urban Scale	11,784	0.7	0.0	0.0	0.0	0.1	0.3	0.5	0.9	1.3	1.8	3.1	10.8
1-H DAILY AVERAGE													
Microscale	59,905	0.6	0.0	0.0	0.1	0.2	0.4	0.5	0.8	1.0	1.2	1.7	4.0
Middle Scale	32,659	0.5	0.0	0.0	0.1	0.1	0.3	0.4	0.6	0.9	1.2	1.9	5.5
Neighborhood Scale	121,328	0.4	0.0	0.0	0.0	0.1	0.2	0.3	0.5	0.8	1.0	1.6	7.0
Urban Scale	11,784	0.3	0.0	0.0	0.0	0.0	0.2	0.3	0.5	0.7	0.8	1.2	2.5
8-H DAILY MAX													
Microscale	59,905	0.8	0.3	0.3	0.3	0.3	0.5	0.7	1.1	1.5	1.8	2.6	5.8
Middle Scale	32,659	0.7	0.1	0.3	0.3	0.3	0.3	0.6	0.9	1.4	1.9	2.8	6.2
Neighborhood Scale	121,328	0.6	0.0	0.3	0.3	0.3	0.3	0.4	0.8	1.2	1.6	2.7	10.9
Urban Scale	11,784	0.5	0.0	0.2	0.3	0.3	0.3	0.4	0.7	1.0	1.3	2.1	4.0

The median hourly CO concentration across the U.S. obtained at microscale monitors was 25% higher than at middle scale and 67% higher than at neighborhood scale. However, measurements at or below the median hourly concentration were almost entirely below the LOD for all scales, thereby limiting the usefulness of hourly median comparisons. The upper percentiles (90% and above), however, were all above the LOD and reveal consistently lower hourly concentrations for the urban scale monitors relative to the other monitors. For example, the 99th percentile of reported hourly values was 2.2, 2.3, and 2.1 ppm for microscale, middle scale and neighborhood scale, respectively, compared to 1.6 ppm for urban scale. Similar patterns were present in the 1-h daily max, 1-h daily average, and 8-h daily max distributions. Overall, the urban scale nationwide distributions tended to have lower concentrations relative to neighborhood scale, middle scale and microscale distributions (Table 3-12).

Distributions categorized by spatial scale and CSA/CBSA are provided in Figure 3-27 for hourly data and in Figure 3-28 for 1-h daily max data for the select CSAs/CBSAs where data were available at multiple scales (not all scales were reported by each CSA/CBSA studied). Tables A-17 through A-26 of Annex A contain tabular distributions for all CSAs/CBSAs except Anchorage. On a city-by-city basis, there was considerable variability when comparing distributions at the available spatial scales. With a few exceptions, however, the distribution of microscale and middle scale monitors tended to be higher than those obtained from neighborhood and urban scale monitors. For example, in CSAs/CBSAs containing both microscale and neighborhood scale monitors (Boston, Denver, Houston, Los Angeles, New York and Phoenix), median hourly concentrations at monitors sited for microscale were 20-40% higher than for middle scale and 0-150% greater than those sited for neighborhood scales. At the 99th percentile, microscale concentrations ranged from 31% less than to 59% greater than middle scale concentrations and from 14% less than to 67% greater than neighborhood scale. For most cities, the median hourly data are near or below the 0.5 ppm LOD reported for most monitors in use. In general, these data suggest that CO concentrations measured with monitors sited at micro- and middle scales, typically near roads, were somewhat elevated compared with neighborhood and urban scale monitor locations. However, the magnitude of these differences varies by city and is difficult to discern given the predominance of CO concentrations near or below the LOD.

Despite differences in concentrations observed at different scales (Figure 3-27 and Figure 3-28), intersampler correlations do not follow a distinct trend with respect to spatial monitoring scale (Table 3-10 and Table 3-11). For instance, intersampler correlation in Denver ranged from 0.46 to 0.76 among microscale monitors and was 0.52 for the correlation between the two neighborhood scale monitors (no monitors in Denver reporting to the AQS are sited at middle scale). Intersampler correlation in Los Angeles ranged from 0.44 to 0.73 for middle scale, and the one pair of neighborhood scale monitors had a correlation of 0.43. Only one monitor was sited each at microscale and urban scale, and 16 of the 24 CO monitors in Los Angeles are not declared to sample at any spatial scale (scale designation = "null"). In Denver, the distribution of hourly CO data obtained at microscale was nearly identical to that obtained at neighborhood scale. In Los Angeles, the microscale data was typically higher than middle, neighborhood, or urban scale data except at the upper end of the distribution, where middle scale data were higher for both hourly and 1-h daily max data (Figure 3-27 and Figure 3-28).

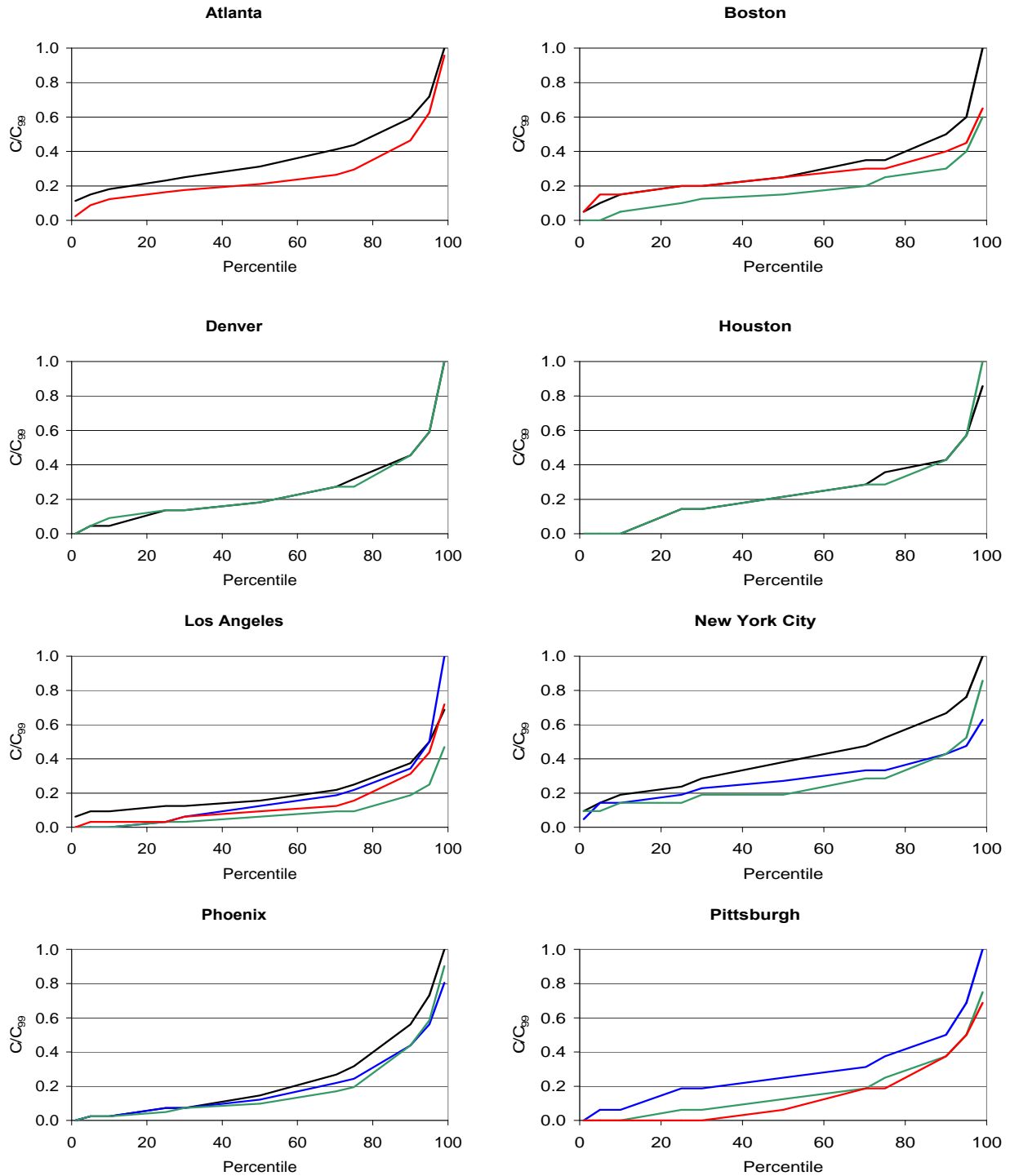


Figure 3-27. Distribution of hourly CO concentration data by city and monitoring scale. For comparison purposes, the y-axis has been scaled to the city-specific 99th percentile concentration. Note that Anchorage, Seattle, and St. Louis CSAs are not included here because these cities do not have monitors sited at different scales.

- microscale
- middle scale
- neighborhood scale
- urban scale

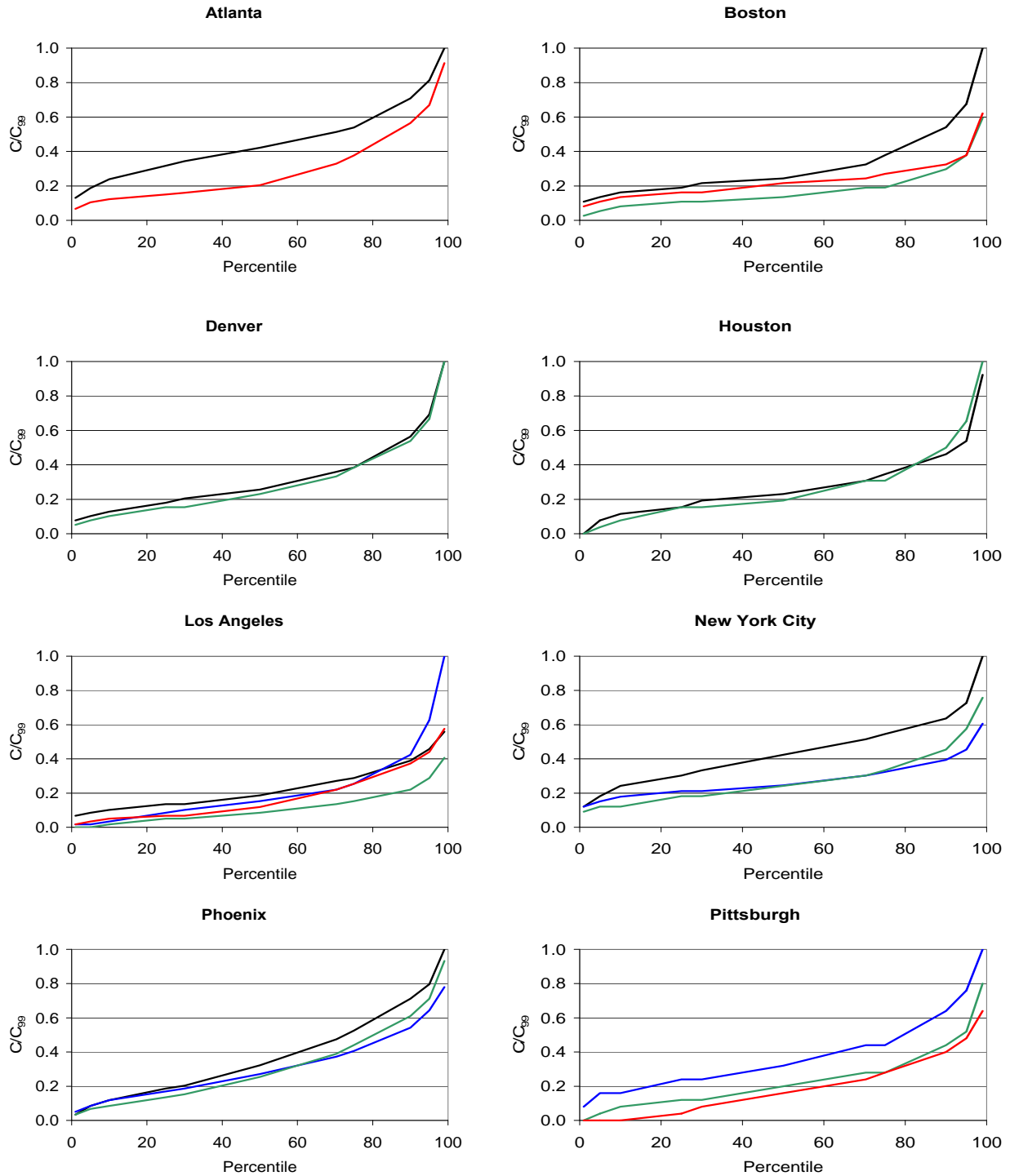
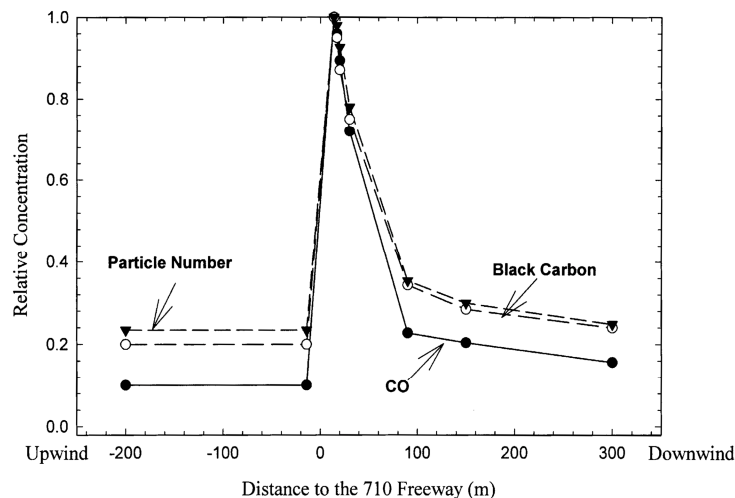


Figure 3-28. Distribution of 1-h daily max CO concentration data by city and monitoring scale. For comparison purposes, the y-axis has been scaled to the city-specific 99th percentile concentration. Note that Anchorage, Seattle, and St. Louis CSAs are not included here because these cities do not have monitors sited at different scales.

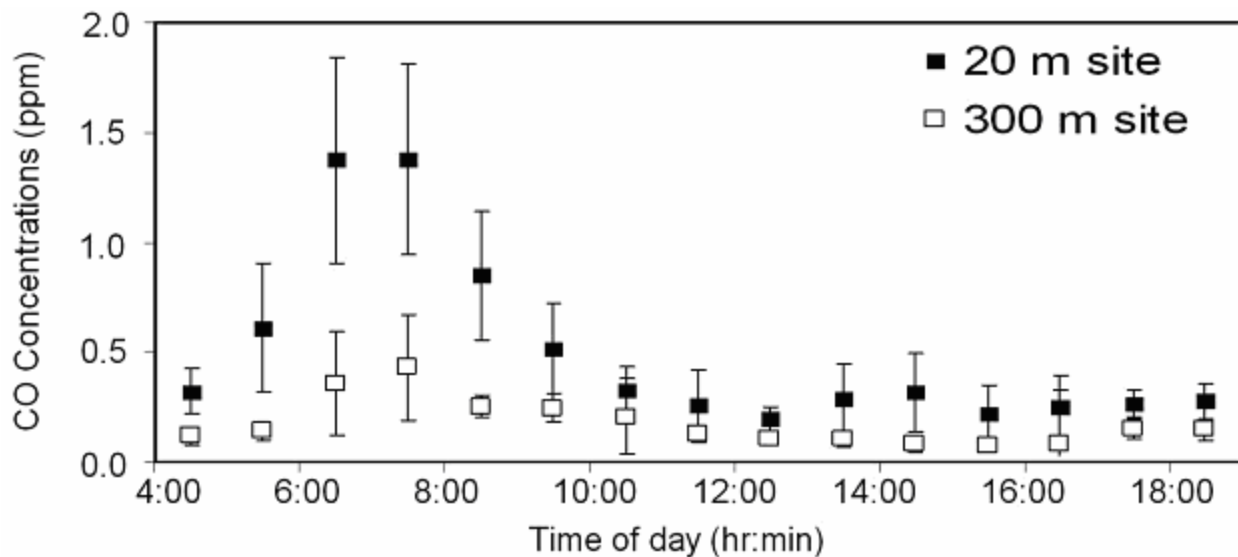
— microscale
 — middle scale
 — neighborhood scale
 — urban scale

The microscale and middle scale CO data reported here are consistent with hourly concentrations reported in the literature for the near-road environment within the U.S. Baldauf et al. (2008, [190239](#)) reported CO concentrations obtained 20 m from an interstate highway in Raleigh, NC, to have a median around 0.25 ppm and with maximum concentration <4.0 ppm. Zhu et al. (2002, [041553](#)) reported CO concentration of 1.9-2.6 ppm at a distance of 17 m from an interstate highway in Los Angeles, with concentration decreasing exponentially with distance from the highway. Zhu et al. (2002, [041553](#)) observed on-road CO concentrations to be approximately 10 times higher than at an upwind monitoring site, as shown in Figure 3-29. Concentrations continued to decrease and were still two times higher than upwind levels at a monitoring site 300 m away. Baldauf et al. (2008, [190239](#)) also reported a drop in concentration at a monitoring site 300 m from the road compared with the 20 m site. Figure 3-30 illustrates the distribution of measurements taken throughout a day. In this plot, the near-road (20 m distance) CO concentrations tended to be significantly higher than those obtained at 300 m, and the daily variability in the CO concentration time series was greater at the 20 m site than at the 300 m site. The ratio of 20 m to 200 m concentrations was higher for the Zhu et al. (2002, [041553](#)) paper. This was likely due to the fact that the 300 m site was always downwind in Zhu et al. (2002, [041553](#)), whereas winds were more variable in Baldauf et al. (2008, [190239](#)). Other near-road measurements reported in the literature are similar to those from the Zhu et al. (2002, [041553](#)) and Baldauf et al. (2008, [190239](#)) studies. Chang et al. (2000, [001276](#)) reported near-road ambient CO measurements obtained in downtown Baltimore (distance to road not specified) in the range of 0.5-1.3 ppm. Riediker et al. (2003, [043761](#)) reported measurements of CO concentration obtained near one of four heavily-trafficked roads in Wake County, NC, to average 1.1 ppm (range: 0.4-1.7 ppm). Neighborhood scale measurements reported in the literature were also consistent with if not slightly lower than those reported by AQS. Gentner et al. (2009, [194034](#)) reported CO concentrations ranging from roughly 0.4-0.9 ppm in Riverside, CA, 1 km east of an interstate highway. Singh et al. (2006, [190136](#)) reported 24-h avg CO concentrations, obtained with a 0.04 ppm LOD CO monitor in Long Beach, CA, within 0.5 km and 1.5 km of two interstate highways, to range from 0.2-1.4 ppm.



Source: Reprinted with Permission of Elsevier Ltd. from Zhu et al. (2002, [041553](#))

Figure 3-29. Relative concentrations of CO and copollutants at various distances from the I-710 freeway in Los Angeles.



Source: Reprinted with Permission of Air and Waste Management Association from Baldauf et al. (2008, [190239](#))

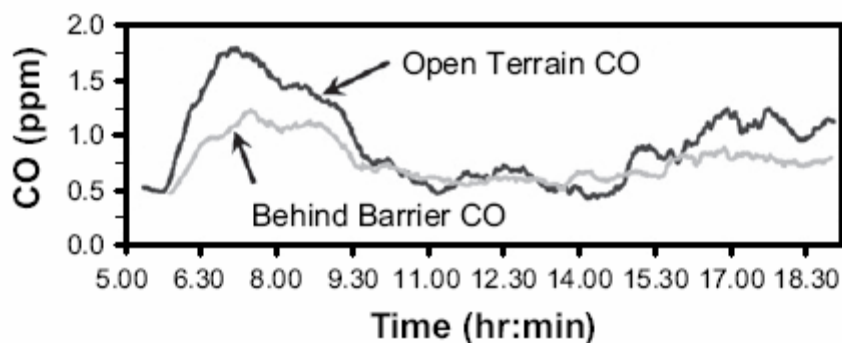
Figure 3-30. CO concentration time series 20 m and 300 m from the I-440 highway in Raleigh, NC. Symbols denote the mean concentration, and whiskers denote standard deviations.

Determinants of spatial variability in ambient CO concentration include roadway density, traffic counts, meteorology, and natural and urban topography. Mobile sources are the largest single source of CO, and their abundance and density affect the magnitude of CO production. Rodes et al. (1998, [010611](#)) compared traffic volume, roadway type, and concentrations of CO and several copollutants in Los Angeles and Sacramento, CA, in a study of on-road traffic emissions. They noted that there was little difference in CO concentration between arterial roads and freeways for Los Angeles. Rodes et al. (1998, [010611](#)) found that traffic was also much more congested throughout Los Angeles. This finding was not surprising given that Los Angeles is a much larger city with substantially higher traffic volumes than Sacramento. Under similar wind conditions, morning concentrations were much higher in Los Angeles than Sacramento. Rodes et al. (1998, [010611](#)) observed that high afternoon winds ventilate Los Angeles, but Sacramento is not as well ventilated. As a result, Sacramento has nearly the same concentrations as Los Angeles in the afternoon. This observation is consistent with measurements by Gentner et al. (2009, [194034](#)), showing that CO concentrations varied inversely with wind speed.

Measured on-road and road-side CO concentrations may also relate to the traffic volume. Among the 291 active sites where monitors met completeness criteria during 2005-2007, 57 were declared by state agencies as microscale with average annual daily traffic (AADT) counts on the nearby roads ranging from 500 vehicles per day at one site in Denver, CO to 133,855 vehicles per day in Tampa, FL with a geometric mean of 17,462 vehicles per day and a geometric standard deviation of 2.5 (Table A-2 of Annex A). Within a geometric standard deviation, the data range from 6,576-40,000 vehicles per day. Only two monitors were sited at roads with 100,000 vehicles per day or more. In contrast, the site where Zhu et al. (2002, [041553](#)) collected data had 160,000-178,000 vehicles per day in 2001 (CalTrans, 2009, [194036](#)). Microscale sites near roads in the mid-range of the traffic count data may record data that are not substantially different from those obtained from neighborhood scale measurements, as indicated in Table 3-12. Likewise, with little microscale data at roads with AADT of more than 100,000 vehicles per day, there is still much uncertainty regarding the magnitude of concentrations in the near-road environment.

Field measurements, computational modeling, and wind tunnel experiments have shown that roadway design, roadside structures and vegetation, and on-road traffic levels can affect concentrations of CO and other pollutant concentrations near roadways. Field measurements reported by Baldauf et al. (2008, [191017](#)) indicated that noise barriers could reduce near-road pollutant concentrations by as much as 50%, although this effect was highly dependent on

meteorological conditions; these results are illustrated in Figure 3-31. This study also showed that the presence of mature vegetation further reduced concentrations and flattened the concentration gradient away from the road. Urban dispersion and wind-field modeling by Bowker et al. (2007, [149997](#)) also demonstrated the influence of noise barriers and vegetation on the concentrations and spatial variability of nonreactive pollutants emitted from traffic sources. Heist et al. (2009, [194037](#)) ran wind tunnel experiments using a model of a road with different roadside features and a tracer gas line source emitted from the simulated road to study how concentrations of gaseous traffic emissions vary spatially in the near-road environment. They demonstrated that noise barriers and roadway design characteristics, such as the presence of embankments and elevated roadway segments, can alter airflow and contaminant dispersion patterns in the near-road environment. For example, their results indicated that roadway design having below-grade sections of road and embankments reduced concentrations away from the road. These results showed similar concentrations as those of Zhu et al. (2002, [041553](#)), both for roadway segments at-grade with no obstructions to air flow and for elevated roadway segments with different road fill conditions. Additionally, Khare et al. (2005, [194016](#)) illustrated in a wind tunnel study that vertical dispersion of a nonreactive gas increased with increasing simulated traffic volume; this effect was also sensitive to changes in approaching wind direction. These studies taken together suggest that localized turbulence induced by roadside structures, roadway design, and traffic provide some mixing and resulting dilution of the CO concentration in the near-road environment; the extent of mixing effects varies by meteorological conditions and the specific roadway design and traffic loading.

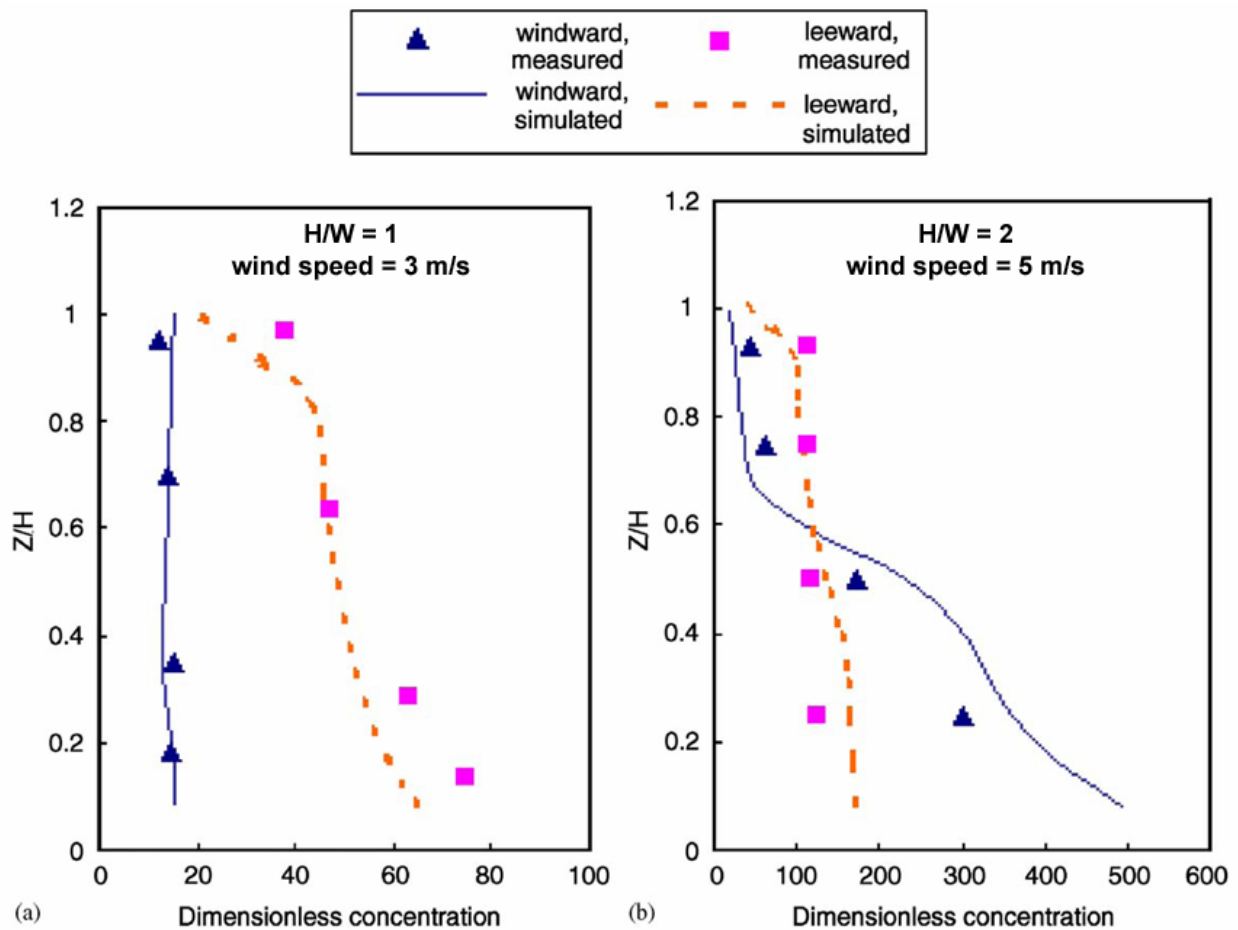


Source: Reprinted with Permission of Elsevier Ltd. from Baldauf et al. (2008, [191017](#))

Figure 3-31. CO concentration profile 10 m from I-440 in Raleigh, NC, behind a noise barrier and in open terrain.

The geometry of urban street canyons has a profound effect on the distribution of CO concentrations on a microscale. A number of studies have performed computational and wind tunnel modeling of street canyons using nonreactive tracers and demonstrated the potential variability in concentration within a canyon (e.g., Borrego et al., 2006, [155697](#); Chang and Meroney, 2003, [090298](#); Kastner-Klein and Plate, 1999, [001961](#); So et al., 2005, [110746](#); Xiaomin et al., 2006, [156165](#)). Because CO is a pollutant with very low reactivity on urban and regional scales, results from these models are directly relevant to CO concentration distributions in street canyons. Parameters influencing street canyon dispersion include canyon height to width ratio (H/W), source positioning, wind speed and direction, building shape, and upstream configuration of buildings. Figure 3-32 shows dimensionless concentrations obtained from wind tunnel and computational fluid dynamics simulations of tracer gas transport and dispersion in an infinitely long street canyon with a line source centered at the bottom of the canyon (Xiaomin et al., 2006, [156165](#)). When the canyon height was equal to the street width (typical of moderate density suburban or urban fringe residential neighborhoods) and lower background wind speed existed, concentrations on the leeward (downwind) canyon wall were four times those of the windward (upwind) wall near ground level.

When the canyon height was twice the street width (typical of higher-density cities) and background winds were somewhat higher, near ground-level concentrations on the windward canyon wall were roughly three times higher than those measured at the leeward wall. These results suggest that the magnitude of microscale CO concentrations may vary by factors of three or four times at different locations within a street canyon and are heavily influenced by wind speed and street canyon topography. The relationship between in-canyon concentration and wind speed and turbulence is well established with concentration varying inversely with the magnitude of wind speed and turbulence (Britter and Hanna, 2003, [090295](#)). When studying the effect of wind direction on street canyon concentration levels for a continuous “line source” of traffic exhaust, concentration levels were at local maxima under two conditions: wind perpendicular to or parallel to the street canyon. Wind gusts at the turbulence interface at the top of the canyon or traffic-based turbulence can also cause dilution of the exhaust concentration within the canyon (Kastner-Klein et al., 2000, [194035](#)).

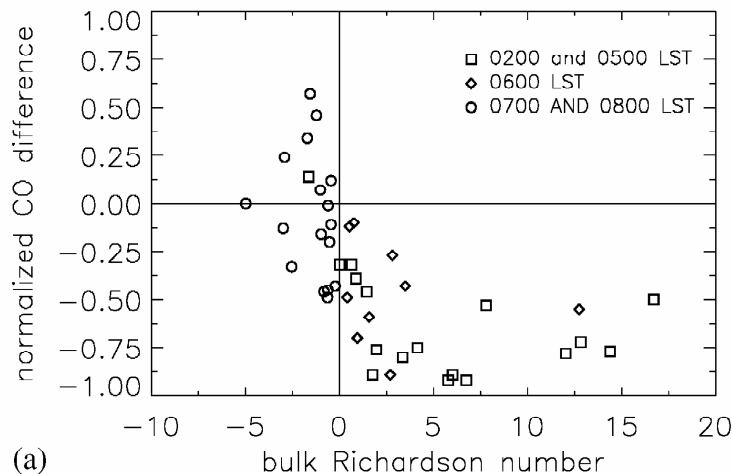


Source: Reprinted with Permission of Elsevier Ltd. from Xiaomin et al. (2006, [156165](#))

Figure 3-32. Dimensionless tracer gas concentration on the windward and leeward sides of the canyon plotted against the elevation of the measurement (Z) scaled by building height (H) under two different H/W and wind speed conditions. Shown are measurements obtained in a wind tunnel (symbols) and model simulations using computational fluid dynamics (lines).

Street canyon field studies support the computational and wind tunnel modeling results described above. In a multisite survey of curbside CO concentration in London, U.K., Croxford and Penn (1998, [087176](#)) observed up to threefold differences in concentration related to the side of the

street on which the monitor was positioned relative to the wind direction, with H/W varying between 0.7 and 1.7 depending on position within the canyon. Bogo et al. (2001, [192378](#)) measured CO concentrations in a street canyon with H/W of 1 in Buenos Aires, Argentina, using a continuous CO monitor. Similar to the Xiaomin et al. (2006, [156165](#)) simulation results for H/W of 1, Bogo et al. (2001, [192378](#)) observed slightly higher leeward concentrations than windward concentrations within the canyon, where recirculating airflow inside the canyon causes pollutants to collect in higher concentration on one side. However, for the case of a deep street canyon (H/W of 5.7) in Naples, Italy, Murena et al. (2008, [194038](#)) observed that the concentrations on two sides of the canyon differed by <15%, with wind direction varying between 10° and 80° from the street axis. Doran et al. (2003, [143352](#)) measured CO concentration in a street canyon in Phoenix, AZ, during the morning hours and observed that CO concentration decreases with elevation above the ground if turbulent mixing is small, but that the difference between ground level and 39th-floor (50 m AGL) measurements of CO concentration decreases when turbulent mixing increases (with maximum measurements at any elevation not exceeding 2 ppm). As shown in Figure 3-33, the larger difference in concentration as a function of turbulent mixing can occur when there are meteorologically stable conditions in the lower boundary layer. These results support findings from the modeling studies that CO concentration can vary by several times within a street canyon and is greatly influenced by local meteorology and building topography.



Source: Reprinted with Permission of Elsevier Ltd. From Doran et al. (2003, [143352](#))

Figure 3-33. Normalized difference between CO measurements taken at ground level and from the 39th floor of a building in a Phoenix, AZ street canyon as a function of bulk Richardson number (Ri). Bulk Ri is a dimensionless number that describes the ratio of potential to kinetic energy, and it is used here as a measure of stability within the street canyon, with greater Ri corresponding to greater stability and values near or less than zero indicating greater mixing.

Research by Kaur and Nieuwenhuijsen (2009, [194014](#)) and Carslaw et al. (2007, [148210](#)) suggests that CO exposures are related to traffic volume and fleet mix in the street-canyon environment. Kaur and Nieuwenhuijsen (2009, [194014](#)) used multiple linear regression to model CO concentration data from central London as a function of mode of transport (broken down by vehicle type), traffic count, wind speed, and temperature. They added each variable successively and found traffic count, temperature, wind speed, and walking to be significant parameters in the model, with traffic count being the strongest determinant. Analysis of variance showed variability in traffic count to explain 78% of the variability in CO levels for these data, and variability in mode of transport explained 6% of the variability. Likewise, Carslaw et al. (2007, [148210](#)) used a generalized additive model to determine how CO concentration data (log-transformed) obtained in central London varied as a function of light- and heavy-duty traffic counts, along-street and cross-street components of

wind, temperature, year, and Julian day. Light-duty vehicle count was a more important determinant of CO concentration than heavy-duty (i.e., diesel) vehicle count in this study. They found that the CO declined steadily with year and that wind was the most significant covariate. In addition to showing meteorology to be an important determinant of concentration, these modeling exercises also suggest a linear or log-linear relationship between concentration and traffic.

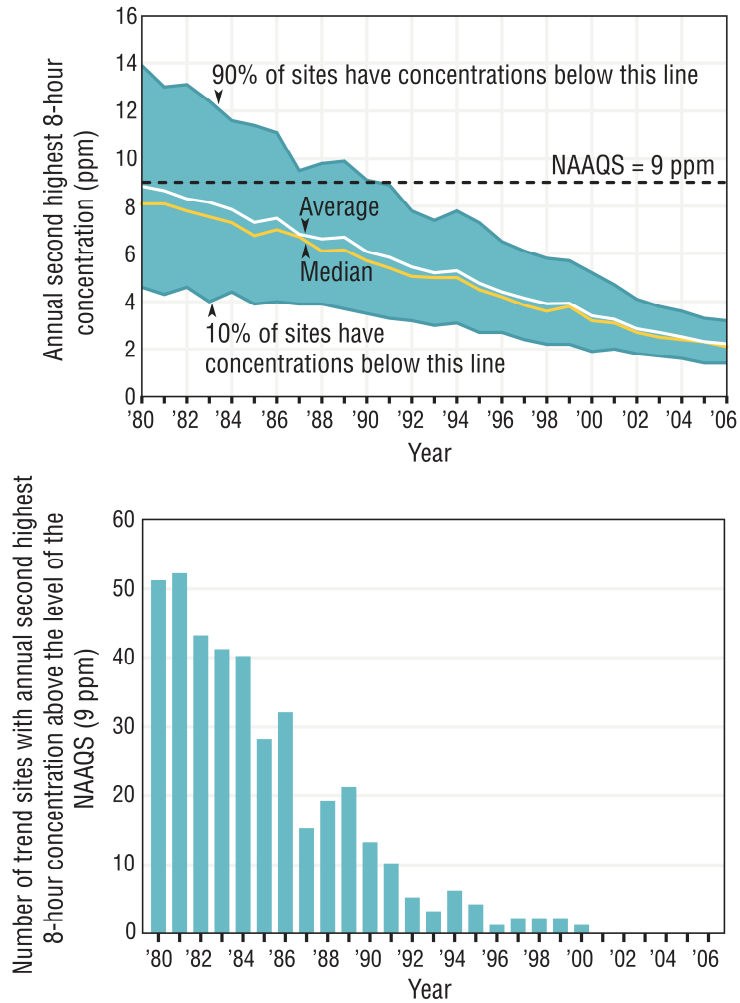
3.5.2. Temporal Variability

3.5.2.1. Multiyear Trends

Figure 3-34 (top) shows ambient CO concentrations in ppm from 1980 to 2006 based on continuous measurements averaged over 8-h time segments. Figure 3-34 (bottom) depicts trends in the annual second-highest 8-h CO concentrations for 144 sites in 102 counties nationwide having data either in the SLAMS network or from other special purpose monitors.

The 2006 annual second highest 8-h CO concentration averaged across 144 monitoring sites nationwide was 75% below that for 1980 and is the lowest recorded during the past 27 yr (Figure 3-34 [top]). Since 1992, more than 90% of these sites have reported second highest CO concentrations below the 8-h NAAQS of 9 ppm. The mean annual second highest 8-h ambient CO concentration has been below 5 ppm since 2004. The downward trend in CO concentrations in the 1990s parallels the downward trend observed in CO emissions, attributed largely to decreased mobile source emissions. In addition, of the 144 sites used to determine this trend, from a total of 375 monitoring sites operating in 2006, the number reporting second-highest 8-h CO concentrations above the level of the NAAQS declined to zero over the same period (Figure 3-34 [bottom]).

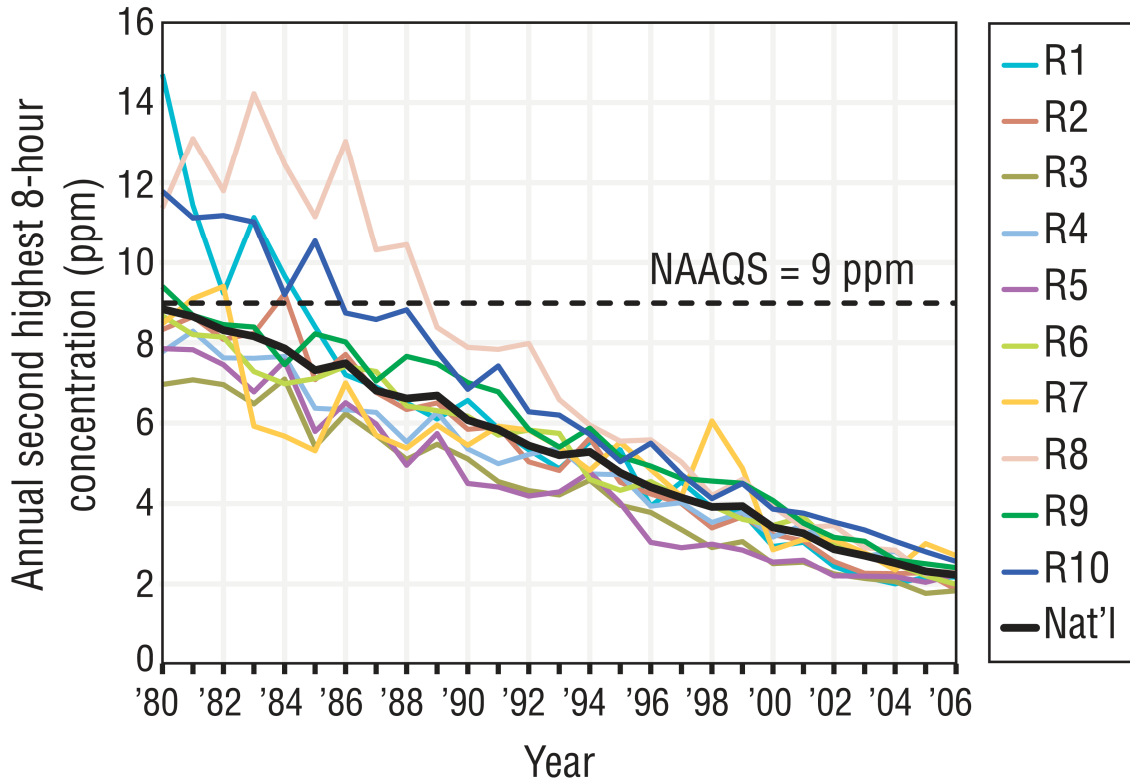
Consistent with the nationwide trends in emissions and concentrations, CO concentrations in all 10 EPA Regions have steadily decreased since 1980, with reductions over this period ranging from 68% in Region 7 to 85% in Region 1 (Figure 3-35). This is also consistent with declining emissions seen in many regions of the U.S., shown in Figure 3-5.



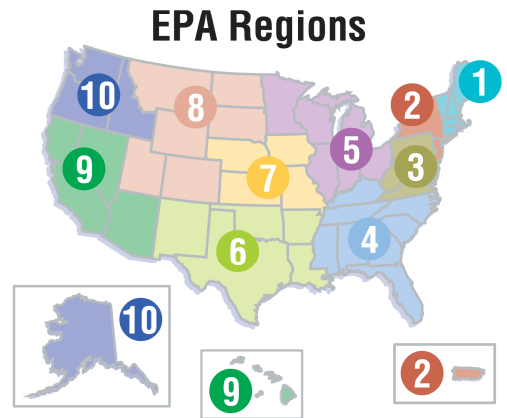
Coverage: 144 monitoring sites in 102 counties nationwide (out of a total of 375 sites measuring CO in 2006) that have sufficient data to assess CO trends since 1980.

Source: U.S. EPA (2008, [157076](#))

Figure 3-34. (Top) Trends in ambient CO in the U.S., 1980-2006, reported as the annual second highest 8-h concentrations (ppm) for the mean, median, 10% and 90% values. (Bottom) Trends in ambient CO in the U.S., 1980-2006, reported as the number of trend sites (y-axis) with annual second highest 8-h concentrations above the level of the NAAQS (9 ppm).



Coverage: 141 monitoring sites in the EPA Regions (out of a total of 375 sites measuring CO in 2006) that have sufficient data to assess CO trends since 1980.



Source: U.S. EPA (2008, [157076](#))

Figure 3-35. Trends in ambient CO in the U.S., 1980-2005, reported as the annual second highest 8-h concentrations (ppm) for the EPA Regions 1 through 10, along with a depiction of the geographic extent of those Regions.

3.5.2.2. Hourly Variation

Weekday and weekend diel variation for the mean, median, 5th, 10th, 90th, and 95th percentiles of hourly CO concentration over 2005-2007 are shown in Figure 3-36 and Figure 3-37, respectively, for the 11 CSAs and CBSAs examined in this assessment. Since these figures represent the distribution of hourly observations over a 3-yr period, any fluctuations or changes in the timing of the daily peaks would result in a broadening of the curves shown in the diel plot compared to the actual daily temporal behavior on any specific day measured by an individual monitor. However, these figures are useful for comparing the general hourly variation in CO concentrations across cities and by day of the week (i.e., weekday versus weekend). The weekday data showed that the Anchorage mean, median, 5th and 10th percentile CO concentration curves exhibit pronounced morning and evening rush hour peak CO levels. Boston, Denver, Houston, Los Angeles, Phoenix, Pittsburgh, and St. Louis all exhibited similar trends, although the magnitude of the concentrations shown was roughly twice as high for Anchorage as the other cities. The curves had less overall variability for Boston, Pittsburgh, and St. Louis. The Atlanta plot shows that the median concentration was fairly constant throughout the 24-h period, with a slightly elevated mean during the morning hours. The 90th and 95th percentile curves exhibit stronger morning and evening CO concentration peaks. New York City shows fairly constant CO mean and median concentration throughout the day, with slight elevations throughout the morning rush hour and a slight trough between 1:00 and 5:00 a.m. The Seattle plot shows a daytime plateau beginning around 5:00 a.m. and lasting until roughly 10:00 p.m., with higher concentrations during morning and afternoon rush hour. Differences in hourly variation among the 11 CSAs and CBSAs reflect city-to-city variation in source characteristics and meteorology. For instance, the rush hour peaks in many cities likely correspond to increased mobile source emissions during those periods. Local meteorology and topography, which influence mixing heights, can also affect hourly variation in CO concentration.

Figure 3-37 illustrates weekend diel trends for the 11 CSAs and CBSAs considered in this assessment. For Anchorage during the period 2005-2007, the mean and median concentration curves peaked during the morning and evening hours. A daytime concentration trough is evident. The 90th and 95th percentiles of concentration were similar but more pronounced. The shape of this plot is also characteristic of Atlanta, Boston, Denver, Houston, Los Angeles, Phoenix, Pittsburgh, Seattle, and St. Louis, although the Anchorage CO concentrations are nearly 100% higher than concentrations in the other cities. The weekend diel plot for New York City shows that the mean and median CO concentrations remain fairly constant throughout the day, with a slight reduction between 2:00 and 7:00 a.m. The 90th and 95th percentile curves illustrate more diel variation.

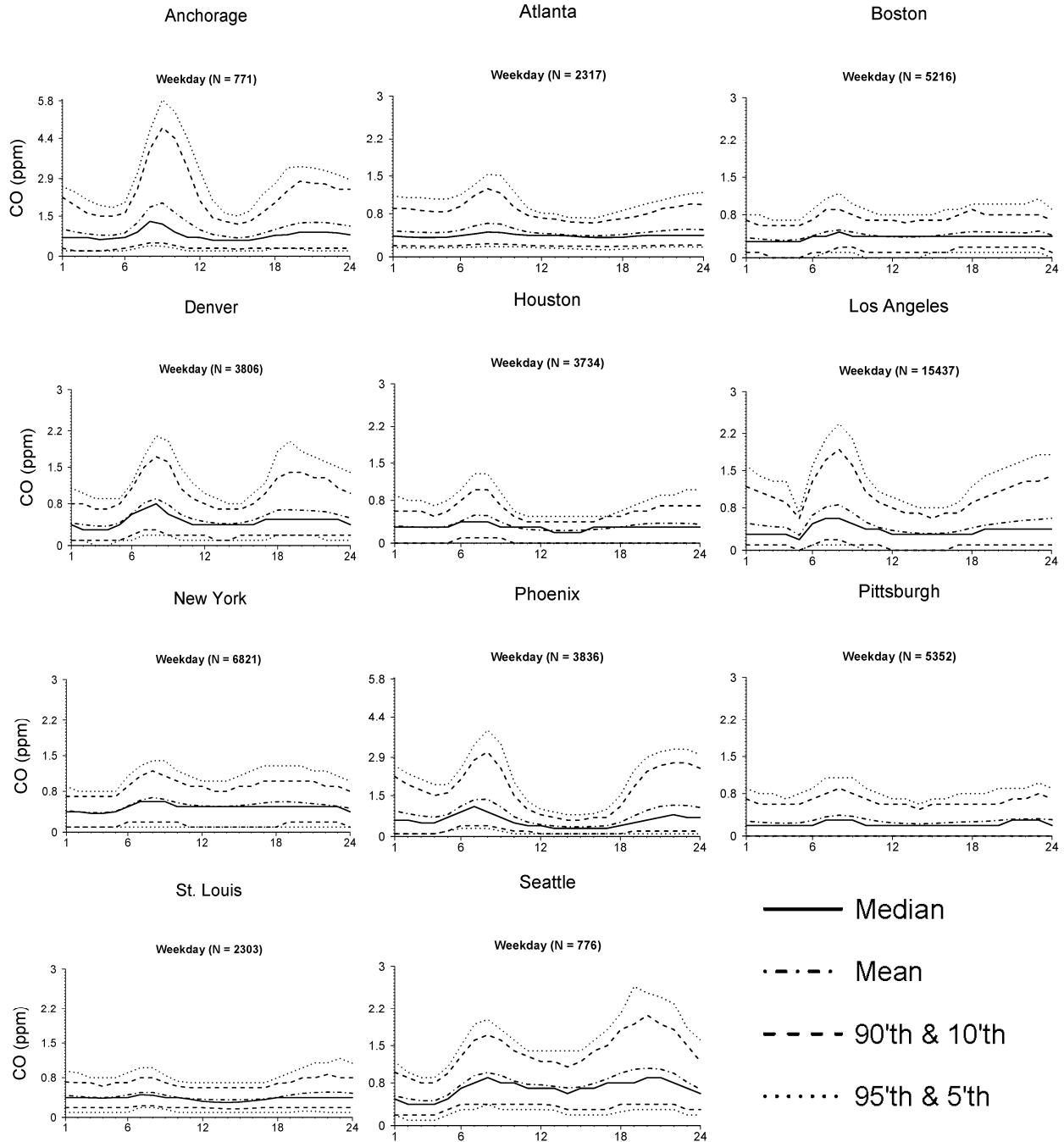


Figure 3-36. Diel plot generated from weekday hourly CO data (ppm) for the 11 CSAs and CBSAs, 2005-2007. Included are the number of monitor days (N) and the median, mean, 5th, 10th, 90th and 95th percentiles of composite CO concentrations plotted by time of day. Note that the y-axis of the Anchorage and Phoenix plots are scaled to 5.8 ppm while the other plots are scaled to 3.0 ppm.

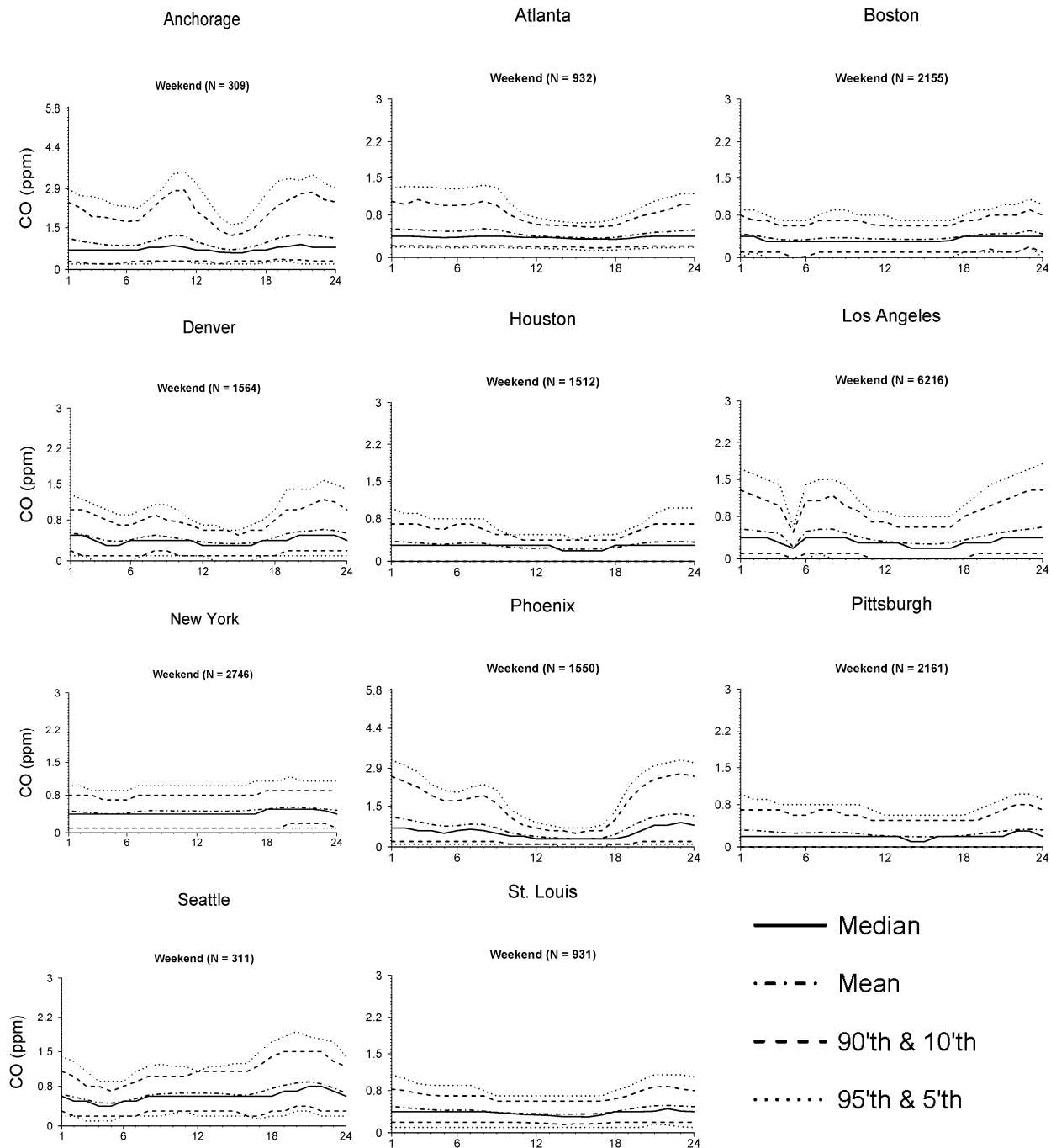


Figure 3-37. Diel plot generated from weekend hourly CO data (ppm) for the 11 CSAs and CBSAs, 2005-2007. Included are the number of monitor days (N) and the median, mean, 5th, 10th, 90th and 95th percentiles of composite CO concentrations plotted by time of day. Note that the y-axis of the Anchorage and Phoenix plots are scaled to 5.8 ppm while the other plots are scaled to 3.0 ppm.

3.5.3. Associations with Copollutants

Associations between hourly CO and other copollutants, including SO₂, NO₂, O₃, PM₁₀, and PM_{2.5} are provided in box plots in Figure 3-38 using AQS data across the U.S. AQS data were obtained from all available co-located monitors across the U.S. after application of the 75% completeness criteria described earlier in Section 3.5.1.1. Pearson correlation coefficients (r) were calculated using 2005-2007 data stratified by season. Correlation plots analogous to Figure 3-38 for select individual cities are provided in Annex A, Figures A-43 to A-48.

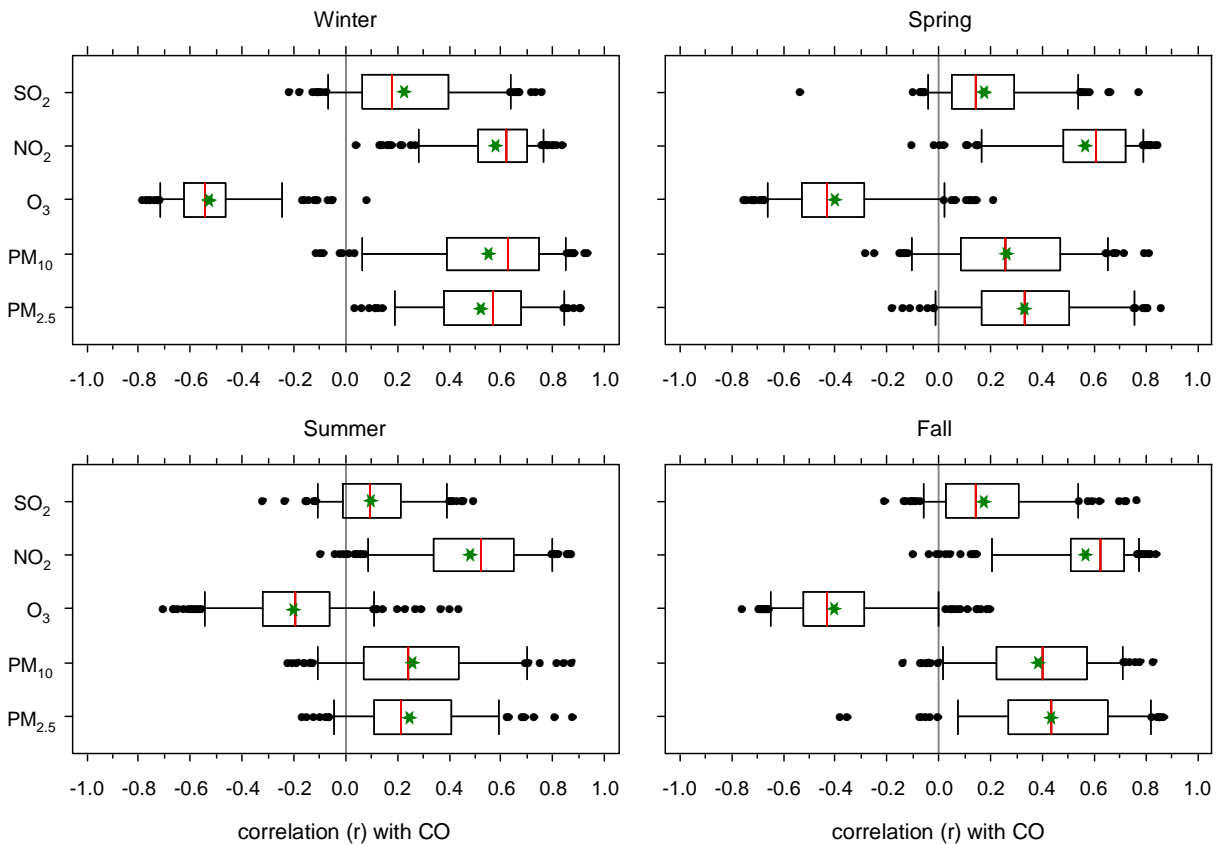


Figure 3-38. Seasonal plots showing the variability in correlations between hourly CO concentration and co-located hourly SO₂, NO₂, O₃, PM₁₀ and PM_{2.5} concentrations. Red bars denote the median, green stars denote the arithmetic mean, the box incorporates the IQR, and the whiskers extend to the 5th and 95th percentiles. Correlations outside the 5th and 95th percentiles are shown as individual points.

In all cases, a wide range of correlations existed between CO and copollutants as illustrated in Figure 3-38. The mean and median correlation between CO and copollutants were positive for NO₂, PM₁₀, and PM_{2.5}; near zero for SO₂; and negative for O₃. These findings reflect common combustion sources for CO, NO₂, and PM. CO is highly correlated with NO₂ and PM_{2.5} because they are both emitted directly during incomplete combustion and because secondary nitrate PM comes from NO_x, which is largely produced from mobile sources. Among those copollutants with positive associations, NO₂ had the highest mean and median correlations, followed by PM_{2.5} and PM₁₀ (correlations vary by season). The IQR of correlations with SO₂ spanned from positive to negative for all seasons; SO₂ would not be expected to correlate well with CO because SO₂ emanates primarily from industrial sources. Correlations between CO and O₃ were almost entirely negative for

winter, when CO emissions tend to be high and O₃ formation is low. During the other three seasons, most of the CO-O₃ correlations were also negative. Given the role of CO in O₃ chemistry, cross-correlation functions were also computed by season for the CO-O₃ relationship (Annex A, Figure A-50). The data showed negative correlations at all lags with minima at zero lag for winter, spring, and fall. During the summer, a small positive peak correlation ($r = 0.071$) was centered at a lag of -8 h and a minima occurred at a lag of 1 h, $r = -0.272$. It is not known whether the positive lagged correlations in summertime are related to interaction of CO with O₃ through chemistry, coinciding independent effects such as peak times for rush hour CO emissions and afternoon O₃ formation, or some combination of interactive and independent effects. However, given the very low magnitude of these correlations, it is clear that many other factors influence the O₃ and CO time series.

Within and between individual metropolitan areas, the distribution of copollutant correlations varied substantially. Figure 3-39 and Figure 3-40 illustrate the correlations between CO and copollutants for Denver, CO, and Los Angeles, CA, to exemplify these differences. Copollutant correlation plots are also shown for other cities in Annex A, Figures A-44 through A-49. For instance, correlations between CO and copollutants are all positive for SO₂, NO₂, PM₁₀, and PM_{2.5} and are all negative for O₃ in Denver. In contrast, the correlations in Los Angeles span from negative to positive for O₃, PM₁₀, and PM_{2.5}, in various seasons. The larger span of correlations for Los Angeles in comparison with Denver could result from several factors. For example, more variation in meteorology, topography, or source distribution with respect to monitor placement in Los Angeles may cause the distribution of copollutant correlations to be wider. In addition, fewer co-located monitors in Denver compared with Los Angeles may be causing some of the observed differences.

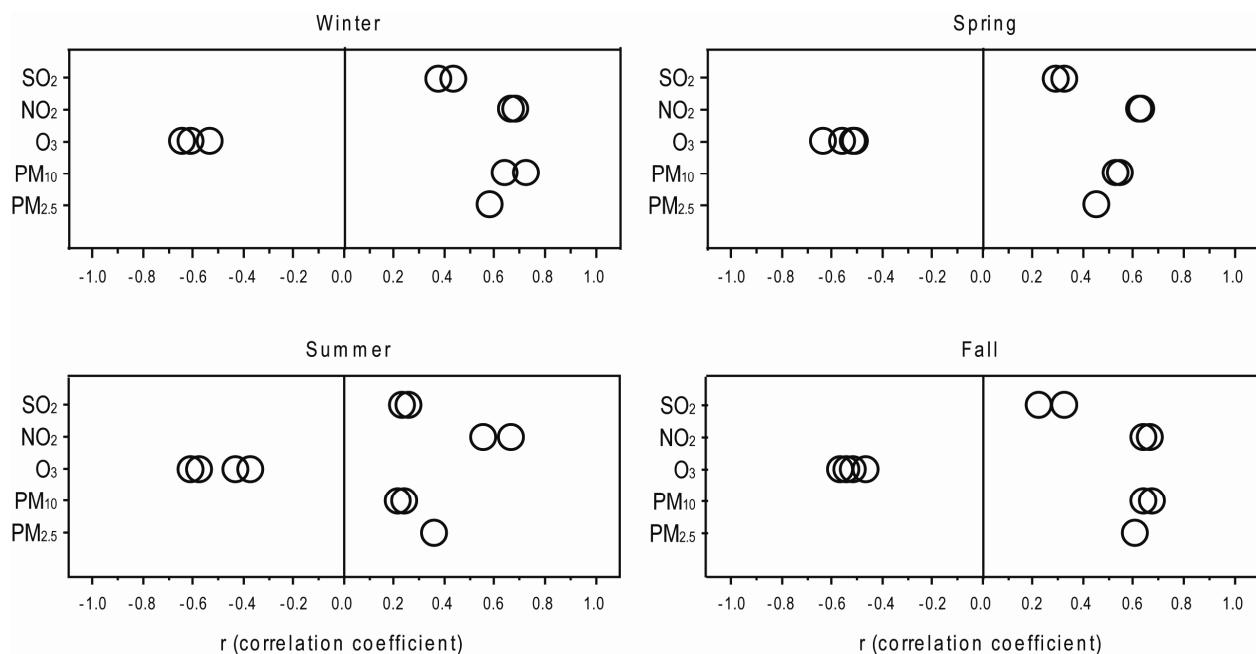


Figure 3-39. Seasonal plots showing the variability in correlations between hourly CO concentration and co-located hourly SO₂, NO₂, O₃, PM₁₀ and PM_{2.5} concentrations for Denver, CO.

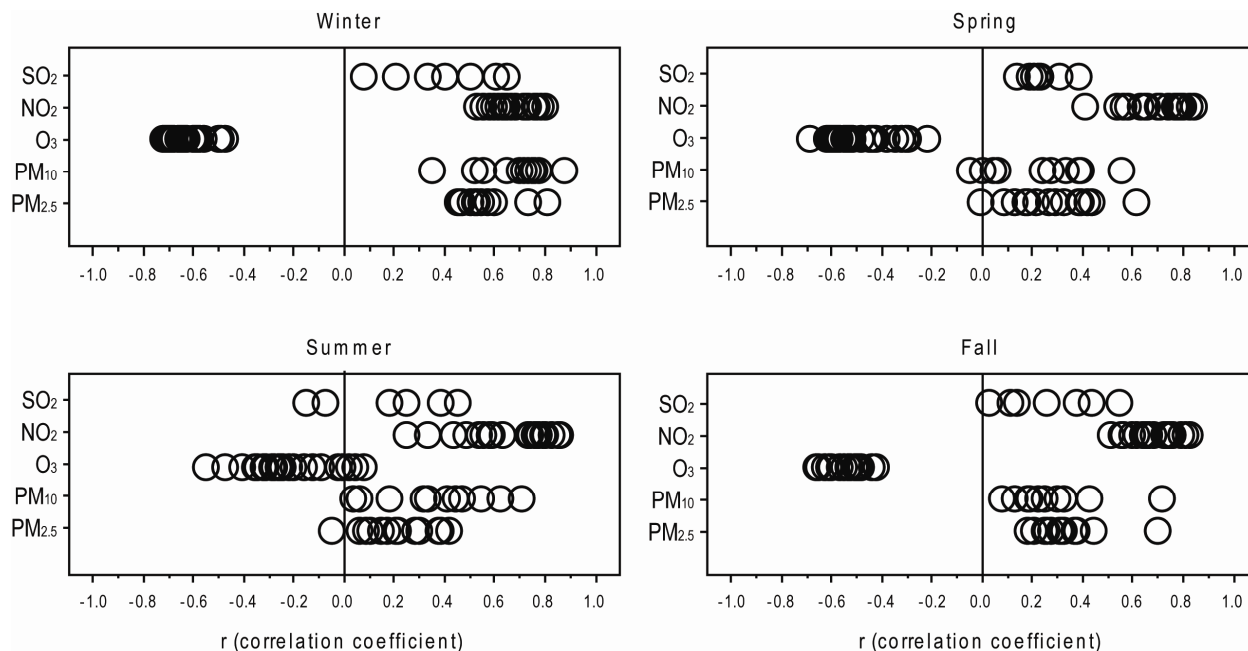
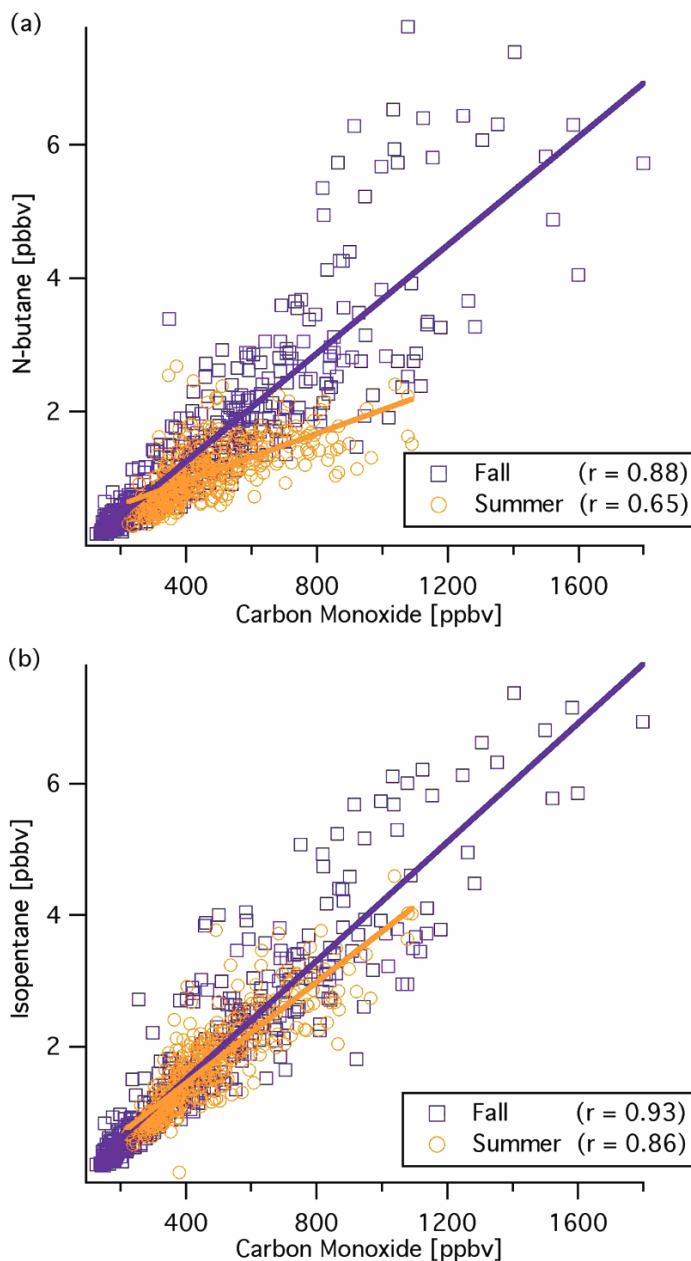


Figure 3-40. Seasonal plots showing the variability in correlations between hourly CO concentration and co-located hourly SO₂, NO₂, O₃, PM₁₀ and PM_{2.5} concentrations for Los Angeles, CA.

Several recent studies reported correlations between ambient CO and other pollutants. Reported relationships were generally consistent with the correlations shown above using AQS data. Sarnat et al. (2001, [019401](#)) reported significant positive Spearman's correlations between CO and NO₂ ($r = 0.76$) and PM_{2.5} ($r = 0.69$) and significant negative correlations between CO and O₃ ($r = -0.67$) in Baltimore (concentration averaging periods not specified). Correlation of CO with SO₂ was insignificant ($r = -0.12$). The Sarnat et al. (2001, [019401](#)) study focused on correlations of ambient and personal PM_{2.5} with gaseous copollutants, so seasonal information is only available for the correlation between PM_{2.5} and CO. High correlation of ambient CO with NO₂ is expected given that both are closely related to mobile source combustion emissions. Sarnat et al (2005, [087531](#)) also reported significant year-round association between CO and PM_{2.5} and significant associations between CO and SO₄²⁻ aerosols. Kim et al. (2006, [089820](#)) measured CO, NO₂, and PM_{2.5} at ambient fixed sites in Toronto, Canada, and found associations, averaged over monitoring stations, of CO with PM_{2.5} (Spearman's $r = 0.38$, nonsignificant) and of CO with NO₂ ($r = 0.72$, significant). Tolbert et al. (2007, [090316](#)) reported correlations between multiple pollutants in Atlanta and also showed the highest Spearman's correlation for CO with NO₂ ($r = 0.70$). CO was also reported to have fairly high correlation with PM_{2.5} elemental carbon (EC) ($r = 0.66$), PM_{2.5} organic carbon (OC) ($r = 0.59$), and PM_{2.5} total carbon (TC) ($r = 0.63$). Correlations were reported to be much lower for CO with O₃ ($r = 0.27$) and PM_{2.5} SO₄²⁻ ($r = 0.14$). The higher correlations of CO with EC, OC, and TC are likely related to the fact that CO and carbonaceous PM are both emitted by mobile sources. Gentner et al. (2009, [194034](#)) analyzed the relationship between ambient CO and VOC concentrations, serving as markers of gasoline vehicle emissions in Riverside, CA. Correlations of CO with two compounds, n-butane and isopentane, are shown in Figure 3-41 for summer and fall. Higher concentrations of n-butane per unit of CO were observed for fall, as well as higher correlation (fall: $r = 0.88$; summer: $r = 0.65$). For isopentane, the slopes of regression are much closer for fall and summer, with higher correlations between isopentane and CO (fall: $r = 0.93$; summer: $r = 0.86$). Gentner et al. (2009, [194034](#)) noted that isopentane vapor fraction was higher in summer than winter and that the n-butane vapor fraction increases in winter. This reflects the higher volatility of n-butane compared with isopentane. In this work, Gentner et al. (2009, [194034](#)) used emissions modeling to estimate that overall VOC emissions from gasoline varies with CO emissions with a ratio of 0.086 with a correlation of $r = 0.80$ in summer. Gentner et al. (2009, [194034](#)) suggest that the near-road slope of

ambient VOC to CO concentration might be influenced by upwind CO concentration and secondary CO production by oxidation of VOCs.



Source: Reprinted with Permission of ACS from Gentner et al. (2009, [194034](#))

Figure 3-41. Linear regression of n-butane and isopentane concentration as a function of CO concentration, Riverside, CA.

3.5.4. Policy-Relevant Background

Background concentrations of pollutants used for informing policy decisions about national standards in the U.S. are commonly referred to at EPA as PRB concentrations. In this assessment, PRB concentrations include contributions from natural sources everywhere in the world and from anthropogenic sources outside the U.S., Canada, and Mexico.

3.5.4.1. Surface-Based Determinations

For this assessment, PRB concentrations of CO were determined from the extensive and long-running network of remote-site baseline CO measurements conducted by NOAA's Earth System Research Laboratory (ESRL), Global Monitoring Division (GMD), as part of their Carbon Cycle Greenhouse Gases Group (CCGG) Cooperative Air Sampling Network (CASN); see <http://www.esrl.noaa.gov/gmd/ccgg/iadv>. Surface-based CO measurements have been made for more than 10 yr with exceptionally high sensitivity and selectivity at locations significantly away from local sources. In this assessment, for example, CO data through December 2007 are available with extensive quality assurance and control information from the worldwide network of 72 stations active in December 2008. ESRL GMD uses the highly sensitive gas chromatography-mercury liberation photometric detection technique with precision to 1 ppb in 50 ppb or 2 ppb in 200 ppb and accuracy to 1.5 ppb in 500 ppb or 2 ppb in 200 ppb.

In order to smooth interannually changing meteorological and emissions effects, data from 2005-2007 at 12 remote sites in the U.S. were used to determine PRB. A map of these sites is shown in Figure 3-42; they are: Cold Bay, AK; Barrow, AK; Shemya Island, AK; Cape Kumukahi, HI; Mauna Loa, HI; Trinidad Head, CA; Point Arena, CA; Wendover, UT; Niwot Ridge, CO; Park Falls, WI; Southern Great Plains, OK; and Key Biscayne, FL. These sites are affected by anthropogenic emissions in North America to varying degrees. Average concentrations for each month and for each of the 3 yr are shown for each site in Figure 3-43. All sites demonstrate the well-known seasonality in background CO with minima in the summer and fall and maxima in the winter and spring in the Northern Hemisphere. Northern Hemisphere summer-time minima are related in large measure to the enhanced photochemical reaction of CO with OH, as described in Section 3.2.2. Analysis for North American PRB is made here by segregating the three Alaska sites (owing to their high latitude) and the two Hawaii sites (owing to their distance from the continent) and treating the remaining seven sites as being more representative of the CONUS surface-level background concentrations. Outside the defined CONUS domain used here, the 3-yr avg CO PRB in Alaska ranged from 127 to 135 ppb with an average of 130 ppb, and from 95.3 to 103.1 ppb with an average of 99.2 ppb in Hawaii. Over the CONUS domain the 3-yr avg CO PRB concentration ranged from 118 to 146 ppb with an average of 132 ppb.

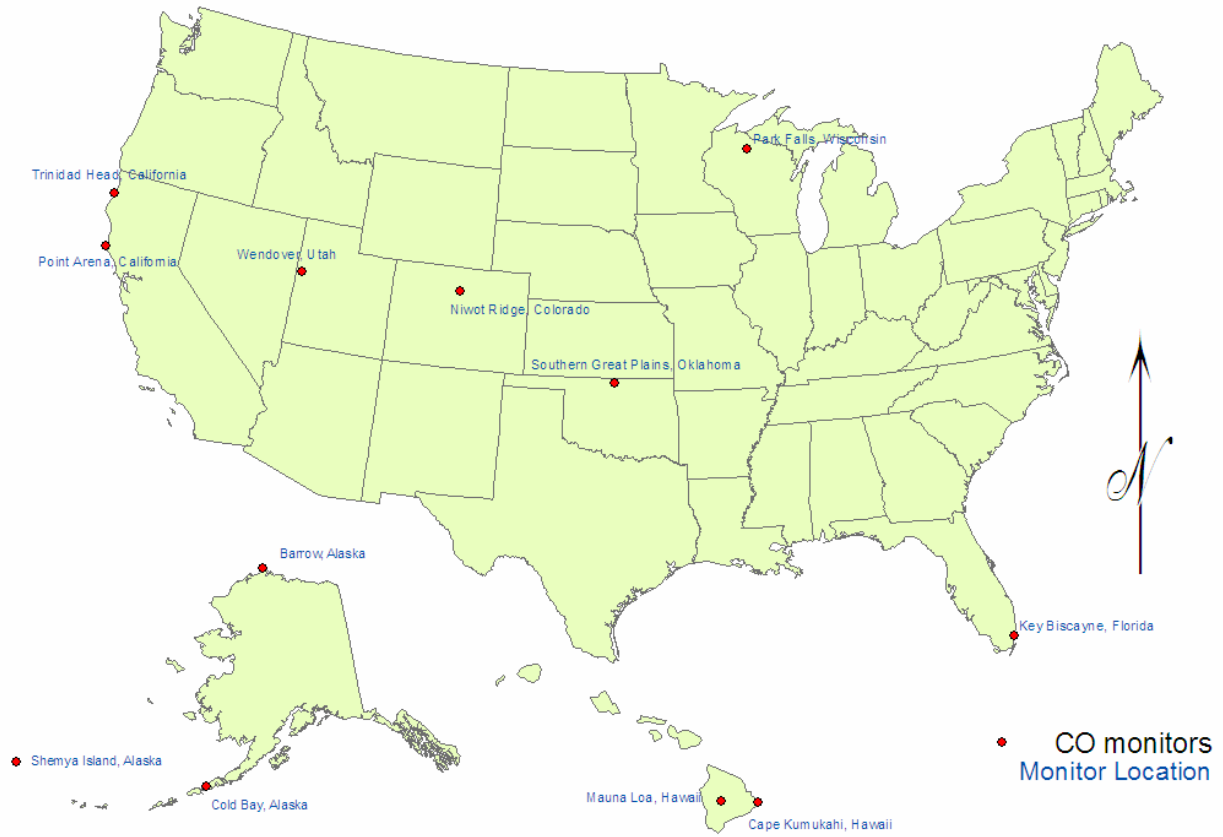


Figure 3-42. Map of the baseline monitor sites used in this assessment to compute PRB concentrations.

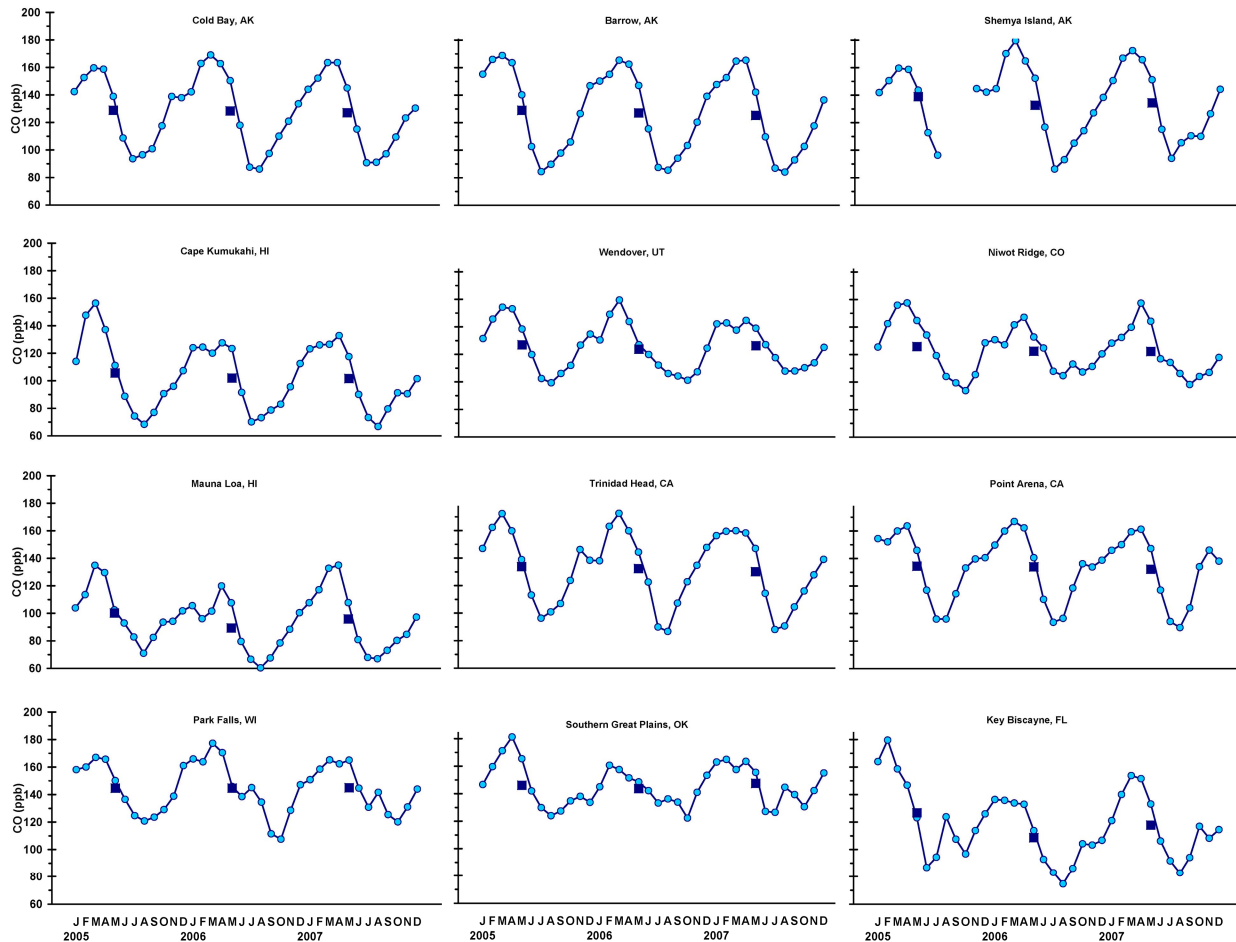


Figure 3-43. Monthly (circles) and annual (squares) average CO concentrations (ppb), 2005-2007. Cold Bay, AK; Barrow, AK; Shemya Island, AK; Cape Kumukahi, HI; Wendover, UT; Niwot Ridge, CO; Mauna Loa, HI; Trinidad Head, CA; Point Arena, CA; Park Falls, WI; Southern Great Plains, OK; and Key Biscayne, FL.

3.5.4.2. Limitations of Other Possible Methods

The significance of CO for surface-level air quality and for its indirect climate forcing effects through CH₄, O₃, and CO₂ as described previously in this chapter, and its long τ relative to that of other primarily urban and regional pollutants make it an important species for measurement and evaluation on multiple spatial, temporal, and chemical scales.

In addition to the ESRL GMD surface network used in this assessment's determination of CO PRB, CO concentrations away from local sources can be measured from space. So, for example, CO has been observed from space by the Measurement of Air Pollution from Satellites (MAPS) instrument on Space Shuttle orbiter flights for three 10-day missions in 1984 and 1994 (Connors et al., 1994, [193755](#)) and by the Measurement of Pollution in the Troposphere (MOPITT) on the Terra satellite since 2000 (Emmons et al., 2004, [193756](#)). Surface spatial coverage with both space-based instruments was limited by the common problems of cloud cover, high surface albedo and emissivities, and image swath pattern and timing, with the result that much of the CONUS, for example, was missed some of the time. In addition, all of these satellite measurements were limited though somewhat differently in the vertical resolution of their total column CO concentration values.

For a determination of a PRB-equivalent background concentration for 2008, the MAPS data would be of no use, except for comparisons on temporal trends, and even that is limited by the very few observations from MAPS. MOPITT data might seem more useful were it not for MOPITT's very low precision and accuracy in the lowest few kilometers above the Earth's surface of its integrated total column CO measurement by thermal infrared radiances (Shindell et al., 2005, [193746](#)). MOPITT CO profile sensitivities are so low at the surface that retrievals at the 850 hPa level, the lowest reported, do not capture the surface concentration accurately but actually represent a broad and deep vertical slice of the lower troposphere with an integral concentration that often peaks well above 850 hPa (Shindell et al., 2006, [091028](#)). Error analysis by Emmons et al. (2004, [193756](#)), reported in Shindell et al. (2006, [091028](#)) revealed that MOPITT concentration error in the lower troposphere was 7% and had greater bias over cleaner sites, which are of most interest when estimating a CONUS PRB.

Since the integrated total column measurements of CO from space-borne instruments are dominated by CO in the mid- and upper troposphere, comparisons to surface measurements are subject to appreciable error. Using a subset of seven to nine of the ESRL GMD network stations in North America, for example, to compare to the MAPS and MOPITT data, Shindell et al. (2005, [193746](#)) found that the satellite data showed an increase of between 3 and 13 ppb CO while the surface data at these locations showed a decrease of 20 ppb in the years 2000-2002 relative to 1994. Mean global concentrations of CO were apparently decreasing before 2000, but that trend has now mostly ended (Duncan and Logan, 2008, [194042](#)), so that the integrated column CO total measured from space may have indicated a false trend.

CO concentrations can also be predicted with numerical CTMs on regional, continental, and global scales. Hence it would, in principle, be possible to predict CO PRB concentrations for the CONUS. The chief limitation to this method comes from the highly uncertain emissions of CO worldwide needed to drive the global CTMs, which in turn set the boundary conditions and chemical flow fields for the finer-scale models that might be used to compute PRB. Interannual variability in CO emissions from global biomass burning is very high, and the emissions source strength of this signal is a very strong component of the CONUS PRB given the CO τ of ~ 57 d. The long τ means that PRB monitoring sites are subject to contamination by regional pollution. Estimates of total global CO emissions used in recent forward and inverse model experiments range from $<1,100$ MT/yr to $>3,300$ MT/yr (Shindell et al., 2005, [193746](#)).

A comprehensive evaluation of 26 state-of-the-science atmospheric chemistry models exercised for present-day and future CO simulations was performed and reported by Shindell et al. (2006, [091028](#)). They found substantial under-prediction of CO in the extra-tropical Northern Hemisphere compared to satellite and local surface observations and large variability among the models as well, even when using identical CH₄ abundances and CO emissions. In North America, for example, the multimodel average underestimated the observations of lower troposphere CO by 60 ppb or more, or by $\sim 50\%$ or more of the measured background concentration at many of the ESRL GMD sites. The Pearson r values for the multimodel average against MOPITT data globally for 2000-2001 was 0.84 ± 0.08 for April at 850 hPa (as near to the surface as tested) but only 0.55 ± 0.11 in October (Shindell et al., 2006, [091028](#)). Shindell et al. (2006, [091028](#)) proposed several reasons why this could contribute to pervasive underprediction: (1) the models do not adequately simulate CO build-up during the wintertime periods of lower OH flux; (2) the models have no seasonal CH₄ cycle with build-up in the Northern Hemisphere winter; and (3) variability in the models' OH concentrations, which accounted for $\sim 80\%$ of the CO intermodel variance (Shindell et al., 2006, [091028](#)).

All of the above methods have their own advantages and disadvantages. The levels determined by the ESRL/GMD network show the temporal and spatial variability of CO levels. Although these sites are subject to North American pollution sources to varying degrees, these data could be used provided this caveat is borne in mind. Resulting errors in estimating excess risks will be very small because the concentrations are only a small fraction of the CO NAAQS.

3.6. Issues in Exposure Assessment

3.6.1. Summary of Findings from 2000 CO AQCD

The 2000 CO AQCD (U.S. EPA, 2000, [000907](#)) describes the results of studies completed prior to 1999 on personal exposures and microenvironmental concentrations of CO. Although these studies may no longer be representative of current exposure levels due to declining ambient CO concentrations, the personal-microenvironmental-ambient relationships are still instructive. Time spent commuting, particularly in cars, was a major contributor to personal CO exposures. Many studies measured in-vehicle concentrations of CO and found elevated concentrations compared to fixed-site monitors. Roadside CO monitors were elevated compared to ambient levels and equal to or lower than in-vehicle levels (Ott et al., 1994, [076546](#); Rodes et al., 1998, [010611](#)). A small portion of the CO concentrations inside a vehicle cabin comes from the vehicle itself, while a substantial fraction comes from roadway mobile source emissions entering the cabin via air exchange. Studies summarized in the 2000 CO AQCD found that in-vehicle CO concentrations were generally two to five times higher than ambient CO concentrations obtained at fixed-site monitors within the cities studied. High-traffic volumes contributed to increased in-vehicle concentrations.

Prior to the 2000 CO AQCD, it was well known that CO levels in residences may be elevated above ambient due to nonambient indoor sources, such as cooking, space heating, and smoking. Separation of indoor CO into ambient and nonambient components was found to be important for determining the effect of ambient CO concentrations, although this had not been done successfully in studies conducted to date. Two large studies performed in Denver, CO, and Washington, DC, in the early 1980s found that fixed-site monitor concentrations were higher than personal exposures for those with low-level exposures, while fixed-site monitor concentrations were lower than exposures for those with high-level exposures (Akland et al., 1985, [011618](#); Johnson, 1984, [024652](#)). Nonambient sources contributing to high-total exposures likely obscured this relationship. In Denver, gas stove operation, passive smoking, and attached garages increased residential indoor exposure by 2.6, 1.6, and 0.4 ppm, respectively, compared to individuals without those sources present. Categorical analyses found significantly higher personal exposures on high-ambient concentration days than on low-ambient concentration days, suggesting that personal exposures are related to ambient levels. Nonambient exposures tend to obscure the relationship between ambient CO concentrations, as measured at ambient monitors, and total personal CO exposure.

3.6.2. General Exposure Concepts

A theoretical model of personal exposure is presented to highlight measurable quantities and the uncertainties that exist in this framework. An individual's time-integrated total exposure to CO can be described based on a compartmentalization of the person's activities throughout a given time period:

$$E_T = \int C_j dt$$

Equation 3-2

where E_T = total (T) exposure over a time-period of interest, C_j = airborne CO concentration at microenvironment j , and dt = portion of the time-period spent in microenvironment j . Equation 3-2 can be decomposed into a model that accounts for exposure to CO of ambient (E_a) and nonambient (E_{na}) origin of the form:

$$E_T = E_a + E_{na}$$

Equation 3-3

Examples of ambient CO sources include industrial and mobile source emissions, biomass combustion, and agricultural processes. Examples of nonambient sources include environmental tobacco smoke (ETS), cooking, and home heating. CO concentrations generated by ambient and

nonambient sources are subject to spatial and temporal variability that can affect estimates of exposure and resulting health effects. Exposure factors affecting interpretation of epidemiologic studies are discussed in detail in Section 3.6.8.

This assessment focuses on the ambient component of exposure because this is more relevant to the NAAQS review. E_a can be expressed in terms of the fraction of time spent in various outdoor and indoor microenvironments (Wallace et al., 2006, [089190](#); Wilson et al., 2000, [010288](#)):

$$E_a = \sum f_o C_o + \sum f_i F_{inf,i} C_{o,i}$$

Equation 3-4

where f = fraction of the relevant time period (equivalent to dt in Equation 3-2), subscript o = index of outdoor microenvironments, subscript i = index of indoor microenvironments, subscript o,i = index of outdoor microenvironments adjacent to a given indoor microenvironment i , and $F_{inf,i}$ = infiltration factor for indoor microenvironment i . Equation 3-4 is subject to the constraint $\sum f_o + \sum f_i = 1$ to reflect the total exposure over a specified time period, and each term on the right hand side of the equation has a summation because it reflects various microenvironmental exposures. Here, “indoors” refers to being inside any aspect of the built environment, e.g., home, office buildings, enclosed vehicles (automobiles, trains, buses), and/or recreational facilities (movies, restaurants, bars). “Outdoor” exposure can occur in parks or yards, on sidewalks, and on bicycles or motorcycles. F_{inf} is a function of the building air exchange characteristics. Assuming steady state ventilation conditions, the infiltration factor is a function of the penetration (P) of CO, the air exchange rate (a) of the microenvironment, and the rate of CO loss (k) in the microenvironment; $F_{inf} = Pa/(a+k)$. Given that $k \rightarrow 0$ for CO, F_{inf} reduces to P . Studies of CO infiltration are reviewed in Section 3.6.5.1. In epidemiologic studies, C_a is often used in lieu of outdoor microenvironmental data to represent these exposures based on the availability of data. Thus it is often assumed that $C_o = C_a$ and that the fraction of time spent outdoors can be expressed cumulatively as f_o ; the indoor terms still retain a summation because infiltration differs among different microenvironments. If an epidemiologic study employs only C_a , then the assumed model of an individual’s exposure to ambient CO, first given in Equation 3-4, is re-expressed solely as a function of C_a :

$$E_a = (f_o + \sum f_i P) C_a$$

Equation 3-5

Meteorology, strength of CO sources, spatial variability of CO concentration, proximity of the study population to sources of CO, design of the epidemiologic study, and other factors determine whether or not Equation 3-5 is a reasonable approximation for Equation 3-4. Errors and uncertainties inherent in use of Equation 3-5 in lieu of Equation 3-4 are described in Section 3.6.8 with respect to implications for interpreting epidemiologic studies. Epidemiologic studies often use concentration measured at a central site monitor to represent ambient concentration; thus α , the ratio between personal exposure to ambient CO and the ambient concentration of CO, is defined as:

$$\alpha = \frac{E_a}{C_a}$$

Equation 3-6

Combination of Equation 3-5 and Equation 3-6 yield:

$$\alpha = f_o + \sum f_i P$$

Equation 3-7

α varies between 0 and 1. If a person’s exposure occurs in a single microenvironment, the ambient component of a microenvironmental CO concentration can be represented as the product of the ambient concentration and P . Wallace et al. (2006, [089190](#)) note that time-activity data and corresponding estimates of P for each microenvironmental exposure are needed to compute an individual’s α with accuracy. If local sources and sinks exist and are significant but not captured by central site monitors, then the ambient component of the local outdoor concentration may be

estimated using dispersion models, land use regression models, receptor models, fine scale CTMs or some combination of these techniques. These techniques are described in Section 3.6.3.

3.6.3. Exposure Modeling

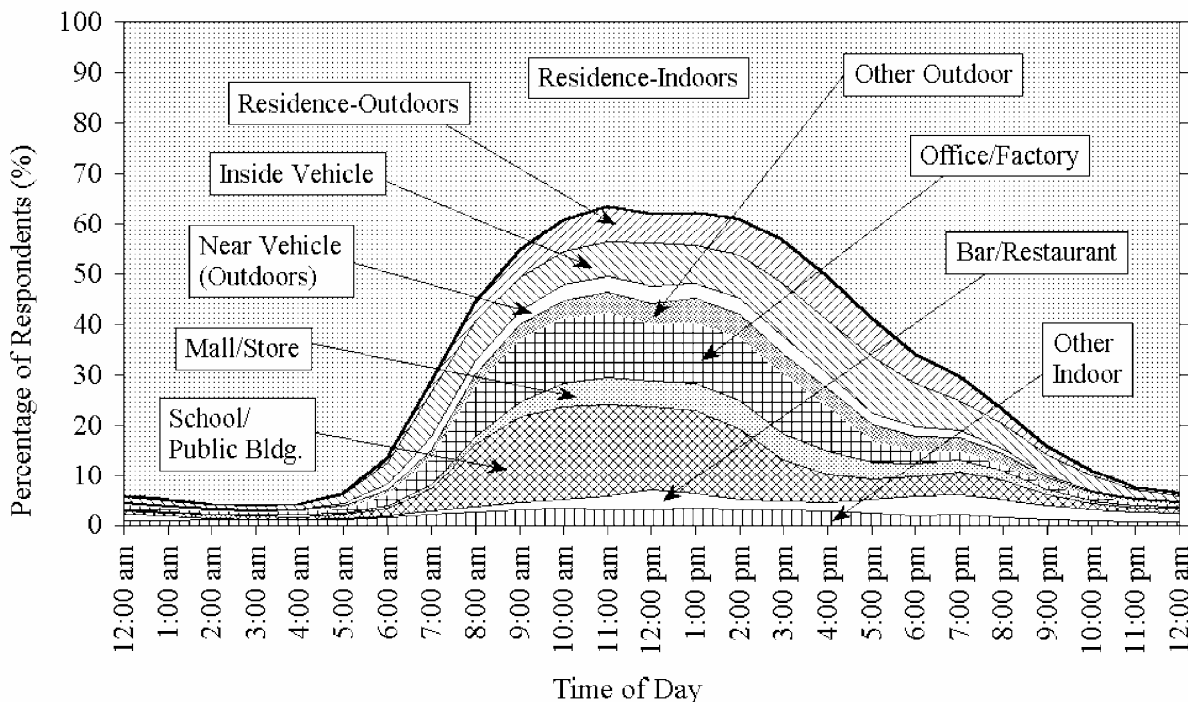
3.6.3.1. Stochastic Population-Based Time-Weighted Microenvironmental Exposure Models

Population-based methods, such as the Air Pollution Exposure (APEX) and Stochastic Human Exposure and Dose Simulation (SHEDS) models, involve stochastic treatment of the model inputs (Burke et al., 2001, [014050](#); U.S. EPA, 2009, [194009](#)). These are described in detail in the 2008 NO_x ISA (U.S. EPA, 2008, [157073](#)), in Annex AX 3.6.1. Stochastic models utilize distributions of pollutant-related and individual-level variables, such as ambient and local CO concentration source contributions and breathing rate respectively, to compute the distribution of individual exposures across the modeled population. The models also have the capability to estimate received dose through a dosimetry model. Using distributions of input parameters in the model framework rather than point estimates allows the models to incorporate uncertainty and variability explicitly into exposure estimates (Zidek et al., 2007, [190076](#)). These models estimate time-weighted exposure for modeled individuals by summing exposure in each microenvironment visited during the exposure period. For example, Bruinen de Bruin et al. (2004, [190943](#)) utilized the EXPOLIS (exposure in polis, or cities) model to predict CO population exposures in Milan, Italy, based on subjects' time-activity data broken into 15-min intervals. The simulation results showed that the U.S. 8-h NAAQS level was exceeded in 1 case out of 1,000. The model also showed that exposures exceeded 20 ppm in 1 case out of 100,000. The results were not shown to be very sensitive to the number of microenvironments (e.g., outdoors, indoors, in-vehicle) included in the model.

The initial set of input data for population exposure models is ambient air quality data, which may come from a monitoring network or model estimates. Estimates of concentrations in a set of microenvironments are generated either by mass balance methods or microenvironmental factors. Microenvironments modeled include indoor residences; other indoor locations, such as schools, offices, and public buildings; and vehicles. The sequence of microenvironments and exertion levels during the exposure period is determined from characteristics of each modeled individual. The APEX model does this by generating a profile for each simulated individual by sampling from distributions of demographic variables such as age, gender, and employment; physiological variables such as height and weight; and situational variables such as living in a house with a gas stove or air conditioning. Activity patterns from a database such as Consolidated Human Activity Database (CHAD) are assigned to the simulated individual using age, gender, and biometric characteristics (U.S. EPA, 2009, [194010](#)). Breathing rates are calculated for each activity based on exertion level, and the corresponding received dose is then computed. For APEX, the CO dosimetry algorithm calculates venous COHb levels using the nonlinear CFK model, as described in Chapter 4. (U.S. EPA, 2008, [191775](#)). Summaries of individual- and population-level metrics are produced, such as maximum exposure or dose, number of individuals exceeding a specified exposure/dose threshold, and number of person-days at or above benchmark exposure levels. The models also consider the nonambient contribution to total exposure. Nonambient source terms are added to the infiltration of ambient pollutants to calculate the total concentration in the microenvironment. Output from model runs with and without nonambient sources can be compared to estimate the ambient contribution to total exposure and dose.

Recent larger-scale human activity databases, such as those developed for the CHAD or the National Human Activity Pattern Survey (NHAPS), have been designed to characterize exposure patterns among much larger population subsets than can be examined during individual panel studies (Klepeis et al., 2001, [002437](#); McCurdy et al., 2000, [000782](#)). CHAD consists of a consolidation of human activity data obtained during several panel studies in which diary or retrospective activity data were obtained, while NHAPS acquired sample population time-activity data through surveys about human activity (Klepeis et al., 2001, [002437](#)). The complex human activity patterns across the population (all ages) are illustrated in Figure 3-44 (Klepeis et al., 2001, [002437](#)), which is presented to illustrate the diversity of daily activities among the entire population as well as the proportion of time spent in each microenvironment. Different patterns would be anticipated when breaking down

activity patterns only for subgroups such as children or the elderly. Population exposures can be estimated using CO concentration data in each microenvironment.



Source: Reprinted with Permission of Nature from Klepeis et al. (2001, [002437](#)).

Figure 3-44. Distribution of time that the sample population spends in various environments, from the NHAPS.

Compartmental models, such as the Indoor Air Model (INDAIR), can be used to assess exposure to infiltrated ambient air pollutants in a deterministic or probabilistic framework (Dimitroulopoulou et al., 2001, [014737](#)). To examine indoor concentrations of ambient CO, Dimitroulopoulou et al. (2006, [090302](#)) used the probabilistic formulation of the INDAIR model to examine indoor exposure to ambient CO, along with NO_x and PM for a given distribution of background CO levels, meteorology, residential air exchange rate, and residential room dimensions. They found that 24-h avg CO concentration increased from 1.86 ppm outdoors to 1.90-1.93 ppm indoors in the absence of nonambient sources, and that indoor 24-h avg CO concentration could increase to 1.93-2.00 ppm in the presence of smoking and to 1.98-2.32 ppm in the presence of gas cooking. Similarity between the outdoor and nonsource indoor concentrations was attributed to the lack of CO loss mechanisms. In the Reducing Urban Pollution Exposure from Road Transport (RUPERT) study, Bell et al. (2004, [192376](#)) presented methodology to use the probabilistic form of INDAIR for development of personal exposure frequency distributions of CO, NO_x, and PM, based on time spent in residential, transportation, school, office, and recreational environments, with inputs from transportation source categories (Chen et al., 2008, [193986](#)).

3.6.3.2. Using Spatial Models to Estimate Exposure

Another set of approaches to improve exposure estimates in urban areas involves construction of a concentration surface over a geographic area, with concentration between monitors estimated using a model to compensate for missing data. The calculated CO concentration surface can then be used to estimate exposures outside residences, schools, workplaces, roadways, or other locations of

interest. This technique does not estimate exposure directly because it does not account for activity patterns or concentrations in different microenvironments. There are two main types of approaches: spatial interpolation of measured concentrations, and regression models using land use, roadway characteristics, and other variables to predict concentrations at receptors in the domain. Rigorous first-principle models, such as dispersion models and CTMs, can also be used for this type of application, but are less suitable because they have intensive resource requirements and are typically applied over larger domains.

The STEMS model provides an example of an integrated-exposure modeling approach using a range of spatial inputs. STEMS maps exposures based on inputs for traffic levels, atmospheric dispersion, background concentrations, and geography. Gulliver and Briggs (2005, [191079](#)) tested the STEMS model for CO and observed some correlation between modeled and measured CO concentrations ($R^2 = 0.41$), which was consistent with results for PM₁₀ and NO_x. Exposures were estimated from the predicted ambient CO concentration using a term similar to α that varied depending on whether the individual was walking or in a vehicle. Gulliver and Briggs (2005, [191079](#)) noted that a limitation to modeling CO is the scarcity of background CO data obtained at rural sites. For this reason, they assumed a constant value obtained from estimates made over the North Atlantic Ocean. Although the authors only presented detailed results for a model of PM₁₀ based on traffic and meteorology in Northampton, U.K., they found that the majority of variation on a given day in modeled exposure among school children was due to differences in travel routes. Variation across days was also influenced by background and meteorological conditions. Similar results can be expected for CO based on the tendency for variation of the CO concentration profile on the neighborhood and microscales (Jerrett et al., 2005, [092864](#)). Flachsbar (1999, [015857](#)) tested numerous meteorological, traffic, and background CO input variables in a regression approach to predicting CO exposure among individuals while traveling in a vehicle. This work showed travel time and average speed of on-road vehicles to be important determinants of CO exposure in a vehicle. Results from individual models of this nature can be pooled to develop a distribution for examination of population effects or for comparison with population exposure models.

Dispersion Models

Dispersion models have been used both for direct estimation of exposure and as inputs for stochastic modeling systems, as described above. Location-based exposures have been predicted using a model such as California Line Source Dispersion Model (CALINE), the American Meteorological Society/Environmental Protection Agency Regulatory Model (AERMOD), CALPUFF (long-range plume transport model created by the California Air Resources Board), or the Operational Street Pollution Model (OSPM) for estimation of street-level ambient CO exposure (e.g., Abdul-Wahab, 2004, [194011](#); Delfino et al., 2009, [190254](#); Zhou and Levy, 2008, [190091](#)). CALINE, CALPUFF, and AERMOD utilize Gaussian dispersion models to describe pollutant transport, while OSPM is a semi-empirical model of airflow and pollutant transport within an infinite street canyon. Delfino et al. (2009, [190254](#)) used CALINE (version 4) to model exposure in the near-road environment for estimation of relative risks of asthma hospitalizations as a function of increases in ambient CO and NO_x concentrations. The concentration at each subject's home was computed with the dispersion model, and then the data were aggregated to estimate a population risk. Zhou and Levy (2008, [190091](#)) used results from an OSPM simulation to compute intake fraction, defined as the fraction of emissions that are inhaled or ingested, for ambient CO and other copollutants. Daytime activity patterns were modeled using both CHAD and the American Community Survey (<http://www.census.gov/acs/www>) to model commuting behaviors that would affect both mobile-source emissions and population-based exposures. With an individualized exposure approach, the model is deterministic. However, population exposures were estimated by performing repeated simulations using various housing characteristics and then computing the probability distribution function for exposure. When comparing street-canyon exposure computed by OSPM with near-road exposure computed simply with a Gaussian dispersion model, Zhou and Levy (2008, [190091](#)) estimated that the street-canyon exposures would be three times greater than those in the general community. Isakov et al. (2009, [191192](#)) developed a methodology to link a chemical transport model, used to compute regional scale spatiotemporally-varying concentration in an urban area, with stochastic population-exposure models to predict annual and seasonal variation in population exposure within urban microenvironments. Although this approach was demonstrated for PM_{2.5}, it is

similar to the one used by Zhou and Levy (2008, [190091](#)) for linking ambient CO concentrations with population activity pattern data to associate the spatial-concentration field with personal exposure to ambient CO.

Land Use Regression Models

Land use regression (LUR) models have also been developed to estimate pollution levels as a function of several land use factors, such as land use designation, traffic counts, home heating usage, point source strength, and population density (Briggs et al., 1997, [025950](#); Gilliland et al., 2005, [098820](#); Ryan and LeMasters, 2007, [156063](#)). LUR is a regression derived from monitored concentration values as a function of data from a combination of the land use factors. The regression is then used for predicting concentration at multiple locations based on the independent variables at those particular locations without monitors. At the census-tract level, a LUR is a multivariate description of pollution as a function of traffic, land use, and topographic variables (Briggs et al., 1997, [025950](#)). Like deterministic-dispersion models, LUR can be performed over wide areas to develop a probability density function of exposure at the urban scale. However, Hoek et al. (2008, [195851](#)) warn of several limitations of LUR, including distinguishing real associations between pollutants and covariates from those of correlated copollutants, limitations in spatial resolution from monitor data, applicability of the LUR model under changing temporal conditions, and introduction of confounding factors when LUR is used in epidemiologic studies.

A GIS platform is typically used to organize the independent variable data and map the results from an LUR simulation. The GIS software creates numerous lattice points for the regression of concentration as a function of the covariates. For instance, Krewski et al. (2009, [191193](#)) computed PM_{2.5} concentrations for the New York City and Los Angeles metropolitan areas. For the Los Angeles analysis, the LUR was estimated at 23 monitors and then applied to simulate PM_{2.5} concentration at 18,000 points in the simulation domain, and an inverse distance weighting (IDW) kriging method was applied to interpolate the predicted concentration. In New York City, the LUR was estimated at 49 monitors for a 3-yr model and at 36 monitors for a model of winter 2000 and then applied to simulate PM_{2.5} concentration at 5,600 locations in the 28-county domain; kriging was employed only for the purpose of visualizing the concentration between monitors. The models explained 69% and 66% of the variation in PM_{2.5} in Los Angeles and New York City, respectively.

GIS-based spatial-smoothing models can be used to estimate concentrations where monitors are not located. Yanosky et al. (2008, [099467](#)) described an approach to estimate PM concentrations, using a combination of reported AQS data and GIS-based and meteorological covariates. Temporally stationary covariates included distance to nearest road for different PM size fractions, urban land use, population density, point-source emissions within 1 and 10 km buffers, and elevation above sea level. Time-varying covariates included area-source emissions, precipitation, and wind speed. In this analysis, the GIS-based covariates were temporally stationary, while the meteorological and PM monitored concentration inputs were time varying. This approach was applied to estimate PM_{2.5}, PM_{10-2.5}, and PM₁₀ exposures for the Nurse's Health Study and provided estimates of concentration at approximately 70,000 nodes with PM_{2.5} and/or PM₁₀ data input from more than 900 AQS sites, with good validation of the PM_{2.5} and PM₁₀ models (Paciorek et al., 2009, [190090](#); Yanosky et al., 2008, [099467](#); Yanosky et al., 2009, [190114](#)).

Marshall et al. (2008, [193983](#)) compared four spatial interpolation techniques for estimation of CO concentrations in Vancouver, BC. The investigators assigned a daily average CO concentration to each of the 51,560 postal-code centroids using one of the following techniques: (1) the concentration from the nearest monitor within 10 km; (2) the average of all monitors within 10 km; (3) the IDW average of all monitors in the area; and (4) the IDW average of the three closest monitors within 50 km. Method 1 (the nearest-monitor approach) and Method 4 (IDW-50 km) had similar mean and median estimated annual average concentrations, although the 10th-90th percentile range was smaller for IDW-50. This is consistent with the averaging of extreme values inherent in IDW methods. The Pearson correlation coefficient between the two methods was 0.88. Methods 2 and 3 were considered sub-optimal and were excluded from further analysis. In the case of Method 2, a single downtown high-concentration monitor skewed the results in the vicinity, partially as a result of the asymmetric layout of the coastal city of Vancouver. Method 3 was too spatially homogenous because it assigned most locations a concentration near the regional average, except for locations immediately adjacent to a monitoring site. LUR results were also reported in this study for

NO and NO₂ and indicated that LUR's higher spatial precision reflects neighborhood-scale effects from nearby land use but may not account for urban-scale variation. Brauer et al. (2008, [156292](#)) also evaluated LUR and IDW-based spatial-interpolation models and suggested that LUR is appropriate for directly-emitted pollutants with high spatial variability; Brauer et al. (2008, [156292](#)) used NO and BC as examples, but CO emitted from mobile sources would also fall in that category. These results highlight the variation in local concentration estimates with choice of estimation technique.

Originally, LUR was used to model NO₂ dispersion. It has been adapted for modeling exposures to other pollutants, although application of LUR to CO exposures has been performed in only a few studies. Findings related to other pollutants are provided because they are instructive in how LUR can be used to predict CO concentrations. Carslaw et al. (2007, [148210](#)) used multiple-regression modeling to examine the effects of traffic volumes, wind components, temperature, and time on concentrations of CO, NO_x, NO₂ (O₃ was also a predictive variable for NO₂), benzene, and butadiene at a single site. These results were used for forecasting concentrations at that site, but the study lacked the spatial resolution to predict concentrations at alternate sites. Cassidy et al. (2007, [199975](#)) applied LUR to analyze the effect of wind, temperature, traffic volume, roadway size, number of stories of surrounding buildings, other sources of pollution, terrain, and time of day on concentrations of CO, PM_{2.5}, and PM₁₀ at 30 street-level sites within Baguio City, Philippines. In this work, they found traffic volume was the only significant predictor of CO during rush-hour periods, while winds significantly predicted early morning concentrations of CO, PM_{2.5}, and PM₁₀. The model was not used for spatial interpolation in this case. Brauer et al. (2003, [155702](#)) used LUR to analyze PM_{2.5} exposure at 40-42 sites each within Stockholm, Sweden, Munich, Germany, and throughout The Netherlands. This study found a measure of traffic density to be the most significant variable predicting PM_{2.5} exposure and used GIS to apply the model at home addresses of asthmatic subjects to estimate exposures. Ryan et al. (2008, [156064](#)) reported on an LUR model developed from monitor and land-use data and then applied at the locations of children to assess their exposure to traffic-derived EC for the Cincinnati Allergy and Air Pollution Study. Ryan et al. (2008, [156064](#)) found traffic to be the most important determinant of diesel exhaust particle exposure. In this case, wind direction was also factored into the model as a determinant of EC mixing. Although these studies differed in the number of sites and in the pollutants of focus, they are instructive in considering how LUR can be employed for estimating CO exposure.

3.6.4. Personal Exposure Monitors for CO

Portable monitors for measuring personal CO exposure include the Langan and Draeger monitors, both of which use electrochemical oxidation-reduction techniques (Langan, 1992, [046120](#)). These monitors continuously log CO concentrations, making them suitable for use in personal monitoring studies. Electrochemical CO sensors typically have an LOD of 1 ppm and a 90% sensor response time (or the time required for the sensor to register 90% of a step change in CO concentration) of 20-60 s. The 2000 CO AQCD (U.S. EPA, 2000, [000907](#)) provided detail on design updates of electrochemical CO sensors made during the 1990s. Commercially available personal CO exposure monitors are not designed to detect concentrations below 1 ppm. Electrochemical personal CO monitors are also typically sensitive to temperature changes, so that data correction is normally required.

3.6.5. Indoor Exposure to CO

3.6.5.1. Infiltration of Ambient CO

CO is a relatively inert gas, making the indoor decay rate negligible compared to typical air exchange rates (~1/h). In the absence of indoor sources, this would lead to an indoor-outdoor concentration ratio (I/O) of approximately 1. For this reason, few studies have calculated I/O for CO. Polidori et al. (2007, [156877](#)) calculated I/O of 0.94-1.21 for two retirement communities in the Los Angeles area. The authors suggested that similarity between I/O for CO and NO_x can be attributed to lack of indoor sources of either gas. Chaloulakou and Mavroidis (2002, [026050](#)) reported I/O using CO measurements in the absence of indoor sources in a school building in Athens, Greece, and

found that I/O varied with season. During the summer, median I/O was reported to be 0.57 on weekdays, 0.91 on Saturdays, and 0.81 on Sundays. In winter, median I/O was reported to be 0.82 during weekdays, 0.90 on Saturdays, and 0.74 on Sundays. In a related study, Chaloulakou et al. (2003, [190945](#)) reported the median I/O over all days as 0.8 for the same school and 0.9 for an Athens office building with no ETS (the presence of other sources was not clearly stated but assumed zero). However, observed indoor values are often greater than outdoor concentrations in the presence of indoor sources. A recent study in the U.K. reported I/O of 3.9-4.3 in homes with gas cookers (Dimitroulopoulou et al., 2006, [090302](#)), which is consistent with previous studies. A multipollutant study conducted in 2000-2001 attempted to measure I/O for CO and calculated residential infiltration factors, but low CO concentrations resulted in a large number of measurements below the LOD (Williams et al., 2003, [053335](#)). Ni Riain et al. (2003, [053792](#)) examined the effects of mechanical ventilation and wind speed on I/O. In this study, the authors measured indoor and outdoor concentrations at two buildings located on a six-lane highway in central London with natural and mechanical ventilation. Ni Riain et al. (2003, [053792](#)) found that outdoor concentrations for each building and ventilation condition ranged from 1.5 ± 0.1 ppm to 1.9 ± 0.1 ppm. Ni Riain et al. (2003, [053792](#)) reported cumulative I/O approaching 0.9 within 30 min of sampling for the mechanical ventilation case and cumulative I/O varying between 0.65 and 0.8 for more than 70 h of sampling for the natural ventilation case. Ni Riain et al. (2003, [053792](#)) found that wind speed and direction influenced the variation in I/O.

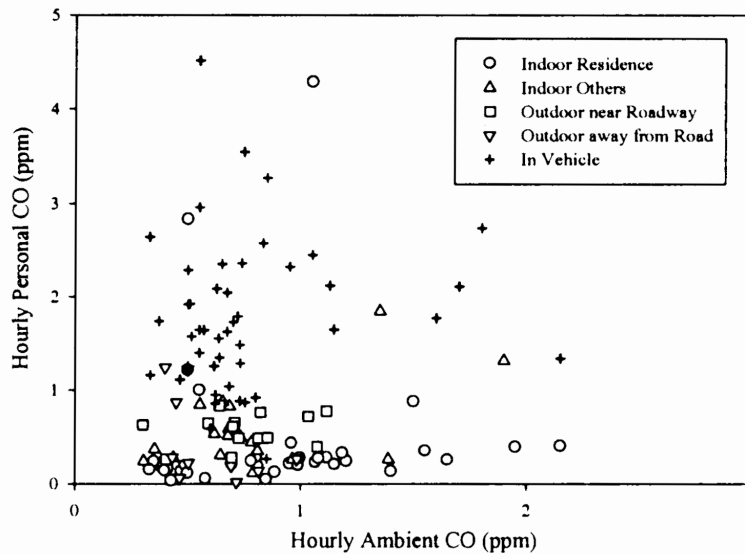
Indoor air flow may affect CO exposure in the absence of indoor sources. Milner et al. (2006, [123100](#)) compared hourly CO concentration time series from different parts of a building (with a mix of natural and mechanical ventilation) located near a busy road and intersection in central London, U.K. They found that, within a given floor, CO concentration is greater in rooms that are closer to busy roads or an intersection. They noted that the correlation coefficient between indoor and outdoor CO concentrations also decreased within the building with distance from the road; the correlation coefficients were reported to be 0.80 for two time series obtained in rooms near the road, while they were reported to range between 0.46 and 0.55 on the sides of the building furthest from the road. The magnitude of the difference between CO concentrations in different rooms located nearer or further from the roads also depended on wind direction. Milner et al. (2006, [123100](#)) noted that I/O tended to decrease with increasing wind speed, but Chaloulakou et al. (2003, [190945](#)) also noted that indoor CO concentration varied inversely with wind speed. Chaloulakou et al. (2003, [190945](#)) attributed their observation to reduced concentrations related to dilution effects. Milner et al. (2006, [123100](#)) stated that this relationship could be due to dilution of CO or to the tendency of people to keep windows closed on windy days. Additionally, CO concentrations were higher on lower floors of the building and varied over a given day throughout the building. These findings suggest that differences in exposure can occur within the same building as a result of differences in air exchange related to access to windows, mechanical ventilation, and outdoor meteorological conditions.

3.6.5.2. Exposure to Nonambient CO

Several papers have investigated the microenvironmental sources of total personal CO exposure. The CDC conducted a survey of ED visits for nonfatal CO poisoning, CO exposure, or potential CO exposure, and found that home heating was the largest known source of CO exposure, prompting 16.4% of CO-related ED visits, followed by motor vehicle exhaust exposure accounting for 8.1% of ED visits (Annest et al., 2008, [190236](#)). Alm et al. (2000, [192374](#); 2001, [020237](#)) studied factors that contributed to elevated CO exposures among preschool children and found that presence of a gas stove at home, ETS, natural ventilation, and living in a high-rise building all contributed to increased CO exposures. Time-activity diaries were linked to personal CO exposures in the EXPOLIS study. Here, Georgoulis et al. (2002, [025563](#)) observed that geometric mean exposure among smokers ranged from 0.33 ppm in Helsinki, Finland, to 3.2 ppm in Athens, Greece, while among nonsmokers it ranged from 0.36 ppm in Helsinki to 1.7 ppm in Milan and ambient CO concentration ranged from 0.42 ppm in Helsinki to 3.2 ppm in Athens. Bruinen de Bruin (2004, [190943](#)) found, for a panel of 46 subjects in Milan, that indoor CO concentrations were 3.4 ppm in the presence of gas cooking and ETS, compared with 2.9 ppm in the presence of ETS only, 2.4 ppm in the presence of gas cooking only, and 1.8 ppm in the absence of indoor CO sources. Scotto di Marco et al. (2005, [144054](#)) reported that average indoor CO increased in the presence of ETS from 0.96-1.2 ppm for the home indoor environment and from 1.0-1.4 ppm for the work indoor

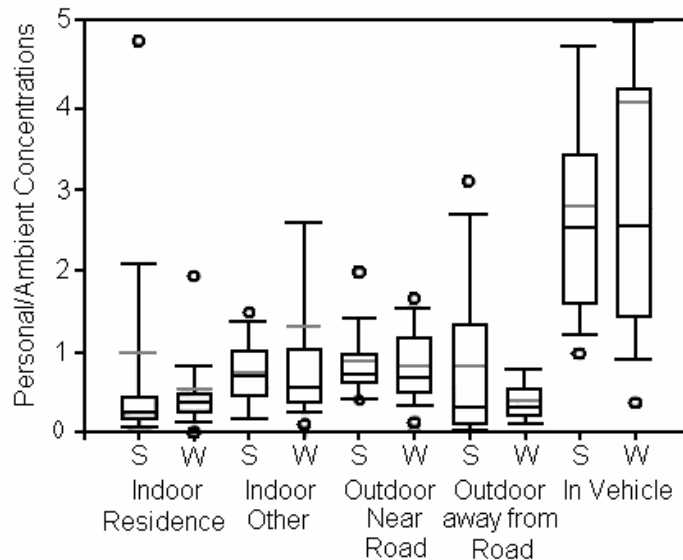
environment. CO concentrations were measured to decrease from 1.5 to 1.3 ppm in other (not home or work) indoor environments, but those locations included garages, restaurants, and bars and could have been differently influenced by CO from cooking, indoor automobiles, or other sources.

Personal CO concentrations can also be much more variable than ambient measurements. Figure 3-45 shows hourly versus personal CO concentration data obtained by Chang et al. (2000, 001276) for a 1998-1999 multipollutant sampling campaign in Baltimore, MD. Personal exposures were obtained in five separate microenvironments in this study. A high degree of scatter is evident in this figure, which suggests that these personal exposures are influenced by both ambient and nonambient sources of CO. Figure 3-46 is a box plot of the personal-to-ambient CO concentration ratio for the same five microenvironments. Wide variability is seen in these plots, particularly during the summer. Much of that variability could be due to the influence of nonambient sources, which would then result in poor correlation between total personal exposure and ambient concentration.



Source: Reprinted with Permission of the Air and Waste Management Association from Chang et al. (2000, 001276)

Figure 3-45. Hourly personal versus ambient CO concentrations obtained in Baltimore, MD, during summer of 1998 in five settings: indoor residence, indoor other, outdoor near road, outdoor away from road, and in vehicle.



Source: Adapted with Permission of the Air and Waste Management Association from Chang et al. (2000, [001276](#))

Figure 3-46. Box plots of the ratio of personal to ambient concentrations obtained in Baltimore, MD, during summer of 1998 and winter of 1999 in five settings: indoor residence, indoor other, outdoor near road, outdoor away from road, and in vehicle. The grey line shows the mean, and the black mid-line shows the median. S = summer; W = winter.

Vehicle self-pollution, defined by Behrentz et al. (2004, [155682](#)) as the fraction of a vehicle's own exhaust entering the vehicle microenvironment, is another potential nonambient source of CO exposure. This has been studied using inert tracer gases to evaluate exposures of children riding school buses. Behrentz et al. (2004, [155682](#)) used sulfur hexafluoride (SF₆) tracer gas emitted from school bus engines to determine the proportion of in-vehicle pollution related to self-pollution. Based on the SF₆ concentration, they calculated that 0.04-0.29% of the bus cabin air contained exhaust for high-emitting diesel engines, 0.01-0.03% for "regular" diesel buses, 0.02-0.04% for buses fitted with a particle trap, and 0.03-0.04% for buses running on compressed natural gas. SF₆ concentrations were higher when bus windows were closed.

3.6.6. Exposure Assessment Studies at Different Spatial Scales

3.6.6.1. Neighborhood to Urban Scale Studies of Ambient CO Exposure

Although several multipollutant exposure studies have been conducted recently in the U.S., (e.g., Sarnat et al., 2006, [089784](#)), most have not included CO in the suite of pollutants, possibly due to high detection limits in personal monitors. A few studies conducted in Europe and Canada measured personal-ambient relationships for CO. This section summarizes CO exposure assessment studies that compare personal exposure measurements with ambient concentration measurements for the purpose of examining how well these measures correspond.

The EXPOLIS study (Georgoulis et al., 2002, [025563](#)) found that 48-h personal exposures were significantly correlated with ambient concentrations in each of five European cities (Athens, Basel, Helsinki, Milan, and Prague). Controlling for source terms, including ETS, traffic, and natural gas appliances, regression coefficients between personal exposure and ambient concentration ranged from 0.28 in Milan to 1.99 in Helsinki and were all statistically significant ($p \leq 0.01$ for all cities except Prague, where $p = 0.05$). The regression coefficient for Helsinki (>1) likely reflects nonambient sources that were not controlled in the study. The ambient concentration was the only variable that was statistically significantly associated with 48-h personal exposure for all five cities

in this study, with correlations between personal CO exposure and ambient CO concentration ranging from 0.33 to 0.77. Georgoulis et al. (2002, [025563](#)) reported that CO exposure in traffic ranged from 0.99 ppm in Helsinki to 4.2 ppm in Athens, while ambient CO concentration ranged from 0.42 ppm in Helsinki to 3.2 ppm in Athens. As part of this study, personal CO exposure was measured for a panel of 50 office workers in Milan (Bruinen de Bruin et al., 2004, [190943](#)). Average measured 1-h personal exposures were 7.3 ppm in comparison with 5.0 ppm for fixed site 1-h measurements. Average 8-h (3.3 ppm) and 24-h (2.1 ppm) CO concentrations were the same for personal and fixed-site measurements. Percentage of time exposed, exposures, and percentage of exposure from the Bruinen de Bruin et al. (2004, [190943](#)) study, in the absence of nonambient CO from ETS and gas cooking, are shown in Table 3-13. The largest percentage of time-weighted CO exposure was attributed to home indoor exposure in the absence of indoor sources, while the highest exposure levels were observed during transit; Scotto di Marco et al. (2005, [144054](#)) found similar results. Bruinen de Bruin et al. (2004, [190943](#)) and Scotto di Marco et al. (2005, [144054](#)) found that mobile source emissions were important contributors to personal exposure, as described in Section 3.6.6.2.

Table 3-13. Percentage of time exposed to ambient CO (adjusted to reflect the absence of nonambient CO from ETS and gas cooking), average CO exposures, and percentage of exposure estimated for the population.

	Percent of time exposed (%)	Exposure (ppm)	Percent of exposure (%)
INDOORS	89.6		81.1
Home	56.5	1.8	49.4
Work	29.1	1.9	26.8
Other	4.1	2.5	4.9
OUTDOORS	1.8		2.1
Home	0.2	2.3	0.2
Work	0.6	2.1	0.6
Other	1.0	2.6	1.2
IN-TRANSIT	8.5		16.8
Walking	3.0	3.0	4.4
Train/metro	0.7	3.0	1.0
Bus/tram	2.0	3.8	3.7
Motorbike	0.2	4.5	0.4
Car/taxi	2.6	5.7	7.2

Source: Reprinted with Permission of Nature from Bruinen de Bruin et al. (2004, [190943](#))

EXPOLIS also looked at the special case of children's exposure to CO because children generally do not produce CO in their daily activities and have no occupational exposures. Alm et al. (2000, [192374](#); 2001, [020237](#)) reported higher personal exposures than ambient concentrations for children aged 3-6 yr in Helsinki. Their mean 1-h daily max exposure was 5.2 ppm, compared to 1.4 ppm measured at a fixed-site monitor. For the average of 8-h and 24-h daily max concentrations, the corresponding values were 2.9 ppm and 2.1 ppm for personal exposure and 0.8 and 0.6 ppm, respectively, for fixed site measurements. The Spearman rank correlation, although statistically significant, was relatively low ($r = 0.15$) between individual 24-h avg exposure and the ambient monitor. The correlation improved when the average exposure of children measured on the same day ($r = 0.33$, 3-6 children) or the same week ($r = 0.55$, 10-23 children) was compared to the monitor data. A regression model using questionnaire data found that parental smoking status, parental education, and presence of a gas stove explained only 12% of the variability in the 8-h max

exposures, indicating that other factors, such as time spent outdoors and proximity to roadways, are likely to be important in determining personal exposure.

Kim et al. (2006, [089820](#)) reported mean CO concentrations of 1.4 ppm for a panel of 28 cardiac-compromised individuals in Toronto, Canada. Corresponding fixed-site monitor mean concentrations ranged from 0.5 to 1.4 ppm, with an overall mean of 1.0 ppm. The observed higher personal exposures may have been due to both indoor sources and proximity to roadways when outdoors. Personal-ambient Spearman correlations ranged from -0.65 to 0.93, with a median of $r = 0.31$, indicating that while moderate correlations are observed overall, inter-individual differences based on time spent in different microenvironments have a strong influence on the observed correlation. Lai et al. (2004, [056811](#)) measured relationships between personal CO exposure and microenvironmental (home indoor, home outdoor, and work indoor) concentrations in Oxford, U.K. The highest personal exposures were associated with smoking, cooking, and transportation, while low correlations were observed between personal and indoor residential concentrations, further indicating the importance of indoor sources and the need to separate ambient contributions to personal exposure from total personal exposure.

The studies presented above present mixed results regarding the association between ambient CO concentration measurements and personal CO exposures. Some personal CO measurements have been reported to be higher than ambient concentrations, while others are similar. Additionally, correlation between ambient CO concentration and personal exposure has varied in the literature. Nonambient (described in Section 3.6.5) and in-transit sources (described in Section 3.6.6.2) have been identified as important contributors to personal exposure. These observations raise questions about where and when ambient CO concentration can be used as a surrogate for personal CO exposure; these concepts are explored further in Section 3.6.8.

3.6.6.2. Microscale Studies of Ambient CO Exposure: Near-Road and On-Road Exposures

The 2007 American Housing Survey (AHS) (U.S. Census Bureau, 2008, [194013](#)) reports that 17.9 million occupied homes nationwide (16.1%) are within ~90 m (300 ft) of a “4-or-more-lane highway, railroad, or airport” and so are exposed to the near-road environment. Within city centers, 6.2 million occupied homes (19.7% of those living in city centers) are within approximately 90 m of a highway, railroad, or airport; whereas in rural areas outside designated Metropolitan Statistical Areas (MSA), 1.4 million occupied homes (9.2% of those in rural areas outside MSAs) are near a highway, railroad, or airport. Those data can be put into context for exposure assessment in the near-road environment; Section 3.5.1.3 describes near-road studies in which ambient CO was measured within the vicinity of a road and microscale AQS data obtained in the near-road environment. The AQS data suggest some spatial variability (20-40% difference between microscale and middle scale monitors, with the hourly microscale concentration having a median of 0.5 ppm and a 99th percentile value of 2.2 ppm), which was much lower than that reported by Zhu et al. (2002, [041553](#)) for the near-road environment, in which the average concentration at 17 m from the road was 2.3 ppm (range 1.9-2.6 ppm) and a factor of about 12.5 lower for the monitoring site located 300 m from the road. The larger discrepancy observed between the Zhu et al. (2002, [041553](#)) data and the AQS data might be attributed to the fact that the sampling equipment used by Zhu et al. (2002, [041553](#)) were downwind of the freeway for the entire sampling period, while the hourly AQS data represents a range of wind speeds and directions that vary across different monitoring sites. For those living in the 16.1% of occupied homes situated in the near-road environment (within ~90 m), median hourly CO concentrations are typically higher than those further from the road, but the magnitude of the outdoor concentration is still in most circumstances measured to be below 2.2 ppm.

Kaur and Nieuwenhuijsen (2009, [194014](#)) and Carslaw et al. (2007, [148210](#)) suggest that CO exposures are related to traffic volume and fleet mix in the street-canyon environment. In this research, Kaur and Nieuwenhuijsen (2009, [194014](#)) developed a multiple linear regression of CO as a function of mode of traffic, broken down by vehicle type, wind speed, temperature, and traffic count for data obtained in central London as part of the DAPPLE study of traffic-related pollution. They added each variable successively and found traffic count, temperature, wind speed, and walking to be significant parameters in the model, with traffic count being the strongest determinant. Analysis of variance showed variability in traffic count to explain 78% of the variability in CO levels for these data, and variability in mode of transport explained 6% of the variability. Likewise, Carslaw et al. (2007, [148210](#)) used a generalized additive model to determine how CO concentration

(log-transformed) varies as a function of year, the along-street and cross-street components of wind, temperature, Julian day, light and heavy traffic counts, and temperature for data obtained in central London. Light-duty vehicle count was a more important determinant of CO concentration than was heavy-duty (i.e., diesel) vehicle count in this study, which is not surprising because gasoline-powered vehicles are known to emit more CO than diesel engines. They found that the CO concentration declined steadily with year and that wind was the most significant covariate. The decline in CO concentration with year, adjusted for all other covariates, was usually significantly different than the simple relationship between concentration and year, but the adjusted and unadjusted trends were similar. In addition to showing meteorology to be an important determinant of concentration, these modeling exercises also suggest a linear or log-linear relationship between concentration and traffic count.

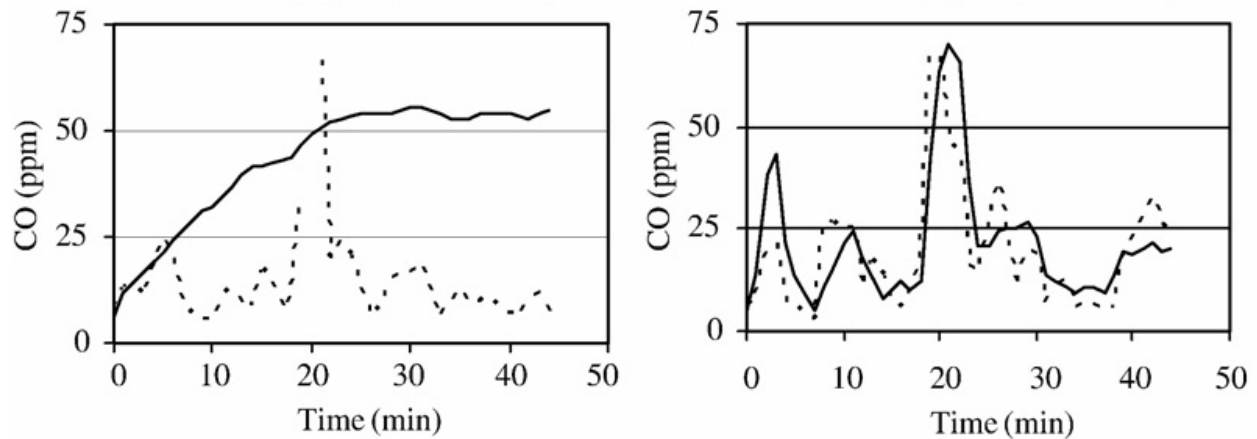
Findings regarding meteorology are consistent with in-vehicle CO concentration studies. Gómez-Perales et al. (2007, [138816](#)) also noted that meteorology can impact in-vehicle exposures, with evening increases in wind speed causing a 50% reduction in CO exposures among bus and minibus commuters. Alm et al. (1999, [047196](#)) made a similar observation in a study of urban commuters' exposure within a vehicle. These observations are sensible given the influence of meteorology on near-road concentrations shown by Baldauf et al. (2008, [190239](#)) and Gokhale and Khare et al (2007, [194015](#)).

A number of studies have focused on transit-time CO exposure, which can occur while in a vehicle or cycling (on-road) or while walking (near-road). Chang et al. (2000, [001276](#)) showed that personal exposures in vehicles were on average 2.8 times higher than ambient concentrations during the summer and 4.1 times higher than ambient concentrations in the winter (Figure 3-46). For the other four microenvironments tested, the average ratio of personal exposure to ambient concentration was ~1. Kaur et al. (2005, [086504](#)) found that transit time exposures in London, U.K., were significantly higher than measurements made at a fixed-site background monitor away from traffic (0.3 ± 0.1 ppm) for car riders (1.3 ± 0.2 ppm), taxi riders (1.1 ± 0.1 ppm), bicyclers (1.1 ± 0.2 ppm), walkers (0.9 ± 0.2 ppm), and bus riders (0.8 ± 0.1 ppm). Curbside measurements (1.5 ± 0.7 ppm) in this study were slightly higher than car riders' exposures. Duci et al. (2003, [044199](#)) found that average in-transit exposures in Athens, Greece, were highest for cars (winter: 21.4 ± 4 ppm), followed by pedestrians (winter: 11.5 ± 2.6 ppm; summer: 10.1 ± 1.7 ppm), buses (winter: 10.4 ± 2.9 ppm; summer: 9.4 ± 3.6 ppm), trolleys (winter: 9.6 ± 1.9 ppm; summer: 8.2 ± 3 ppm), and rail transit (winter: 4 ± 0.6 ppm; summer: 3.4 ± 0.7 ppm). Duci et al. (2003, [044199](#)) did not provide fixed-site CO concentrations but stated that in-transit exposures were higher in each case. Gómez-Perales et al. (2004, [054418](#)) measured CO exposures on buses, minibuses, and metro cars in Mexico City, Mexico, to be 12 ppm, 15 ppm, and 7 ppm, respectively. These values are much higher than CONUS measurements and those presented by Kaur et al. (2005, [086504](#)), but the relative difference between the minibus and bus exposures in the Gómez-Perales et al. study are similar to those seen for the taxi-to-bus or car-to-bus comparisons in Kaur et al. (2005, [086504](#)). These studies indicate that on-road exposures might be influenced by vehicle type, but that city-to-city differences are likely larger than differences between different modes of transport.

Additional analyses from the EXPOLIS study indicated that on-road mobile source emissions were the most important source of CO exposure for non-ETS-exposed subjects (Bruinen de Bruin et al., 2004, [190943](#); Scotto Di Marco et al., 2005, [144054](#)). Scotto di Marco et al. (2005, [144054](#)) found that, for a panel of 201 adult Helsinki, Finland, residents (aged 25-55 yr), subjects spent 8.1% (1.9 h) of their time in transit, which accounted for 12.6% of their total exposure (range of means = 0.96 ppm on a train – 2.8 ppm in a car). Similarly, in a panel study of 50 office workers, Bruinen de Bruin et al. (2004, [190943](#)) found that, in the absence of nonambient sources, the subjects spent 8.5% (2 h) of their time in transit, which accounted for 16.8% of their total exposure, with 2.6% of time spent in a car or taxi accounting for 7.2% of exposure (mean = 5.7 ppm). Commuting time was an important predictor of exposure, such that subjects living in low CO concentration suburban areas and commuting to work experienced higher exposures than urban residents with short commute times. According to the 2007 AHS (U.S. Census Bureau, 2008, [194013](#)), 110.1 million U.S. workers (87.8% of those working) commute to work in automobiles. 32.8% of U.S. workers work at home or commute less than 15 min to work, 32.1% commute 15-29 min to work, 15.1% commute 30-44 min to work, 5.7% commute 45-59 min to work, and 5.0% commute 1 h or longer to work.

Vehicle ventilation can be an important determinant of in-vehicle concentrations. A study from Abi Esber and El Fadel (2008, [190939](#)) in Beirut, Lebanon, is presented because the authors observed in-vehicle CO concentration time series under a range of ventilation conditions, although

the in-vehicle CO concentrations measured are substantially higher than those typically observed in the U.S. Abi Esber and El Fadel (2008, [190939](#)) reported results from CO concentration measurements taken directly outside and within an automobile in Beirut, Lebanon, during the morning commute period of 7:30-9:30 a.m under three different ventilation conditions. Figure 3-47 shows that the time series for the cabin and outdoor CO samples are very similar for the fresh air scenario. However, for the recirculating air ventilation scenario, the in-vehicle concentration increases and then reaches a plateau at a higher level. Abi Esber et al. (2007, [190941](#)) stated that unaccounted sources of CO cause the build-up of in-cabin CO concentrations when the ventilation is set to recirculation mode. The correspondence between in-vehicle and outside-vehicle concentrations for the fresh air ventilation experiments, and lack thereof for the recirculation mode ventilation experiments, observed by Abi Esber and El Fadel (2008, [190939](#)) suggests that in-vehicle concentrations of ambient CO are affected by mode of ventilation.



Source: Reprinted with Permission of Elsevier Ltd. from Abi Esber and El Fadel (2008, [190939](#))

Figure 3-47. Comparison of in-vehicle (solid line) and outside-the-vehicle (dotted line) results for (left) driving with windows closed and air conditioner in recirculating air mode, and (right) driving with windows closed and air conditioner in fresh air mode.

Substantial variability can occur over time within a vehicle. Riediker et al. (2003, [043761](#)) measured CO concentrations inside highway patrol cars during shifts. Troopers recorded in a time-activity diary the ventilation settings of their cars and exit/entry from the vehicle, and the air conditioning was typically set to recirculation mode during the shifts. Riediker et al. (2003, [043761](#)) found that CO concentrations (mean \pm SD: 2.6 ± 1.1 ppm) were higher than ambient monitor concentrations (0.8 ± 0.3 ppm). They were also higher than roadside CO concentrations (1.1 ± 0.3 ppm), indicating that either the vehicle itself contributes to in-cabin CO or on-road concentrations are higher than roadside concentrations or both. Riediker et al. (2003, [043761](#)) noted that within-shift variability was higher than between-shift variability, which underscores the variability in police officers' activities during a given shift. Data were not segregated by ventilation settings, although the police officers typically operated the air conditioning continually because the study was performed during the summer. Alm et al. (1999, [047196](#)) reported in-vehicle CO concentrations of 5.7 ppm in the morning and 3.1 ppm in the afternoon commute for Kuopio, Finland. These data indicate that within-shift variability observed by Riediker et al. (2003, [043761](#)) might be related to time of day. Likewise, Rodes et al. (1998, [010611](#)) reported CO concentrations in vehicles in Sacramento and Los Angeles under different driving conditions (arterial, freeway, high-occupancy-vehicle freeway lane, and "maximum" conditions at rush-hour and nonrush-hour times). They measured peak in-vehicle concentrations spanning 7-67 ppm on a freeway during rush hour, although the mean for each scenario was <6 ppm. In comparison, the peak roadside concentration ranged from 3 to 11 ppm and the peak ambient CO concentration was 1.3 ppm at the time of the measurements. The Rodes et al. (1998, [010611](#)) data agree with results from the Riediker et al.

(2003, [043761](#)) and Alm et al. (1999, [047196](#)) studies showing that substantial variability in CO concentration inside the cabin of a vehicle can occur during the course of a commute.

In their review of roadway exposures to CO and PM, Kaur et al. (2007, [190070](#)) listed a number of factors that may influence near-road or on-road exposure. Vertical CO concentration gradients have been documented in which concentrations decreased with height; lower breathing zone height among children may make them more likely to be exposed to higher CO tailpipe emissions. With respect to transportation, Kaur et al. (2007, [190070](#)) suggested that vehicle ventilation, speed, position in traffic, and start/stop activity influence in-vehicle exposures. Abi Esber and El Fadel (2008, [190939](#)) and Riediker et al. (2003, [043761](#)) illustrated the effect of vehicle ventilation on in-vehicle concentrations. The influence of vehicle speed and start/stop activity is consistent with the turbulence research of Khare et al. (2005, [194016](#)) and Gokhale and Khare (2007, [194015](#)) that suggested an increase in traffic volume and vehicle movement acts to dilute the on-road concentration of CO discussed in Section 3.5.1.3.

3.6.7. Association between Personal CO Exposure and Copollutants

Since incomplete combustion is the primary source of ambient CO in urban areas, exposure to ambient CO is accompanied by exposure to other combustion-related pollutants, such as NO_x, PM, and VOCs. Thus, ambient CO is often considered a surrogate for exposure to traffic-generated pollutants. However, the specific mix of CO with NO_x and PM depends on the source; for example, the mixture generated by gasoline engines differs from that produced by natural gas combustion. Correlations between ambient CO and ambient PM_{2.5}, PM₁₀, NO₂, SO₂, and O₃ from AQS data and the peer-reviewed literature were presented in Section 3.5.3. Nationwide, ambient CO was most highly correlated with ambient NO₂, followed by PM_{2.5} and PM₁₀. Correlations between CO and PM_{2.5} were not consistently positive on a national basis; correlations spanned from negative to positive for ambient CO with ambient SO₂ and ambient PM₁₀, and ambient CO was negatively correlated with ambient O₃. The correlation between ambient CO and specific ambient VOCs depends on parameters such as ambient temperature and the volatility of a specific compound.

Relationships between personal CO exposures and copollutants were reported less frequently in the literature, but results from these studies were consistent with the findings cited above. In a study of personal exposures to CO, PM_{2.5}, and ultrafine PM in a street canyon, Kaur et al. (2005, [086504](#)) found low Pearson's correlation of total personal CO exposure with personal PM_{2.5} exposure ($r = 0.23$). Personal CO exposure had much better correlation with personal ultrafine particle (UFP) exposure ($r = 0.68$). Chang et al. (2000, [001276](#)) reported correlations of personal CO exposure with personal PM_{2.5}, personal toluene, and personal benzene exposures in Baltimore, MD, at five locations, labeled indoor residential, indoor nonresidential, outdoors near roadway, outdoors away from road, and in vehicle. Much variability was observed in the correlations for different locations and seasons (winter versus summer). In general, the correlations of personal CO with personal VOCs tended to be stronger in the winter. Chang et al. (2000, [001276](#)) suggested that lower wintertime indoor air exchange rates could increase exposure to nonambient CO and VOC sources, such as ETS, and hence increase correlations between personal exposure of CO to VOCs. Significant associations of CO with benzene and toluene were also observed in vehicle microenvironments.

3.6.8. Implications for Epidemiology

Exposure error can be an important contributor to variability in epidemiologic study results. Community time-series studies may involve thousands or millions of people whose exposure and health status is estimated over the course of a few years using a short monitoring interval (hours to days). Community-averaged concentration is typically used as a surrogate for ambient exposure in community time-series studies. Exposures and health effects are spatially aggregated over the time intervals of interest because community time-series studies are designed to examine health effects and their potential causes at the community level (e.g., Bell et al., 2009, [194033](#)). A longitudinal cohort epidemiology study typically involves hundreds or thousands of subjects followed over several years or decades. Concentrations are generally aggregated over time and by community to estimate exposures (e.g., Rosenlund et al., 2006, [089796](#)). In addition, panel studies, which consist of a relatively small sample (typically tens) of study participants followed over a period of days to months, have been used to examine the health effects associated with exposure to ambient

concentrations of air pollutants. Panel studies include time-activity diary studies (Akland et al., 1985, [011618](#); Bruinen de Bruin et al., 2004, [190942](#); Scotto Di Marco et al., 2005, [144054](#)). These studies may apply a microenvironmental model to represent exposure to an air pollutant.

The importance of exposure misclassification varies with study design and is dependent on the spatial and temporal aspects of the design. For example, the use of a community-averaged CO concentration in a community time-series epidemiologic study may not allow for adequate examination of the role of spatial variability. Other factors that could influence exposure estimates include spatial and temporal variability related to source strength, topography of the natural and built environment, and meteorology; measurement errors; use of ambient CO concentration as a surrogate for ambient CO exposure; and the presence of CO in a mixture of combustion-related pollutants. The following sections will consider various sources of error and how they affect the interpretation of results from epidemiologic studies of different designs.

3.6.8.1. Measurement Error

Measurement Error at Community-Based Ambient Monitors and Exposure Assessment

Because CO concentrations measured with community-based ambient monitors are often used as surrogates for ambient CO exposure in epidemiology studies, the limitations of the instrumentation are important to consider. As stated in Section 3.4.2, among the 291 monitors meeting completeness criteria for 2005-2007, only 8 were monitors with LOD = 0.04 ppm; the other monitors had LOD of 0.5 ppm. Among the nationwide AQS data for 2005-2007 from these 291 monitors, more than 50% of the hourly CO concentration data were below the LOD of the instrumentation. Data below the LOD adds uncertainty to the association between CO exposure and health effects estimates. Additionally, many of the monitors are not sited for a specific measurement scale, and a given scale classification can represent a range of CO source conditions, as described in Section 3.5.1.3. These factors also contribute uncertainty in interpretation of measurements.

Instrumental measurement error, other than that related to high LOD, is not expected to bias health effect estimates substantially in most circumstances. Because there will be some random component to instrumental measurement error, the correlation of the measured CO concentration with the true CO concentration will likely be <1. When analyzing the effect of instrument error for measuring nonreactive ambient pollutants, Zeger et al. (2000, [001949](#)) stated that the instrument error for ambient measurements “is close to the Berkson type.” In the Berkson error model, the measured-exposure estimate is used instead of the true exposure, based on the assumption that the average measurement is the average of the true exposure. It is generally expected that the health effects estimate will not be biased by using measured values with error but may have more uncertainty than would an estimate based on the true-average exposure. In order for instrument error to cause substantial bias in health effects estimates, the error term (the difference between the true concentrations and the measured concentrations) must be strongly correlated with the measured concentrations.

Measurement Error for Personal Exposure Monitors

Personal electrochemical CO monitors are subject to interference and drift and have a relatively high LOD (~1 ppm) relative to current ambient concentrations. Previous studies in the 1980s and 1990s, when ambient levels were higher, involved successful deployment of these monitors, but more recent exposure studies have avoided personal CO measurements because there are now a high percentage of nondetects. The lack of a suitable personal monitor for measuring low-level exposures (<1 ppm) has hampered field studies assessing personal exposure to ambient CO. Chang et al. (2001, [019216](#)) evaluated the Langan CO monitor as part of an air quality sampling manifold. At relatively high (0.4-3.0 ppm) CO concentrations, the instrument correlated well ($R^2 = 0.93$) with a reference NDIR CO monitor, with the Langan underestimating the CO concentration by 41%. When ambient levels fell consistently below that level, coefficient of determination (R^2) between the Langan and reference monitor fell to $R^2 = 0.40$ in summer and $R^2 = 0.59$ in winter, with

the arithmetic average concentration underestimated by 47% in summer and by 63% in winter. Chang et al. (2001, [019216](#)) pointed out the need for frequent instrument zeroing to minimize instrument drift. Abi Esber and El Fadel (2007, [190940](#)) evaluated a similar personal electrochemical CO sensor, the GEM™ 2000, by comparing measured concentrations with those obtained through co-located grab-bag sampling in a vehicle cabin. Differences between the GEM™ 2000 and the reference samples were fairly low during weekday driving (differences = 2.1-10.6%). Differences on Sundays, when traffic was significantly lower than during weekdays, were dependent on vehicle ventilation conditions, with better agreement when vehicle ventilation allowed for higher cabin CO concentrations (differences = 3.4-5.6%). But the electrochemical sensor did not compare well with reference values when concentrations were low (differences = 20-71%). In general, it is difficult to separate the large instrumental measurement error seen at concentrations below instrument LOD from variation related to nonambient CO sources. This large variation in personal measurements can result in high levels of classical measurement error (Sheppard et al., 2005, [079176](#)).

3.6.8.2. Exposure Issues Related to Nonambient CO

The focus of the ISA is on ambient CO because that is relevant to the NAAQS. Uncertainty related to nonambient CO exposure may make it difficult to distinguish the effect of ambient CO on health effects. Wallace and Ziegenfus (1985, [011656](#)) used NHANES II (1976-1980) data to evaluate the relationship between COHb levels and ambient CO concentration in 20 U.S. cities. They found a significant slope of 0.066% per 1 ppm increase of CO concentration. However, there was much scatter in the data, and variability in ambient CO concentration only accounted for 3% of the variation in COHb. The authors attributed this scatter to variability in nonambient sources such as gas cooking and ETS. This finding illustrates the importance of considering the relative role of ambient and nonambient CO in total personal exposure.

Ambient and nonambient CO are chemically identical and so exert the same health effects. At the same time, ambient and nonambient sources are distinct and not correlated with each other (Wilson and Suh, 1997, [077408](#)) and so would not confound the association between ambient CO exposure and the health effect (see also Sheppard et al., 2005, [079176](#)). Zeger and Diggle (2001, [026017](#)) noted that, because ambient and nonambient CO exposures are uncorrelated, in a health effects model the regression coefficient of ambient concentration should be equal to the product of α (the ratio of ambient exposure to ambient concentration) and the regression coefficient obtained when average personal exposure is used. The confidence intervals around the estimate obtained using total personal exposure would be wider because nonambient CO concentrations add variability. This is true even for the case when the chemical compound is the same for the ambient and nonambient pollutants, as in the case of CO. Likewise, Sheppard et al. (2005, [079176](#)) simulated ambient and nonambient exposures to a nonreactive pollutant and observed that nonambient exposure has no effect on the association between ambient exposure and health outcomes for the case where ambient and nonambient concentrations were independent. Hence, the bias that will be introduced to epidemiologic models by using ambient CO concentration instead of personal exposure to ambient CO is given by the average α . Random variations in daily values of α would not change the health effects estimate but would also widen the confidence intervals around the health effect estimate.

3.6.8.3. Spatial Variability

CO concentration is known to be spatially heterogeneous, as evidenced by the near-road and in-vehicle studies cited in Sections 3.5.1.3 and 3.6.6.2, as well as the intraurban correlations provided in Section 3.5.1.2 and Tables A-9 through A-16 of Annex A. Results from Zhu et al. (2002, [041553](#)), which showed a large CO concentration gradient in the near-road environment, support the contention that CO exposures for those living in the near-road environment but far from a monitor might be underestimated. Conversely, exposures for those living away from roads might be overestimated by near-road CO concentration measurements. Exposure error may occur if the ambient CO concentration measured at the central site monitor is used as an ambient exposure surrogate and differs from the actual ambient CO concentration outside a subject's residence and/or worksite (in the absence of indoor CO sources). Averaging data from a large number of samplers will dampen intersampler variability, and use of multiple monitors over smaller land areas may allow for

more variability to be incorporated into an epidemiologic analysis. This is consistent with conclusions presented in the 2000 AQCD (U.S. EPA, 2000, [000907](#)).

Community exposure may not be well represented when monitors cover large areas with several subcommunities having different sources and topographies. The intersampler correlations of AQS data from monitors, presented in Section 3.5.1.2, reflect how well the time series of concentration data correspond across metropolitan areas. Overall, the data show moderate site-to-site correlation; for example, in the Los Angeles CSA the mean of the correlation was 0.50, and within one standard deviation of the mean, the range of correlations was 0.36-0.65. Bell et al. (2009, [194033](#)) tested the association between monitor density and 1-h max CO effect estimates for CVD hospitalizations for 126 U.S. counties and found an 8% increase in effect estimate size (95% CI: -7% to -24%) with an IQR decrease in area covered by the monitor. This difference was not statistically significant but suggested that the magnitude of the effect estimate might be related to monitor coverage. Sarnat et al. (2009, [180084](#)) studied the spatial variability of CO, along with NO₂, O₃, and PM_{2.5}, in the Atlanta, GA, metropolitan area and how spatial variability affects interpretation of epidemiologic results, using time-series data for circulatory disease ED visits. Sensitivity to spatial variability was examined at slightly greater than neighborhood scale (8 km) in this study. Interestingly, Sarnat et al. (2009, [180084](#)) found that relative risk varied with distance between the monitor and study population when comparing urban to rural locations, but distance of the study population to the monitor was not an important factor when comparing urban population groups. This suggests that, even for spatially heterogeneous CO, urban scale measures may produce results comparable to neighborhood-scale exposures in some circumstances. This may be due to comparability of sites throughout a city, for example, as a result of similar traffic patterns. However, Sarnat et al. (2009, [180084](#)) caution that, because their study was limited to 8 km radii, it is not possible to interpret this work with respect to near-road and on-road microscale exposures.

3.6.8.4. Temporal Variability

Temporal Correlation

Within a city, lack of correlation of relevant time series at various sites results in smoothing the exposure/surrogate concentration function over time and resulting loss of peak structure from the data series. At the same time if monitors are well correlated across a metropolitan area, even if the magnitude of concentration varies over space, time series analyses should provide comparable results across larger spatial areas. Such temporal correlation resulted in the small variation in relative risk estimates within the metropolitan region in Sarnat et al. (2009, [180084](#)), where peak rush-hour times were similar throughout the city, in comparison with the rural area where temporal driving patterns were different. Burnett and Goldberg (2003, [042798](#)) found that community time-series epidemiologic study results reflect actual population dynamics only when five conditions are met: environmental covariates are fixed spatially but vary temporally; the probability of the health effect estimate is small at any given time; each member of the population has the same probability of the health effect estimate at any given time after adjusting for risk factors; each member of the population is equally affected by environmental covariates; and, if risk factors are averaged across members of the population, they will exhibit smooth temporal variation. Note that for this study, Burnett and Goldberg (2003, [042798](#)) analyzed mortality related to PM exposure, but the results are not specific to a given pollutant or health effect and thus are generalized here for time-series analysis. Dominici et al. (2000, [005828](#)) noted that ensuring correlation between ambient and community average exposure time-series air pollutant data is made difficult by limitations in availability and duration of detailed ambient concentration and exposure time-series data, resulting in a source of uncertainty. If sufficient data are available and the time series of concentration data adequately represent population dynamics, then high temporal correlation between sampling sites should limit bias in health effects estimates, even if the magnitude of the concentrations differ.

Seasonality

Community time-series epidemiologic studies can be designed to investigate seasonal effects by incorporating seasonal interaction terms for the exposure surrogate and/or meteorology (e.g., Dominici et al., 2000, [005828](#)). Sheppard et al. (2005, [079176](#)) examined the role of seasonality on epidemiologic models. They found that α for the population will vary seasonally. This makes sense because α is a function of the amount of time spent indoors and outdoors and of indoor ventilation. Given that use of ambient CO concentration instead of ambient CO exposure biases the coefficient used in epidemiologic models by α , Sheppard et al. (2005, [079176](#)) found that seasonal trends causing a change in α would contribute additional positive or negative bias, depending on the season and region of the country. However, several studies discussed in Chapter 5 investigated seasonal effects. No consistent seasonal pattern across health outcomes was observed in these studies.

3.6.8.5. CO Exposure in Copollutant Mixtures

Because CO exposures most often occur together with exposure to other combustion-related pollutants, especially in traffic, interpretation of health studies using ambient CO data can be a challenge, as discussed further in Chapter 5. Ambient CO concentrations from AQS data (Section 3.5.3) have been shown to be correlated with ambient concentrations of NO₂ and VOCs, and personal CO exposures have been correlated with personal PM and VOC exposures (Section 3.6.7). Correlation between factors is one condition for confounding, so it is possible that coexistence of CO with NO₂ or VOCs could confound estimates of the health effects of ambient CO concentrations, and CO concentration could potentially confound estimates of the health effects of NO₂ or VOCs. For this to be true, both CO and the copollutant would have to be correlated with the health outcome of interest. The moderately high correlations between ambient CO and copollutants make it difficult to discern the extent to which CO and other compounds are associated with a given health effect.

It is also possible that the factor of interest may be the multipollutant mixture emitted from on-road or other combustion processes. The HEI Report on Traffic Related Pollutants (HEI, 2009, [191009](#)) suggests that ambient CO, NO₂, and benzene could all be considered as surrogates for mobile source-related pollution, but none are ideal surrogates for mobile-source pollution because ambient CO concentration tends to decrease rapidly with distance from the source (e.g., Baldauf et al., 2008, [190239](#); Zhu et al., 2002, [041553](#)), NO₂ is reactive and benzene is volatile. Additionally, PM components of mobile source emissions change rapidly in size and composition from secondary formation and other atmospheric processing. Given that the mixture of mobile source-related emissions changes rapidly as a result of these factors, the ratio of CO to other components of mobile-source emissions also changes. Hence, even if CO is itself stable within the mixture of copollutants, the dynamic evolution of the mixture may change the representativeness of CO as an indicator of that mixture over time. Additionally, reductions in CO emissions over the past 30 yr have brought ambient CO concentrations down substantially, with more than half of hourly measurements below the LOD for most instruments (Section 3.5.1.1). Furthermore, CO and other copollutants found in mobile-source emissions have multiple anthropogenic and biogenic sources and, as a result, are difficult to attribute solely to mobile source pollution (Section 3.2). For all of these reasons, the representativeness of CO as an indicator of the multipollutant mixture of mobile-source emissions has not been clearly determined.

3.6.8.6. Conclusions

This section presents considerations for exposure assessment and the exposure errors and uncertainties that can potentially affect health effects estimates. These issues can be categorized into the following areas: measurement, nonambient sources, spatial variability, temporal variability, and CO in copollutant mixtures. Potential influences of each of these sources on health effect estimates derived from panel, time-series, and longitudinal epidemiologic studies are described above. Additionally, error sources have the potential to interact with each other. For example, CO concentrations have been shown to decrease rapidly with distance from a highway, and so spatial variability is an important issue in assessing CO exposure. Exposure error may occur if the ambient CO concentration measured at the central site monitor is used as an ambient exposure surrogate and differs from the actual ambient CO concentration outside a subject's residence and/or worksite.

However in time-series epidemiologic studies, spatial variability will only be an important source of error if the time series of CO concentration at different locations are not well correlated in time. The spatial variability of CO, in mixture with the dynamically changing group of mobile source pollutants, adds to the difficulty of quantifying the health effects related specifically to CO compared with those related to other combustion-related copollutants. In most circumstances, exposure error tends to bias a health effect estimate downward (Sheppard et al., 2005, [079176](#); Zeger et al., 2000, [001949](#)). Insufficient spatial or temporal resolution to capture true variability and correlation of CO with copollutants are examples of sources of uncertainty that could widen confidence intervals and so reduce the statistical significance of health effects estimates.

3.7. Summary and Conclusions

3.7.1. CO Sources, Emissions, and Chemistry

In the U.S., on-road mobile sources constituted more than half, or ~61 MT out of ~117 MT, of total CO emissions in the 2002 NEI and BEIS, which are the most recent publicly available CO emission datasets meeting EPA's data quality assurance objectives. In metropolitan areas in the U.S., for example, as much as 75% of all CO emissions can come from on-road vehicle exhaust (U.S. EPA, 2006, [157070](#)). The majority of these on-road CO emissions derive from gasoline-powered vehicles since the O₂ content, pressure, and temperature required for diesel fuel ignition do not produce large quantities of CO. Anthropogenic CO emissions are estimated to have decreased 35% between 1990 and 2002. On-road vehicle sector emissions controls have produced nearly all these national-level CO reductions. Nationally, biogenic emissions, excluding fires, were estimated to contribute ~5%, or ~5.8 MT, of total CO emissions from all sources in 2002, and fires in 2002 added another 16%, or ~18.5 MT, to the national CO emissions total. Although these estimates are generated using well-established approaches, uncertainties inherent in the emission factors and models used to represent sources for which emissions have not been directly measured and vary by source category, season, and region.

In addition to being emitted directly by incomplete combustion, CO is produced by photooxidation of CH₄ and other VOCs in the atmosphere, including NMHCs. Estimating the CO yield from oxidation of HCs larger than CH₄ requires computing the yields of several intermediate products and reactants from oxidation of the parent molecules. The major pathway for removal of CO from the atmosphere is reaction with OH to produce CO₂ and HO₂. The mean photochemical lifetime (τ) of CO in the northern hemisphere is ~57 days. During winter at high latitudes, CO has nearly no photochemical reactivity on urban and regional scales.

3.7.2. Climate Forcing Effects Related to CO

Recent data do not alter the current well-established understanding of the role of urban and regional CO in continental- and global-scale chemistry outlined in the 2000 CO AQCD (U.S. EPA, 2000, [000907](#)) and subsequently confirmed in the recent global assessments of climate change by the Intergovernmental Panel on Climate Change (IPCC, 2001, [156587](#); IPCC, 2007, [092765](#)). CO is a weak direct contributor to RF and greenhouse warming. Sinha and Toumi (1996, [193747](#)) estimated the direct RF of CO computed for all-sky conditions at the tropopause to be 0.024 W/m² based on an assumed change in CO mean global concentrations from 25 to 100 ppb since preindustrial times. The direct RF attributed to CO over this time-frame is ~1.5% of the direct RF for CO₂ estimated by the IPCC (Forster et al., 2007, [092936](#)).

More importantly, CO can indirectly cause increased RF because it reacts with tropospheric OH and thus can increase the lifetime of trace gases in the atmosphere including the GHGs CH₄ and O₃. Additionally, the major pathway for removal of CO from the atmosphere is reaction with OH to produce CO₂. CH₄, O₃, and CO₂ absorb infrared radiation from the Earth's surface and contribute to the greenhouse effect. Indirect RF attributed to 1750-2005 emissions of CO through changes in concentration of the GHGs O₃, CH₄, and CO₂ was estimated by Forster et al. (2007, [092936](#)) to be ~0.2 W/m² or ~12% of the direct RF of CO₂ (Figure 3-7). The future direct and indirect integrated

RF for year 2000 emissions of CO was estimated to be $\sim 0.2 \text{ W/m}^2\cdot\text{yr}$ with $\sim 50\%$ uncertainty over both 20-yr and 100-yr time horizons (Figure 3-8). The RF related to short-lived CO is $\sim 25\%$ of that for CO₂ for a 20-yr time horizon, but only $\sim 7\%$ of that for longer-lived CO₂ over a 100-yr time horizon. Overall, the evidence reviewed in this assessment is sufficient to conclude that **a causal relationship exists between current atmospheric concentrations of CO and effects on climate.**

3.7.3. Ambient CO Measurements

As of August 2009, 24 automated FRMs and no FEMs had been approved for monitoring CO. All EPA FRMs for CO operate on the principle of nondispersive infrared (NDIR) detection and can include gas filter correlation (GFC). Current specifications for CO monitoring are designed to help states demonstrate whether they have met compliance criteria, with requirements for an LOD of 1 ppm. The reported LOD for 20 of the 24 FRMs is 0.5 ppm, and four models of FRMs are in operation with an LOD of 0.04 ppm. FRMs with higher LOD also are limited to a precision of 0.1 ppm and are more subject to drift compared with newer monitors with automatic drift correction options.

For 2005-2007, there were 291 CO monitors meeting the 75% completeness requirements and reporting values year-round to the AQS in the 50 states, plus the District of Columbia, Puerto Rico, and the Virgin Islands. 57 monitors across the U.S. have been sited at microscale to capture near-road concentrations, 31 have been sited at middle scale, and 119 are sited for neighborhood scale monitoring; among the remaining 84 monitors, states did not declare the spatial scale of monitoring for 71 monitors, and 13 are sited for monitoring urban or regional scale. For CO, traffic is the major source in an urban setting and therefore microscale data are sited “to represent distributions within street canyons, over sidewalks, and near major roadways” while middle scale monitors are sited to represent “air quality along a commercially developed street or shopping plaza, freeway corridors, parking lots and feeder streets” (40 CFR Part 58 Appendix D). At middle and neighborhood scales, required minimum monitor distance from a road is directly related to the road’s average daily traffic count to capture community averages. Ambient monitors for CO and other criteria pollutants are located to monitor compliance rather than population exposures. However, AQS monitors are often used for exposure assessment. When comparing CO monitor location with population density, it was observed that population coverage varies both within and between cities.

3.7.4. Environmental CO Concentrations

CO concentration data for 1-h and 8-h intervals were available for 243 counties and autonomous cities or municipalities that maintained active CO monitoring stations meeting the 75% completeness criteria for the years 2005-2007. There were no violations of the 1-h or 8-h NAAQS in those years. The nationwide mean, median, and interquartile range for 1-h measurements reported between 2005 and 2007 were 0.5, 0.4, and 0.4 ppm, respectively, and these statistics did not change by more than 0.1 ppm for each year of the 3-yr period. More than 50% of the data nationwide were below the LOD for the majority of monitors in use. The nationwide mean, median, and interquartile range for 8-h daily max concentrations, reported between 2005 and 2007, were 0.7, 0.5, and 0.5 ppm, respectively. Half of the 8-h daily max concentrations fell below the LOD for the majority of CO monitors in the field. The 2006 annual second highest 8-h CO concentration, averaged across 144 monitoring sites nationwide, was 75% below that for 1980 and is the lowest concentration recorded during the past 27 yr. The mean annual second highest 8-h ambient CO concentration has been below 5 ppm since 2004. The downward trend in CO concentrations in the 1990s parallels the downward trend observed in CO emissions and can be attributed largely to decreased mobile source emissions.

The correlation structures for measurements at the monitors in each of the 11 CSAs/CBSAs examined for this assessment reveal a wide range of responses between monitors in each city and among the cities. While this wide range is produced by the interactions of many physical and chemical elements, the location of each monitor and the uniqueness of its immediate surroundings can often explain much of the agreement or lack thereof. CO concentrations can be elevated near roadways and decrease with increasing distance from the road. Anchorage, AK, had concentrations roughly twice those of the other metropolitan areas. Most of the CSAs/CBSAs examined here had

diel concentration curves with pronounced morning and evening rush hour peak CO levels, although diel CO concentrations had less variability for New York City, Atlanta, and Seattle than for the other eight cities. For most metropolitan areas examined here, concentrations were generally highest in the winter (December-February) and fall (September-November) and decreased, on average, during the spring (March-May) and summer (June-August). Measurements near or below the 0.5 ppm LOD for most instruments, coupled with the coarsely reported measurement resolution of 0.1 ppm, can artificially influence the comparison statistics shown in the tables and result in apparent heterogeneity in the box plots (Figure 3-19 and Figure 3-22).

CO measurements obtained at different monitoring scales were compared to assess spatial variability of CO concentration. The median hourly CO concentration across the U.S. obtained at microscale monitors was 25% higher than at middle scale and 67% higher than at neighborhood scale. The microscale and middle scale CO data reported here are consistent with hourly concentrations reported in the literature for the near-road environment within the United States, with CO concentration decaying with downwind distance from the road. Determinants of spatial variability of ambient CO concentration within the near-road environment include roadway density, traffic counts, meteorology, and natural and urban topography.

In all cases, a wide range of correlations existed between CO and copollutants computed from AQS data. The mean and median correlations between CO and copollutants were positive for NO₂, PM₁₀, and PM_{2.5}; near zero for SO₂; and negative for O₃. These findings might reflect common combustion sources for CO, NO₂, and PM. Among those copollutants with positive associations, NO₂ had the highest mean and median correlations, followed by PM_{2.5} and PM₁₀. Within and between individual metropolitan areas, the distribution of copollutant correlations varied substantially. Studies in the literature also found fairly high correlations of CO with EC and certain VOCs.

This assessment has used data from 2005-2007 at 12 remote sites as part of the international CCGG CASN in the CONUS, Alaska, and Hawaii to determine PRB. All sites demonstrate the well-known seasonality in background CO, with minima in the summer and fall and maxima in the winter and spring. The 3-yr avg CO PRB in Alaska was 130 ppb; in Hawaii it was 99 ppb; and over the CONUS it was 132 ppb.

3.7.5. Exposure Assessment and Implications for Epidemiology

Very few recent exposure assessment studies involve ambient CO concentration data. The studies of personal exposure to ambient CO presented here generally found that the largest percentage of time in which an individual is exposed to ambient CO occurs indoors, but the highest ambient CO exposure levels occur in transit. In-vehicle CO concentrations are typically reported to be between 2 and 5 times higher than ambient concentrations, although peak in-vehicle concentrations more than an order of magnitude higher than corresponding ambient monitor concentrations have also been reported. Among commuters, exposures were higher for those traveling in automobiles in comparison with those traveling on buses and motorbikes and with those cycling or walking. Ambient CO exposure in automobiles has been demonstrated to vary with vehicle ventilation settings, and a very small portion of that exposure is thought to come from the vehicle in which the exposed person travels. High near-road CO concentrations can be important for those living in the near-road environment because virtually all of ambient CO infiltrates indoors. Hence, indoor exposure to ambient CO is determined by the CO concentration outside the building. Residents of the 17.9 million occupied homes located within approximately 90 m of a highway, railroad, or airport may be exposed to elevated ambient CO levels. However, CO concentration in the near-road environment has been shown to decrease sharply with downwind distance from a highway, wind direction, emission source strength (e.g., number of vehicles on a highway). Natural and urban topography also influence localized ambient CO levels.

Recent exposure assessment studies support one of the main conclusions of the 2000 CO AQCD, that central-site ambient CO monitors may overestimate or underestimate individuals' personal exposure to ambient CO because ambient CO concentration is spatially variable, particularly when analyzing exposures in the near-road environment. Exposure error may occur if the ambient CO concentration measured at the central-site monitor is used as an ambient exposure surrogate and differs from the actual ambient CO concentration outside a subject's residence and/or worksite. For example, measurement at a "hot spot" could skew community exposure estimates upwards, and likewise measurement at a location with few nearby CO sources could skew exposure

estimates downwards. Correlations across CO monitors can vary widely from within and between cities across the U.S. as a function of natural and urban topography, meteorology, and strength and proximity to sources. Typically, intersampler correlation ranges from 0.35 to 0.65 for monitors sited at different scales within a metropolitan area, although it can be greater than 0.8 in some areas. Health effects estimates from time-series epidemiologic studies are not biased by spatial variability in CO concentrations if concentrations at different locations are correlated in time. Additionally, exposure assessment is complicated by the existence of CO in multipollutant mixtures emitted by combustion processes. Because ambient CO exists in a mixture with volatile and reactive pollutants, the correlation between exposure to ambient CO and copollutants can vary substantially over time and across locations. For this reason, it is difficult to quantify the effects related specifically to CO exposure compared with those related to another combustion-related pollutant or mix of pollutants. In most circumstances, exposure error tends to bias a health effect estimate downward. Spatial and temporal variability not fully captured by ambient monitors and correlation of CO with copollutants are examples of sources of uncertainty that could widen confidence intervals of health effects estimates.

References

- Abdul-Wahab SA (2004). An application and evaluation of the CAL3QHC model for predicting carbon monoxide concentrations from motor vehicles near a roadway intersection in Muscat, Oman. *Environ Manage*, 34: 372-382. [194011](#)
- Abi-Esber L; El-Fadel M (2008). In-vehicle CO ingestion: Validation through field measurements and mass balance simulations. *Sci Total Environ*, 394: 75-89. [190939](#)
- Abi-Esber L; El-Fadel M; Nuwayhid I; Saliba N (2007). The effect of different ventilation modes on in-vehicle carbon monoxide exposure. *Atmos Environ*, 41: 3644-3657. [190941](#)
- Abi-Esber L; El-Fadel M; Shihadeh A (2007). Comparison of trip average in-vehicle and exterior CO determinations by continuous and grab sampling using an electrochemical sensing method. *Atmos Environ*, 41: 6087-6094. [190940](#)
- Akland GG; Hartwell TD; Johnson TR; Whitmore RW (1985). Measuring human exposure to carbon monoxide in Washington, DC, and Denver, Colorado, during the winter of 1982-1983. *Environ Sci Technol*, 19: 911-918. [011618](#)
- Alm S; Jantunen MJ; Vartiainen M (1999). Urban commuter exposure to particle matter and carbon monoxide inside an automobile. *J Expo Sci Environ Epidemiol*, 9: 237-244. [047196](#)
- Alm S; Mukala K; Jantunen MJ (2000). Personal carbon monoxide exposures of preschool children in Helsinki, Finland: Levels and determinants. *Atmos Environ*, 34: 277-285. [192374](#)
- Alm S; Mukala K; Tiittanen P; Jantunen MJ (2001). Personal carbon monoxide exposures of preschool children in Helsinki, Finland-comparison to ambient air concentrations. *Atmos Environ*, 35: 6259-6266. [020237](#)
- Altshuller AP (1991). Estimating product yields of carbon-containing products from the atmospheric photooxidation of ambient air alkenes. *J Atmos Chem*, 13: 131-154. [192375](#)
- Andreae MO (1991). Biomass burning: its history, use, and distribution and its impact on environmental quality and global climate. In Levine JS (Ed.), *Global Biomass Burning: Atmospheric, Climatic, and Biospheric Implications* (pp. 1-21). Cambridge, MA: MIT Press. [078147](#)
- Annest JH; Clower J; Yip F; Stock A; Lucas M; Iqbal S (2008). Nonfatal, unintentional, non-fire-related carbon monoxide exposures-United States, 2004-2006. *JAMA*, 300: 896-9. [190236](#)
- Baldauf R; Thoma E; Hays M; Shores R; Kinsey J; Gullett B; Kimbrough S; Isakov V; Long T; Snow R; Khlystov A; Weinstein J; Chen FL; Seila R; Olson D; Gilmour I; Cho SH; Watkins N; Rowley P; Bang J (2008). Traffic and meteorological impacts on near-road air quality: Summary of methods and trends from the Raleigh near-road study. *J Air Waste Manag Assoc*, 58: 865-878. [190239](#)
- Baldauf R; Thoma E; Khlystov A; Isakov V; Bowker G; Long T; Snow R (2008). Impacts of noise barriers on near-road air quality. *Atmos Environ*, 42: 7502-7507. [191017](#)
- Behrentz E; Fitz DR; Pankratz DV; Sabin LD; Colome SD; Fruin SA; Winer AM (2004). Measuring self-pollution in school buses using a tracer gas technique. *Atmos Environ*, 38: 3735-3746. [155682](#)
- Bell M; Namdeo A; Chen H; Ashmore M; Terry A; Dimitroulopoulou S (2004). Reducing Urban Pollution Exposure from Road Transport (RUPERT). In *Urban Transport* (pp. 829-838). Southampton, UK: WIT Press. [192376](#)
- Bell ML; Peng RD; Dominici F; Samet JM (2009). Emergency hospital admissions for cardiovascular diseases and ambient levels of carbon monoxide: results for 126 U.S. urban counties, 1999-2005. *Circulation*, 120: 949-955. [194033](#)
- Bergamaschi P; Hein R; Heimann M; Crutzen PJ (2000). Inverse modeling of the global CO cycle 1. Inversion of CO mixing ratios. *J Geophys Res*, 105: 1909-1927. [192377](#)

Note: Hyperlinks to the reference citations throughout this document will take you to the NCEA HERO database (Health and Environmental Research Online) at <http://epa.gov/hero>. HERO is a database of scientific literature used by U.S. EPA in the process of developing science assessments such as the Integrated Science Assessments (ISAs) and the Integrated Risk Information System (IRIS)

- Berntsen T; Fuglestvedt JS; Joshi M; Shine KP; Stuber N; Sausen R; Li L; Hauglustaine DA; Ponater M (2005). Response of climate to regional emissions of ozone precursors: Sensitivities and warming potentials. *Tellus B Chem Phys Meteorol*, 57: 283-304. [193241](#)
- Berntsen T; Fuglestvedt JS; Myhre G; Stordal F; Berglen TF (2006). Abatement of greenhouse gases: Does location matter? *Clim Change*, 74: 377-411. [193244](#)
- Bey I; Jacob DJ; Yantosca RM; Logan JA; Field B; Fiore AM; Li Q; Liu H; Mickley LJ; Schultz MG (2001). Global modeling of tropospheric chemistry with assimilated meteorology: model description and evaluation. *J Geophys Res*, 106: 23073-23095. [051218](#)
- Bishop GA; Stedman DH (2008). A decade of on-road emissions measurements. *Environ Sci Tech*, 42: 1651-1656. [194670](#)
- Bogo H; Gomez DR; Reich SL; Negri RM; Roman ES (2001). Traffic pollution in a downtown site of Buenos Aires City. *Atmos Environ*, 35: 1717-1727. [192378](#)
- Borrego C; Tchepel O; Costa AM; Martins H; Ferreira J; Miranda AI (2006). Traffic-related particulate air pollution exposure in urban areas. *Atmos Environ*, 40: 7205-7214. [155697](#)
- Bowker GE; Baldauf R; Isakov V; Khlystov A; Petersen W (2007). The effects of roadside structures on the transport and dispersion of ultrafine particles from highways. *Atmos Environ*, 41: 8128-8139. [149997](#)
- Brauer M; Hoek G; van Vliet P; Meliefste K; Fischer P; Gehring U; Heinrich J; Cyrys J; Bellander T; Lewne M; Brunekreef B (2003). Estimating long-term average particulate air pollution concentrations: application of traffic indicators and geographic information systems. *Epidemiology*, 14: 228-239. [155702](#)
- Brauer M; Lencar C; Tamburic L; Koehoorn M; Demers P; Karr C (2008). A cohort study of traffic-related air pollution impacts on birth outcomes. *Environ Health Perspect*, 116: 680-686. [156292](#)
- Brewer DA; Oglaruso MA; Augustsson TR; Levine JS (1984). The oxidation of isoprene in the troposphere: Mechanism and model calculations. *Atmos Environ*, 18: 2723-2744. [194402](#)
- Briggs DJ; Collins S; Elliott P; Fischer P; Kingham S; Lebret E; Pryn K; Van Reeuwijk H; Smallbone K; Van Der Veen A (1997). Mapping urban air pollution using GIS: a regression-based approach. *Int J Geogr Inform Sci*, 11: 699-718. [025950](#)
- Britter RE; Hanna SR (2003). Flow and dispersion in urban areas. *Annu Rev Fluid Mech*, 35: 469-496. [090295](#)
- Bruinen de Bruin Y; Carrer P; Jantunen M; Hänninen O; Scotto di Marco G; Kephelopoulos S; Cavallo D; Maroni M (2004). Personal carbon monoxide exposure levels: Contribution of local sources to exposures and microenvironment concentrations in Milan. *J Expo Anal Environ Epidemiol*, 14: 312-322. [190943](#)
- Bruinen de Bruin Y; Hanninen O; Carrer P; Maroni M; Kephelopoulos S; Scotto di Marco G; Jantunen M (2004). Simulation of working population exposures to carbon monoxide using EXPOLIS-Milan microenvironment concentration and time-activity data. *J Expo Anal Environ Epidemiol*, 14: 154-163. [190942](#)
- Burgard DA; Bishop GA; Stedman DH; Gessner VH; Daeschlein C (2006). Remote sensing of in-use heavy-duty diesel trucks. *Environ Sci Technol*, 40: 6938-6942. [193222](#)
- Burke JM; Zufall MJ; Ozkaynak H (2001). A population exposure model for particulate matter: case study results for PM_{2.5} in Philadelphia, PA. *J Expo Sci Environ Epidemiol*, 11: 470-489. [014050](#)
- Burnett RT; Goldberg MS (2003). Size-fractionated particulate mass and daily mortality in eight Canadian cities. *Health Effects Institute*. Boston, MA. [042798](#)
- CalTrans (2009). CalTrans. Retrieved 02-AUG-09, from <http://traffic-counts.dot.ca.gov/>. [194036](#)
- Carslaw DC; Beevers SD; Tate JE (2007). Modelling and assessing trends in traffic-related emissions using a generalised additive modelling approach. *Atmos Environ*, 41: 5289-5299. [148210](#)
- Carter WPL (1998). Updated maximum incremental reactivity scale for regulatory applications. Air Pollution Research Center and College of Engineering, Center for Environmental Research and Technology. University of California, Riverside CA. [192380](#)
- Cassidy BE, Alabanza-Akers MA, Akers TA, Hall DB, Ryan PB, Bayer CW, Naehar LP (2007). Particulate matter and carbon monoxide multiple regression models using environmental characteristics in a high diesel-use area of Baguio City, Philippines. *Sci Total Environ*, 381: 47-58. [199975](#)

- Chaloulakou A; Mavroidis I (2002). Comparison of indoor and outdoor concentrations of CO at a public school: Evaluation of an indoor air quality model. *Atmos Environ*, 36: 1769-1781. [026050](#)
- Chaloulakou A; Mavroidis I; Duci A (2003). Indoor and outdoor carbon monoxide concentration relationships at different microenvironments in the Athens area. *Chemosphere*, 52: 1007-1019. [190945](#)
- Chang C-H; Meroney RN (2003). Concentration and flow distributions in urban street canyons: wind tunnel and computational data. *J Wind Eng Ind Aerod*, 91: 1141-1154. [090298](#)
- Chang L-T; Koutrakis P; Catalano PJ; Suh HH (2000). Hourly personal exposures to fine particles and gaseous pollutants-- results from Baltimore, Maryland. *J Air Waste Manag Assoc*, 50: 1223-1235. [001276](#)
- Chang L-T; Suh HH; Wolfson JM; Misra K; Allen GA; Catalano PJ; Koutrakis P (2001). Laboratory and field evaluation of measurement methods for one-hour exposures to O₃, PM₂₅, and CO. *J Air Waste Manag Assoc*, 51: 1414-1422. [019216](#)
- Chen H; Namdeo A; Bell M (2008). Classification of road traffic and roadside pollution concentrations for assessment of personal exposure. *Environ Modell Softw*, 23: 282-287. [193986](#)
- Collins WJ; Derwent RG; Johnson CE; Stevenson DS (2002). The oxidation of organic compounds in the troposphere and their global warming potentials. *Clim Change*, 52: 453-479. [044156](#)
- Connors VS; Gormsen BB; Nolf S; Reichle HG (1994). Space-borne observations of the global distribution of carbon monoxide in the middle troposphere during April and October 1994. *J Geophys Res*, 104: 21455-21470. [193755](#)
- Conrad R; Seiler W (1985). Influence of temperature, moisture, and organic carbon on the flux of H₂ and CO between soil and atmosphere: field studies in subtropical regions. *J Geophys Res*, 90: 5699-5709. [029520](#)
- Croxford B; Penn A (1998). Siting considerations for urban pollution monitors. *Atmos Environ*, 32: 1049-1057. [087176](#)
- Crutzen PJ (1987). Role of the tropics in atmospheric chemistry. In Dickinson RE (Ed.), *Geophysiology of Amazonia: Vegetation and climate interactions* (pp. -). New York, NY: John Wiley and Sons. [002848](#)
- Crutzen PJ; Delany AC; Greenberg J; Haagenson P; Heidt L; Lueb R; Pollock W; Seiler W; Wartburg A; Zimmerman P (1985). Tropospheric chemical composition measurements in Brazil during the dry season. *J Atmos Chem*, 2: 233-256. [194403](#)
- Daniel JS; Solomon S (1998). On the climate forcing of carbon monoxide. *J Geophys Res*, 103: 13249-13260. [193235](#)
- Delfino RJ; Chang J; Wu J; Ren C; Tjoa T; Nickerson B; Cooper D; Gillen DL (2009). Repeated hospital encounters for asthma in children and exposure to traffic-related air pollution near the home. *Ann Allergy Asthma Immunol*, 102: 138-44. [190254](#)
- Derwent RG; Collins WJ; Johnson CE; Stevenson DS (2001). Transient behaviour of tropospheric ozone precursors in a global 3-D CTM and their indirect greenhouse effects. *Clim Change*, 49: 463-487. [047912](#)
- Dimitroulopoulou C; Ashmore MR; Byrne MA; Kinnersley RP (2001). Modelling of indoor exposure to nitrogen dioxide in the UK. *Atmos Environ*, 35: 269-279. [014737](#)
- Dimitroulopoulou C; Ashmore MR; Hill MTR; Byrne MA; Kinnersley R (2006). INDAIR: a probabilistic model of indoor air pollution in UK homes. *Atmos Environ*, 40: 6362-6379. [090302](#)
- Dominici F; Zeger SL; Samet JM (2000). A measurement error model for time-series studies of air pollution and mortality. *Biostatistics*, 1: 157-175. [005828](#)
- Doran JC; Berkowitz CM; Coulter RL; Shaw WJ; Spicer CW (2003). The 2001 Phoenix Sunrise experiment: vertical mixing and chemistry during the morning transition in Phoenix. *Atmos Environ*, 37: 2365-2377. [143352](#)
- Duci A; Chaloulakou A; Spyrellis N (2003). Exposure to carbon monoxide in the Athens urban area during commuting. *Sci Total Environ*, 309: 47-58. [044199](#)
- Duncan BN; Logan JA (2008). Model analysis of the factors regulating the trends and variability of carbon monoxide between 1988 and 1997. *Atmos Chem Phys*, 8: 7389-7403. [194042](#)
- Edwards DP; Emmons LK; Hauglustaine DA; Chu DA; Gille JC; Kaufman YJ; Petron G; Yurganov LN; Giglio L; Deeter MN; Yudin V; Ziskin DC; Warner J; Lamarque J-F; Francis GL; Ho SP; Mao D; Chen J; Grechko EI; Drummond JR (2004). Observations of carbon monoxide and aerosols from the Terra satellite: Northern Hemisphere variability. *J Geophys Res*, 109: D24202. [199889](#)

- Emmons LK; Deeter MN; Gille JC; Edwards DP; Attie JL; Warner J; Ziskin D; Francis G; Khattatov B; Yudin V; Lamarque JF; Ho SP; Mao D; Chen JS; Drummond J; Novelli P; Sachse G; Coffey MT; Hannigan JW; Gerbig C; Kawakami S; Kondo Y; Takegawa N; Schlager H; Baehr J; Ziereis H (2004). Validation of Measurements of Pollution In The Troposphere (MOPITT) CO retrievals with aircraft in situ profiles. *J Geophys Res*, 109: D03309. [193756](#)
- Fehsenfeld FC; Ancellet G; Bates TS; Goldstein AH; Hardesty RM; Honrath R; Law KS; Lewis AC; Leaitch R; McKeen S; Meagher J; Parrish DD; Pszenny AAP; Russell PB; Schlager H; Seinfeld J; Talbot R; Zbinden R (2006). International consortium for atmospheric research on transport and transformation (ICARTT): North America to Europe -overview of the 2004 summer field study . *J Geophys Res*, 111: D23S01.1-D23S01.36. [190531](#)
- Finlayson-Pitts BJ; Pitts JN Jr (2000). *Chemistry of the upper and lower atmosphere: theory, experiments and applications*. San Diego, CA: Academic Press. [055565](#)
- Fiore AM; Jacob DJ; Field BD; Streets DG; Fernandes SD; Jang C (2002). Linking ozone pollution and climate change: the case for controlling methane. *Geophys Res Lett*, 2919: 1919. [051221](#)
- Fiore AM; West JJ; Horowitz LW; Naik V; Schwartzkopf MD (2008). Characterizing the tropospheric ozone response to methane emission controls and the benefits to climate and air quality. *J Geophys Res*, 113: D08307. [193749](#)
- Fishman J; Bowman KW; Burrows JP; Richter A; Chance KV; Edwards DP; Martin RV; Morris GA; Pierce RB; Ziemke JR; Al-Saadi JA; Creilson JK; Schaack TK; Thompson AM (2008). Remote sensing of tropospheric pollution from space. *Bull Am Meteorol Soc*, 89: 805-821. [193927](#)
- Flachsbart PG (1999). Models of exposure to carbon monoxide inside a vehicle on a Honolulu highway. *J Expo Sci Environ Epidemiol*, 9: 245-260. [015857](#)
- Forster P; Ramaswamy V; Artaxo P; Berntsen T; Betts R; Fahey DW; Haywood J; Lean J; Lowe DC; Myhre G; Nganga J; Prinn R; Raga G; Schultz M; Van Dorland R (2007). Changes in atmospheric constituents and in radiative forcing, Chapter 2. In Solomon S, Qin D; Manning M; Chen Z; Marquis M; Averyt KB; Tignor M; Miller HL (Ed.), IPCC Fourth Assessment Report (AR4): Climate Change 2007: Working Group I Report: The Physical Science Basis. (pp. 129-234). Cambridge, U.K. and New York, NY: Intergovernmental Panel on Climate Change; Cambridge University Press. [092936](#)
- Fuglestad J; Berntsen T; Myhre G; Rypdal K; Skeie RB (2008). Climate forcing from the transport sectors. *PNAS*, 105: 454-458. [193242](#)
- Fuglestad JS; Berntsen TK; Isaksen ISA; Mao H; Liang X-Z; Wang W-C (1999). Climatic forcing of nitrogen oxides through changes in tropospheric ozone and methane; global 3D model studies. *Atmos Environ*, 33: 961-978. [047431](#)
- Gentner DR; Harley RA; Miller AM; Goldstein AH (2009). Diurnal and seasonal variability of gasoline-related volatile organic compound emissions in Riverside, California. *Environ Sci Technol*, 43: 4247-4252. [194034](#)
- Georgoulis LB; Hanninen O; Samoli E; Katsouyanni K; Kunzli N; Polanska L; De Bruin YB; Alm S; Jantunen M (2002). Personal carbon monoxide exposure in five European cities and its determinants. *Atmos Environ*, 36: 963-974. [025563](#)
- Gilliland F; Avol E; Kinney P; Jerrett M; Dvonch T; Lurmann F; Buckley T; Breyse P; Keeler G; de Villiers T; McConnell R (2005). Air pollution exposure assessment for epidemiologic studies of pregnant women and children: lessons learned from the Centers for Children's Environmental Health and Disease Prevention Research. *Environ Health Perspect*, 113: 1447-54. [098820](#)
- Gokhale S; Khare M (2007). Statistical behavior of carbon monoxide from vehicular exhausts in urban environments. *Environ Modell Softw*, 22: 526-535. [194015](#)
- Goldstein A; Galbally I (2007). Known and unexplored organic constituents in the earth's atmosphere. *Environ Sci Technol*, 41: 1514-1521. [193247](#)
- Gómez-Perales JE; Colville RN; Fernández-Bremauntz AA; Gutiérrez-Avedoy V; Páramo-Figueroa VH; Blanco-Jiménez S; Bueno-López E; Bernabé-Cabanillas R; Mandujano F; Hidalgo-Navarro M; Nieuwenhuijsen MJ (2007). Bus, minibus, metro inter-comparison of commuters' exposure to air pollution in Mexico City. *Atmos Environ*, 41: 890-901. [138816](#)

- Gómez-Perales JE; Colville RN; Nieuwenhuijsen MJ; Fernández-Bremauntz A; Gutiérrez-Avedoy VJ; Páramo-Figueroa VH; Blanco-Jiménez S; Bueno-López E; Mandujano F; Bernabé-Cabanillas R (2004). Commuters' exposure to PM_{2.5}, CO, and benzene in public transport in the metropolitan area of Mexico City. *Atmos Environ*, 38: 1219-1229. [054418](#)
- Gulliver J; Briggs DJ (2005). Time-space modeling of journey-time exposure to traffic-related air pollution using GIS. *Environ Res*, 97: 10-25. [191079](#)
- Hanst PL; Spence JW; Edney EO (1980). Carbon monoxide production in photooxidation of organic molecules in the air. *Atmos Environ*, 14: 1077-1088. [011988](#)
- Harley RA; Marr LC; Lehner JK; Giddings SN (2005). Changes in motor vehicle emissions on diurnal to decadal time scales and effects on atmospheric composition. *Environ Sci Technol*, 39: 5356-5362. [088154](#)
- Harley RA; McKeen SA; Pearson J; Rodgers MO; Lonneman WA (2001). Analysis of motor vehicle emissions during the Nashville/Middle Tennessee Ozone Study. *J Geophys Res*, 106: 3559-3567. [193922](#)
- Hauglustaine DA; Hourdin F; Jourdain L; Filiberti MA; Walters S; Lamarque JF; Holland EA (2004). Interactive chemistry in the Laboratoire de Meteorologie Dynamique general circulation model: Description and background tropospheric chemistry evaluation. *J Geophys Res*, 109: D04314. [193191](#)
- HEI (2009). Traffic-related air pollution: A critical review of the literature on emissions, exposure, and health effects. Health Effects Institute. Boston. Special Report 17. [191009](#)
- Heist DK; Perry SG; Brixey LA (2009). A wind tunnel study of the effect of roadway configurations on the dispersion of traffic-related pollution. *Atmos Environ*, In Press: In Press. [194037](#)
- Hoek G; Beelen R; de Hoogh K; Vienneau D; Gulliver J; Fischer P; Briggs D (2008). A review of land-use regression models to assess spatial variation of outdoor air pollution. *Atmos Environ*, 42: 7561-7578. [195851](#)
- Horowitz LW; Walters S; Mauzerall DL; Emmons LK; Rasch PJ; Granier C; Tie X; Lamarque J-F; Schultz MG; Tyndall GS; Orlando JJ; Brasseur GP (2003). A global simulation of tropospheric ozone and related tracers: Description and evaluation of MOZART, version 2. *J Geophys Res*, 108: D24. [057770](#)
- Hudman RC; Jacob DJ; Turquety S; Leibensperger EM; Murray LT; Wu S; Gilliland AB; Avery M; Bertram TH; Brune W; Cohen RC; Dibb JE; Flocke FM; Fried A; Holloway J; Neuman JA; Orville R; Perring A; Ren X; Sachse GW; Singh HB; Swanson A; Wooldridge PJ (2007). Surface and lightning sources of nitrogen oxides over the United States: Magnitudes, chemical evolution, and outflow. *J Geophys Res*, 112: D12S05. [089474](#)
- Hudman RC; Murray LT; Jacob DJ; Millet DB; Turquety S; Wu S; Blake DR; Goldstein AH; Holloway J; Sachse GW (2008). Biogenic versus anthropogenic sources of CO in the United States. *Geophys Res Lett*, 35: L04801. [191253](#)
- Inman RE; Ingersoll RB; Levy EA (1971). Soil: a natural sink for carbon monoxide. *Science*, 172: 1229-1231. [010972](#)
- IPCC (2001). *Climate Change 2001: The Scientific Basis*. Contribution of Working Group I to the Third Assessment Report (TAR) of the Intergovernmental Panel on Climate Change [Houghton, J.T., Y. Ding, D.J. Griggs, M. Noguer, P.J. van der Linden, X. Dai, K. Maskell, and C.A. Johnson (eds.)]. Cambridge, UK and New York, NY, USA: Intergovernmental Panel on Climate Change, Cambridge University Press. [156587](#)
- IPCC (2007). *Climate Change 2007: The Physical Science Basis*. Contribution of Working Group I to the Fourth Assessment Report (AR4) of the Intergovernmental Panel on Climate Change. Cambridge, UK and New York, NY: Intergovernmental Panel on Climate Change, Cambridge University Press. [092765](#)
- Isakov V; Touma JS; Burke J; Lobdell DT; Palma T; Rosenbaum A; Ozkaynak H (2009). Combining regional- and local-scale air quality models with exposure models for use in environmental health studies. *J Air Waste Manag Assoc*, 59: 461-472. [191192](#)
- Isaksen ISA; Hov O (1987). Calculation of trends in the tropospheric concentration of O₃, OH, CO, CH₄ and NO_x. *Tellus B Chem Phys Meteorol*, 39: 271-285. [019490](#)
- Jacob DJ; Wofsy SC (1990). Budgets of reactive nitrogen, hydrocarbons, and ozone over the Amazon forest during the wet season. *J Geophys Res*, 95: 16,737-16,754. [029668](#)
- Jeffries HE (1995). Photochemical air pollution. In Singh, H. B. (Ed.), *Composition, chemistry, and climate of the atmosphere* New York, NY: Van Nostrand Reinhold. [003055](#)

- Jerrett M; Arain A; Kanaroglou P; Beckerman B; Potoglou D; Sahsuvaroglu T; Morrison J; Giovis C (2005). A review and evaluation of intraurban air pollution exposure models. *J Expo Sci Environ Epidemiol*, 15: 185-204. [092864](#)
- Johnson CE; Derwent RG (1996). Relative radiative forcing consequences of global emissions of hydrocarbons, carbon monoxide, and NOX from human activities estimated with a zonally averaged two-dimensional model. *Clim Change*, 34: 439-462. [193192](#)
- Johnson TR (1984). A study of personal exposure to carbon monoxide in Denver, Colorado. U.S. Environmental Protection Agency. Research Triangle Park, NC. EPA-600/4-84-014. [024652](#)
- Joshi M; Shine KP; Ponater M; Stuber N; Sausen R; Li (2003). A comparison of climate response to different radiative forcings in three general circulation models: Towards an improved metric of climate change. *Clim Dynam*, 20: 843-854. [193752](#)
- Kanakidou M; Crutzen PJ (1999). The photochemical source of carbon monoxide: importance, uncertainties and feedbacks. *Chemosphere Global Change Sci*, 1: 91-109. [011760](#)
- Kanakidou M; Singh HB; Valentin KM; Crutzen PJ (1991). A two-dimensional study of ethane and propane oxidation in the troposphere. *J Geophys Res*, 96: 15,395-15,413. [029701](#)
- Kastner-Klein P; Fedorovich E; Ois Sini JF; Mestayer PG (2000). Experimental and numerical verification of similarity concept for dispersion of car exhaust gases in urban street canyons. *Environ Monit Assess*, 65: 353-361. [194035](#)
- Kastner-Klein P; Plate EJ (1999). Wind-tunnel study of concentration fields in street canyons. *Atmos Environ*, 33: 3973-3979. [001961](#)
- Kaur S; Nieuwenhuijsen M; Colvile R (2005). Personal exposure of street canyon intersection users to PM2.5, ultrafine particle counts and carbon monoxide in central London, UK. *Atmos Environ*, 39: 3629-3641. [086504](#)
- Kaur S; Nieuwenhuijsen MJ (2009). Determinants of personal exposure to PM2.5, ultrafine particle counts, and CO in a transport microenvironment. *Environ Sci Technol*, 43: 4737-4743. [194014](#)
- Kaur S; Nieuwenhuijsen MJ; Colvile RN (2007). Fine particulate matter and carbon monoxide exposure concentrations in urban street transport microenvironments. *Atmos Environ*, 41: 4781-4810. [190070](#)
- Khalil MAK; Rasmussen RA (1990). Atmospheric carbon monoxide: latitudinal distribution of sources. *Geophys Res Lett*, 17: 1913-1916. [012443](#)
- Khalil MAK; Rasmussen RA (1990). The global cycle of carbon monoxide: trends and mass balance. *Chemosphere*, 20: 227-242. [012352](#)
- Khare M; Chaudhry KK; Gowda RMM; Ahmad K (2005). Effects of the homogeneous traffic on vertical dispersion parameter in the near field of roadways – A wind tunnel study. *Environ Monit Assess*, 10: 55-62. [194016](#)
- Kim D; Sass-Kortsak A; Purdham JT; Dales RE; Brook JR (2006). Associations between personal exposures and fixed-site ambient measurements of fine particulate matter, nitrogen dioxide, and carbon monoxide in Toronto, Canada. *J Expo Sci Environ Epidemiol*, 16: 172-183. [089820](#)
- King GM (1999). Characteristics and significance of atmospheric carbon monoxide consumption by soils. *Chemosphere*, 1: 53-63. [002828](#)
- Kirchhoff VWJH; Marinho EVA (1990). Surface carbon monoxide measurements in Amazonia. *J Geophys Res*, 95: 16933-16943. [194406](#)
- Klepeis NE; Nelson WC; Ott WR; Robinson JPTsang AM; Switzer P; Behar JV; Hern SC; Engelmann WH (2001). The National Human Activity Pattern Survey (NHAPS): a resource for assessing exposure to environmental pollutants. *J Expo Sci Environ Epidemiol*, 11: 231-252. [002437](#)
- Krewski D; Jerrett M; Burnett RT; Ma R; Hughes E; Shi Y; Turner MC; Pope AC III; Thurston G; Calle EE; Thun MJ (2009). Extended follow-up and spatial analysis of the American Cancer Society study linking particulate air pollution and mortality. Health Effects Institute. Cambridge, MA. Report Nr. 140. [191193](#)
- Kristjansson JE (2002). Studies of the aerosol indirect effect from sulfate and black carbon aerosols. *J Geophys Res*, 107: 4246. [045282](#)
- Lai HK; Kendall M; Ferrier H; Lindup I; Alm S; Hanninen O; Jantunen M; Mathys P; Colvile R; Ashmore MR; Cullinan P; Nieuwenhuijsen MJ (2004). Personal exposures and microenvironment concentrations of PM2.5, VOC, NO2 and CO in Oxford, UK. *Atmos Environ*, 38: 6399-6410. [056811](#)

- Langan L (1992). Portability in measuring exposure to carbon monoxide. Presented at In: Measuring, understanding, and predicting exposures in the 21st century: proceedings of the conference; November 1991; Atlanta, GA. *J. Exposure Anal. Environ. Epidemiol.* 1(suppl. 1): 223-239. [046120](#)
- Lelieveld J; Berresheim H; Borrmann S; Crutzen PJ; Dentener FJ; Fischer H; Feichter J; Flatau PJ; Heland J; Holzinger R; Korrmann R; Lawrence MG; Levin Z; Markowicz KM; Mihalopoulos N; Minikin A; Ramanathan V; De Reus M; Roelofs GJ; Scheeren HA; Sciare J; Schlager H; Schultz M; Siegmund P; Steil B; Stephanou EG; Stier P; Traub M; Warneke C; Williams J; Ziereis H (2002). Global air pollution crossroads over the Mediterranean. *Science*, 298: 794-799. [190361](#)
- Lobert JM; Scharffe DH; Hao WM; Kuhlbusch TA; Seuwen R; Warneck P; Crutzen PJ (1991). Experimental evaluation of biomass burning emissions: Nitrogen and carbon containing compounds. In Levine JS (Ed.), *Global biomass burning: Atmospheric, climatic, and biospheric implications* (pp. 289-304). Cambridge, MA: MIT Press. [029473](#)
- Manning MR; Brenninkmeijer CAM; Allan W (1997). Atmospheric carbon monoxide budget of the southern hemisphere: Implications of $^{13}\text{C}/^{12}\text{C}$ measurements. *J Geophys Res*, 102: 10673-10682. [194401](#)
- Marshall JD; Nethery E; Brauer M (2008). Within-urban variability in ambient air pollution: comparison of estimation methods. *Atmos Environ*, 42: 1359-1369. [193983](#)
- McCurdy T; Glen G; Smith L; Lakkadi Y (2000). The National Exposure Research Laboratory's consolidated human activity database. *J Expo Sci Environ Epidemiol*, 10: 566-578. [000782](#)
- Menon S; Hansen J; Nazarenko L; Luo Y (2002). Climate effects of black carbon aerosols in China and India. *Science*, 297: 2250-2253. [155978](#)
- Michie RN; McElroy FF; Sokash JA; Thompson VL; Dayton DP; Sutcliffe CR (1983). Performance test results and comparative data for designated reference methods for carbon monoxide. U.S. Environmental Protection Agency. Research Triangle Park. EPA-600/S4-83-013. [194043](#)
- Millet DB; Jacob DJ; Turquety S; Hudman RC; Wu S; Fried A; Walega J; Heikes BG; Blake DR; Singh HB; Anderson BE; Clarke AD (2006). Formaldehyde distribution over North America: Implications for satellite retrievals of formaldehyde columns and isoprene emission. *J Geophys Res*, 111: D24S02. [195106](#)
- Milner JT; ApSimon HM; Croxford B (2006). Spatial variation of CO concentrations within an office building and outdoor influences. *Atmos Environ*, 40: 6338-6348. [123100](#)
- Mobley D; Deslauriers M; Rojas-Brachos L (2005). Improving emission inventories for effective air-quality management across North America: A NARSTO assessment. NARSTO. Pasco, WA. NARSTO-05-001. [194008](#)
- Murena F; Garofalo N; Favale F (2008). Monitoring CO concentration at leeward and windward sides in a deep street canyon. *Atmos Environ*, 42: 8204-8210. [194038](#)
- Naik V; Mauzerall D; Horowitz L; Schwarzkopf MD; Ramaswamy V; Oppenheimer M (2005). Net radiative forcing due to changes in regional emissions of tropospheric ozone precursors. *J Geophys Res*, 110: D24306. [193194](#)
- Ni Riain CM; Mark D; Davies M; Harrison RM; Byrne MA (2003). Averaging periods for indoor-outdoor ratios of pollution in naturally ventilated non-domestic buildings near a busy road. *Atmos Environ*, 37: 4121-4132. [053792](#)
- NRC (1999). *Ozone-forming potential of reformulated gasoline*. Washington, DC: National Research Council, National Academy of Sciences. [010614](#)
- Ott W; Switzer P; Willits N (1994). Carbon monoxide exposures inside an automobile traveling on an urban arterial highway. *J Air Waste Manag Assoc*, 44: 1010-1018. [076546](#)
- Paciorek CJ; Yanosky JD; Puett RC; Laden F; Suh HH (2009). Practical large-scale spatio-temporal modeling of particulate matter concentrations. *Ann Appl Stat*, 3: 370-397. [190090](#)
- Parrish DD (2006). Critical evaluation of US on-road vehicle emission inventories. *Atmos Environ*, 40: 2288-2300. [090352](#)
- Parrish DD; Trainer M; Hereid D; Williams EJ; Olszyna KJ; Harley RA; Meagher JF; Fehsenfeld FC (2002). Decadal change in carbon monoxide to nitrogen oxide ratio in US vehicular emissions. *J Geophys Res*, 107: 4140. [052472](#)
- Pfister G; Hess PG; Emmons LK; Lamarque JF; Wiedinmyer C; Edwards DP; Petron G; Gille JC; Sachse GW (2005). Quantifying CO emissions from the 2004 Alaskan wildfires using MOPITT CO data. *Geophys Res Lett*, 32: L11809. [093009](#)

- Pokharel SS; Bishop GA; Stedman DH (2002). An on-road motor vehicle emissions inventory for Denver: An efficient alternative to modeling. *Atmos Environ*, 36: 5177-5184. [052473](#)
- Pokharel SS; Bishop GA; Stedman DH (2003). Emissions reductions as a result of automobile improvement. *Environ Sci Technol*, 37: 5097-5101. [053740](#)
- Polidori A; Arhami M; Sioutas C; Delfino RJ; Allen R (2007). Indoor/outdoor relationships, trends, and carbonaceous content of fine particulate matter in retirement homes of the Los Angeles Basin. *J Air Waste Manag Assoc*, 57: 366-379. [156877](#)
- Pollack AK; Lindhjem C; Stoeckenius TE; Tran C; Mansell G; Jimenez M; Wilson G; Coulter-Burke S (2004). Final Report: Evaluation of the US EPA MOBILE6 highway vehicle emission factor model. ENVIRON International Corporation. Novato, CA. CRC Project E-64. [184461](#)
- Prather MJ (1996). Natural modes and timescales in atmospheric chemistry: Theory, GWPs for CH₄ and CO, and runaway growth. *Geophys Res Lett*, 23: 2597-2600. [193195](#)
- Riediker M; Williams R; Devlin R; Griggs T; Bromberg P (2003). Exposure to particulate matter, volatile organic compounds, and other air pollutants inside patrol cars. *Environ Sci Technol*, 37: 2084-2093. [043761](#)
- Rind D; Lerner J (1996). Use of on-line tracers as a diagnostic tool in general circulation model development: 1. Horizontal and vertical transport in the troposphere. *J Geophys Res*, 101: 12667-12683. [193750](#)
- Rodes C; Sheldon L; Whitaker D; Clayton A; Fitzgerald K; Flanagan J; DiGenova F; Hering S; Frazier C (1998). Measuring concentrations of selected air pollutants inside California vehicles [final report]. California Environmental Protection Agency, Air Resources Board; South Coast Air Quality Management District. Sacramento, CA. <http://www.arb.ca.gov/research/abstracts/95-339.htm>. [010611](#)
- Rosenlund M; Berglund N; Pershagen G; Hallqvist J; Jonson T; Bellander T (2006). Long-term exposure to urban air pollution and myocardial infarction. *Epidemiology*, 17: 383-390. [089796](#)
- Rotstajn LD; Penner JE (2001). Indirect aerosol forcing, quasi-forcing, and climate response. *J Clim*, 14: 2960-2975. [193754](#)
- Ryan PH; LeMasters GK (2007). A review of land-use regression models for characterizing intraurban air pollution exposure. *Inhal Toxicol*, 19: 127. [156063](#)
- Ryan PH; LeMasters GK; Levin L; Burkle J; Biswas P; Hu S; Grinshpun S; Reponen T (2008). A land-use regression model for estimating microenvironmental diesel exposure given multiple addresses from birth through childhood. *Sci Total Environ*, 404: 139-147. [156064](#)
- Sarnat JA; Brown KW; Schwartz J; Coull BA; Koutrakis P (2005). Ambient gas concentrations and personal particulate matter exposures: implications for studying the health effects of particles. *Epidemiology*, 16: 385-395. [087531](#)
- Sarnat JA; Schwartz J; Catalano PJ; Suh HH (2001). Gaseous pollutants in particulate matter epidemiology: Confounders or surrogates? *Environ Health Perspect*, 109: 1053-1061. [019401](#)
- Sarnat SE; Coull BA; Schwartz J; Gold DR; Suh HH (2006). Factors affecting the association between ambient concentrations and personal exposures to particles and gases. *Environ Health Perspect*, 114: 649-654. [089784](#)
- Sarnat SE; Klein M; Sarnat JA; Flanders WD; Waller LA; Mulholland JA; Russell AG; Tolbert PE (2009). An examination of exposure measurement error from air pollutant spatial variability in time-series studies. *J Expo Sci Environ Epidemiol*, In Press: 1-12. [180084](#)
- Scotto Di Marco G; Kephelopoulos S; Ruuskanen J; Jantunen M (2005). Personal carbon monoxide exposure in Helsinki, Finland. *Atmos Environ*, 39: 2697-2707. [144054](#)
- Sheppard L; Slaughter JC; Schildcrout J; Liu L-JS; Lumley T (2005). Exposure and measurement contributions to estimates of acute air pollution effects. *J Expo Sci Environ Epidemiol*, 15: 366-376. [079176](#)
- Shindell DT; Faluvegi G; Bell N; Schmidt GA (2005). An emissions-based view of climate forcing by methane and tropospheric ozone. *Geophys Res Lett*, 32: L04803. [080129](#)
- Shindell DT; Faluvegi G; Emmons LK (2005). Inferring carbon monoxide pollution changes from space-based observations. *J Geophys Res*, 110: D23303. [193746](#)
- Shindell DT; Faluvegi G; Koch DM; Schmidt GA; Unger N; Bauer SE (2009). Improved attribution of climate forcing to emissions. *Science*, 326: 716-718. [201599](#)

- Shindell DT; Faluvegi G; Stevenson DS; Krol MC; Emmons LK; Lamarque J-F; Petron G; Dentener FJ; Ellingsen K; Schultz MG; Wild O; Amann M; Atherton CS; Bergmann DJ; Bey I; Butler T; Cofala J; Collins WJ (2006). Multimodel simulations of carbon monoxide: comparison with observations and projected near-future changes. *J Geophys Res*, 111: D19306. [091028](#)
- Shindell DT; Faluvegi G; Unger N; Aguilar E; Shmidt GA; Koch DM; Bauer SE; Miller RL (2006). Simulations of pre-industrial, present-day, and 2100 conditions in the NASA GISS composition and climate model G-PUCCINI. *Atmos Chem Phys*, 6: 4427-4459. [193751](#)
- Singh M; Phuleria HC; Bowers K; Sioutas C (2006). Seasonal and spatial trends in particle number concentrations and size distributions at the children's health study sites in Southern California. *J Expo Sci Environ Epidemiol*, 16: 3-18. [190136](#)
- Sinha A; Toumi R (1996). A comparison of climate forcings due to chlorofluorocarbons and carbon monoxide. *Geophys Res Lett*, 23: 65-68. [193747](#)
- So ESP; Chan ATY; Wong AYT (2005). Large-eddy simulations of wind flow and pollutant dispersion in a street canyon. *Atmos Environ*, 39: 3573-3582. [110746](#)
- Thompson AM; Cicerone RJ (1986). Possible perturbations to atmospheric CO, CH₄, and OH. *J Geophys Res*, 91: 10,853-10,864. [019374](#)
- Tolbert PE; Klein M; Peel JL; Sarnat SE; Sarnat JA (2007). Multipollutant modeling issues in a study of ambient air quality and emergency department visits in Atlanta. *J Expo Sci Environ Epidemiol*, 17: S29-S35. [090316](#)
- U.S. Census Bureau (2008). American Housing Survey for the United States: 2007. U.S. Government Printing Office. Washington, DC. [194013](#)
- U.S. EPA (2000). Air quality criteria for carbon monoxide. National Center for Environmental Assessment, Office of Research and Development, U.S. Environmental Protection Agency. Research Triangle Park, NC. EPA 600/P-99/001F. [000907](#)
- U.S. EPA (2006). 2002 National Emissions Inventory Data and Documentation. Retrieved 02-DEC-09, from <http://www.epa.gov/ttnchie1/net/2002inventory.html>. [157070](#)
- U.S. EPA (2006). Air quality criteria for ozone and related photochemical oxidants. EPA. DC. [088089](#)
- U.S. EPA (2006). Cold temperature effects on vehicle HC emissions: draft report. U.S. Environmental Protection Agency. Washington, DC. EPA420-D-06-001. <http://www.epa.gov/oms/regs/toxics/420d06001.pdf>. [199897](#)
- U.S. EPA (2008). Integrated Science Assessment for Oxides of Nitrogen - Health Criteria. U.S. Environmental Protection Agency. Research Triangle Park, NC. EPA/600/R-08/071. [157073](#)
- U.S. EPA (2008). Inventory of U.S. greenhouse gas emissions and sinks: 1990 – 2006. US Environmental Protection Agency. Washington, DC. [184463](#)
- U.S. EPA (2008). Total Risk Integrated Methodology (TRIM) Air Pollutants Exposure Model Documentation (TRIM.Expo/APEX, Version 4.3). Volume 1: User's Guide. U.S. Environmental Protection Agency, Office of Air Quality Planning and Standards. Research Triangle Park, NC. EPA-452/B-08-001b. [191775](#)
- U.S. EPA (2008). U.S. EPA's 2008 Report on the Environment (Final Report). U.S. Environmental Protection Agency. DC. [157076](#)
- U.S. EPA (2009). Consolidated Human Activity Database. Retrieved 27-AUG-09, from <http://www.epa.gov/chadnet1/>. [194010](#)
- U.S. EPA (2009). Human exposure modeling - Air pollutants exposure model (APEX/TRIM.Expo Inhalation). Retrieved 27-AUG-09, from http://www.epa.gov/ttn/fera/human_apex.html. [194009](#)
- Unger N; Shindell DT; Wang TS (2009). Climate forcing by the on-road transportation and power generation sectors. *Atmos Environ*, 43: 3077-3085. [193238](#)
- van der Werf GR; Randerson JT; Giglio L; Collatz GJ; Kasibhatla PS; Arellano Jr AF (2006). Interannual variability in global biomass burning emissions from 1997 to 2004. *Atmos Chem Phys*, 6: 3423-3441. [157084](#)
- Wallace L; Williams R; Suggs J; Jones P (2006). Estimating contributions of outdoor fine particles to indoor concentrations and personal exposures: effects of household characteristics and personal activities. U.S. Environmental Protection Agency; National Exposure Research Laboratory. Research Triangle Park, NC. EPA/600/R-06/023. [089190](#)

- Wallace LA; Ziegenfuss RC (1985). Comparison of carboxyhemoglobin concentrations in adult nonsmokers with ambient carbon monoxide levels. *J Air Waste Manag Assoc*, 35: 944-949. [011656](#)
- Wang C; Prinn RG (1999). Impact of emissions, chemistry and climate on atmospheric carbon monoxide: 100-yr predictions from a global chemistry-climate model. *Chemosphere Global Change Sci*, 1: 73-81. [011758](#)
- Wigley TML; Smith SJ; Prather MJ (2002). Radiative forcing due to reactive gas emissions. *J Clim*, 15: 2690-2696. [047883](#)
- Wild O; Prather MJ (2000). Excitation of the primary tropospheric chemical mode in a global three-dimensional model. *J Geophys Res*, 105: 24,647-24,660. [052402](#)
- Wild O; Prather MJ; Akimoto H (2001). Indirect long-term global radiative cooling from NOX emissions. *Geophys Res Lett*, 28: 1719-1722. [193196](#)
- Williams R; Suggs J; Rea A; Leovic K; Vette A; Croghan C; Sheldon L; Rodes C; Thornburg J; Ejire A; Herbst M; Sanders W Jr (2003). The Research Triangle Park particulate matter panel study: PM mass concentration relationships. *Atmos Environ*, 37: 5349-5363. [053335](#)
- Wilson WE; Mage DT; Grant LD (2000). Estimating separately personal exposure to ambient and nonambient particulate matter for epidemiology and risk assessment: why and how. *J Air Waste Manag Assoc*, 50: 1167-1183. [010288](#)
- Wilson WE; Suh HH (1997). Fine particles and coarse particles: concentration relationships relevant to epidemiologic studies. *J Air Waste Manag Assoc*, 47: 1238-1249. [077408](#)
- Wuebbles DJ; Hayhoe K (2002). Atmospheric methane and global change. *Earth Sci Rev*, 57: 177-210. [044159](#)
- Xiaomin X; Zhen H; Jiasong W (2006). The impact of urban street layout on local atmospheric environment. *Build Environ*, 41: 1352-1363. [156165](#)
- Yanosky JD; Paciorek CJ; Schwartz J; Laden F; Puett R; Suh HH (2008). Spatio-temporal modeling of chronic PM10 exposure for the Nurses' Health Study. *Atmos Environ*, 42(18): 4047-4062. [099467](#)
- Yanosky JD; Paciorek CJ; Suh HH (2009). Predicting chronic fine and coarse particulate exposures using spatiotemporal models for the northeastern and midwestern United States. *Environ Health Perspect*, 117: 522-529. [190114](#)
- Zeger SL; Diggle PJ (2001). Correction: exposure measurement error in time-series air pollution studies. *Environ Health Perspect*, 109: A517. [026017](#)
- Zeger SL; Thomas D; Dominici F; Samet JM; Schwartz J; Dockery D; Cohen A (2000). Exposure measurement error in time-series studies of air pollution: concepts and consequences. *Environ Health Perspect*, 108: 419-426. [001949](#)
- Zhou Y; Levy JI (2008). The impact of urban street canyons on population exposure to traffic-related primary pollutants. *Atmos Environ*, 42: 3087-3098. [190091](#)
- Zhu Y; Hinds WC; Kim S; Shen S; Sioutas C (2002). Study of ultrafine particles near a major highway with heavy-duty diesel traffic. *Atmos Environ*, 36: 4323-4335. [041553](#)
- Zidek JV; Shaddick G; Meloche J; Chatfield C; White R (2007). A framework for predicting personal exposures to environmental hazards. *Environ Ecol Stat*, 14: 411-431. [190076](#)
- Zimmerman PR; Chatfield RB; Fishman J; Crutzen PJ; Hanst PL (1978). Estimates on the production of CO and H2 from the oxidation of hydrocarbon emissions from vegetation. *Geophys Res Lett*, 5: 679-682. [010758](#)